THE ABRASIVE WEAR BEHAVIOUR OF MINERAL-FILLED POLYPROPYLENE

by

Brian Michael Sole

A thesis submitted to the Faculty of Engineering, University of Cape Town in fulfilment of the degree of Doctor of Philosophy

Department of Materials Engineering
University of Cape Town
February 1997

ABSTRACT

Polypropylene is an extremely versatile polymer because its properties can be modified to meet specific requirements. The use of polypropylene in domestic and automobile applications has initiated research focused on the tribological behaviour of the material. In the present study, polypropylene grades have been subjected to both mild and severe abrasive wear conditions with specific emphasis on the surface property of scratch resistance. The experimental work has covered the effect of polymer crystallinity, mineral fillers, and the nature of the abrasive counterface on the wear behaviour of polypropylene. The wear behaviours of polymethyl-methacrylate, polycarbonate, acrylonitrile-butadiene-styrene, and high density polyethylene have been determined for comparative purposes.

The abrasive wear rates have been measured and the material deformation and removal mechanisms have been identified and characterised in terms of the physical properties of the polymer and the individual fillers, and in terms of the macroscopic mechanical behaviour of the filled composite materials. Investigative techniques used in this study included mechanical testing, optical and scanning electron microscopy, surface profilometry, and differential scanning calorimetry.

Under two-body abrasive wear conditions, the unfilled and modified polypropylene materials exhibit a ductile mode of material deformation and removal. The filled grades show increased abrasive wear rates which correlate with their reduced strain to failure. Although these wear rates are not widely sensitive to the physical properties of the specific fillers, the size and shape of the filler particles control the microdeformation mechanisms of the composite materials.

The deformation mechanisms prevalent during single-point scratch tests are shown to model the bulk abrasive properties of the respective polymers. The bulk hardness of the composite and the physical properties of the filler materials influence the scratch performance. Five scratch track morphologies have been identified and related to a transition in wear behaviour with changing abrasive counterface geometry.

The specific scratch resistance of the polymers is assessed by four different methods. The visibility of surface scratching is shown to be influenced by both the hardness of the material and the level of pigmentation and variegation of the polymer surface.

ACKNOWLEDGEMENTS

I would like to express my appreciation to all those who have assisted me in the course of this work, in particular:

Dr Neville Scott, Mr Mark Domingo and the Polypropylene Technical Research and Development team at Polifin for their advice and suggestions, technical assistance, and the supply of materials for this research.

Professor Anthony Ball, my supervisor, and Professor Colin Allen, for their helpful discussions and support.

Mr Glen Newins, Mr Nicholas Dreze, and Mr Dave Dean for help in maintaining the test apparatus and preparation of test specimens; Mrs Mira Topic for laboratory assistance; and Mr James Petersen and Mr Bernard Greeves for photographic assistance.

Mrs Anne Ball for her administrative support.

To my sister, Kathy, for her help with the preparation of this manuscript.

The technical staff at Plastamid for their assistance and use of the injection moulding and polymer testing equipment. In particular, I am extremely grateful to Mr Charles Goldman and Mr Gerome Julius.

The staff and students in the Department of Materials Engineering for their support and encouragement, and the interesting discussions on Friday afternoons. To Mat United, it was a great three years.

The financial support of Polifin Limited is gratefully acknowledged.

GLOSSARY OF ABBREVIATIONS AND SYMBOLS

ABS	acrylonitrile-butadiene-styrene
DSC	differential scanning calorimetry
HDPE	high density polyethylene
MWD	molecular weight distribution
PA6,6	polyamide 6,6
PC	polycarbonate
PET	polyethyleneterepthalate
PMMA	polymethylmethacrylate
POM	polyoxymethylene
PP	polypropylene
PS	polystyrene
PTFE	polytetrafluoroethylene
rpm	revolutions per minute
SEM	scanning electron microscopy

α	included half-angle of cone (°)
A_f	specific surface area ($mm^2\ g^{-1}$)
A_s	sliding contact area (mm^2)
β	average asperity tip radius (μm)
δ	standard deviation of asperity heights
d_s	scratch track width (μm)
ε	elongation to break (%)
E	Young's Modulus ($N\ mm^{-2}$)
E_c	Young's Modulus of composite ($N\ mm^{-2}$)
E_f	Young's Modulus of filler ($N\ mm^{-2}$)
E_m	Young's Modulus of matrix ($N\ mm^{-2}$)
ϕ	volumetric packing factor
θ	base angle of cone (°)
h	penetration depth (μm)

TABLE OF CONTENTS

	Page
ABSTRACT	i
ACKNOWLEDGEMENTS	iii
GLOSSARY OF ABBREVIATIONS AND SYMBOLS	iv
TABLE OF CONTENTS	vi
1. INTRODUCTION	**1**
1.1. Research Approach	2
2. LITERATURE REVIEW	**4**
2.1. Polymer Concepts	4
2.1.1. Introduction	4
2.1.2. Polymeric crystal structure	4
2.1.3. Polymer morphology	6
2.1.4. Molecular weight and distribution	8
2.2. Microstructure - Property Relationships	9
2.2.1. Introduction	9
2.2.2. Molecular weight and crystallinity	10
2.2.3. Effect of strain rate on tensile properties	12
2.3. Mechanical Properties of Filled Polypropylene	12
2.3.1. Introduction	12
2.3.2. Theoretical models for mechanical behaviour	13
2.3.3. Reported results on the mechanical behaviour of filled polypropylene	15
2.4. The Wear of Polymers	20
2.4.1. Introduction	20
2.4.2. Wear Mechanisms	21
2.4.2.1. Adhesive wear	22
2.4.2.2. Chemical wear	22

3.4.3. Density measurements 53
3.4.4. Differential Scanning Calorimetry (DSC) 53
3.5. Mechanical Tests 54
3.5.1. Tensile tests 54
3.5.2. Flexural bend tests 54
3.5.3. Hardness tests 55
3.5.3.1. Vickers microhardness 55
3.5.3.2. Shore D hardness 55
3.5.3.3. Ball indentor hardness tests 55
3.6. Tribology Tests 56
3.6.1. Abrasion testing 56
3.6.1.1. Calibration of the abrasive belt rig 57
3.6.2. Single-point scratch test 58
3.6.3. Abrasive scrub testing and gloss measurement 59
3.6.3.1. Test procedure and operating parameters 61

4. RESULTS **62**
4.1. Materials Characterisation 62
4.1.1. Polymer characterisation 62
4.1.2. Filler characterisation 64
4.1.2.1. Weight fraction analysis 64
4.1.2.2. Filler morphology 65
4.1.2.3. Filler dispersion and orientation 66
4.1.2.3.1. Nature of the filler - matrix interface 67
4.2. Mechanical Testing 69
4.2.1. Tensile tests 69
4.2.1.2. Effect of the base polypropylene homopolymer 69
4.2.1.3. Effect of mineral fillers 72
4.2.1.3.1. Effect of filler shape 75
4.2.1.3.2. Effect of filler size 76

4.2.1.3.3. Effect of the base polypropylene grade 79
4.2.1.4. SEM analysis of tensile fracture samples 80
4.2.1.4.1. Tensile fracture at low filler content 81
4.2.1.4.2. Tensile fracture at high filler content 82
4.2.2. Flexural tests 85
4.2.2.1. Effect of mineral fillers 87
4.2.2.1.1. Effect of filler shape 87
4.2.2.1.2. Effect of filler size 88
4.2.3. Hardness tests 90
4.2.3.1. Vickers microhardness 90
4.2.3.2. Shore D hardness 90
4.2.3.3. Ball indentation hardness tests 90
4.3. Tribology Test Results 91
4.3.1. Abrasive wear tests 91
4.3.1.1. Effect of the base polypropylene homopolymer 92
4.3.1.2. Abrasion of the comparative polymers 94
4.3.1.3. Effect of filler addition on the abrasive wear rate 96
4.3.1.3.1. Effect of filler particle shape and size 103
4.3.1.4. Effect of abrasive particle size on the wear rate 105
4.3.2. Single-point scratch tests 107
4.3.2.1. Rockwell C Diamond indentor tests 107
4.3.2.1.1. The effect of fillers on the scratch behaviour 110
4.3.2.2. Variable included angle scratch tests 113
4.3.2.2.1. Polypropylene and the comparative polymers 114

4.3.2.2.2. The effect of fillers on the variable included angle scratch behaviour 117
4.3.3. Abrasive scrub tests 118
4.3.3.1. Result analysis by surface roughness 120
4.3.3.2. Result analysis by gloss measurement 121
4.3.3.3. Result analysis by material deformation 124
4.3.3.4. Result analysis by visual assessment / ranking 126

5. DISCUSSION **128**
5.1. Introduction 128
5.2. Mechanical Properties 128
5.2.1. Effect of the base polypropylene homopolymer 128
5.2.2. Effect of mineral fillers on the mechanical behaviour 133
5.2.2.1. Effect of filler particle shape 134
5.2.2.2. Effect of filler particle size 136
5.2.2.3. Effect of filler content 139
5.2.2.4. Effect of filler surface treatments 139
5.2.2.5. Overview 140
5.3. Abrasive Wear Properties 140
5.3.1. Influence of abrasive grit size on the wear rate 140
5.3.2. Effect of the base polypropylene homopolymer 142
5.3.2.1. Abrasion against the coarse abrasive belts 143
5.3.2.2. Abrasion against the fine abrasive belts 144
5.3.3. Abrasive wear behaviour of the comparative polymers 145
5.3.4. Effect of mineral fillers on the abrasive wear rate 146
5.3.4.1. Abrasion under high applied contact stresses 149

5.3.4.2. Abrasion under low applied contact stresses 149
5.3.4.3. Influence of mechanical properties on the wear rates of the filled composites 150
5.4. Single-Point Scratch Tests 154
5.4.1. Polypropylene and the comparative polymers 154
5.4.2. Polypropylene and the filled composites 161
5.5. Abrasive Scrub Tests 163
5.5.1. Polypropylene and the comparative polymers 164
5.5.2. Polypropylene and the filled composites 165

6. CONCLUSIONS **167**

7. REFERENCES **170**

APPENDIX A. Properties of the mineral fillers **180**
A.1 Talc fillers 180
A.1.1 Luzenac 00S 180
A.1.2 Luzenac Steaplast 9000 180
A.2 $CaCO_3$ 181
A.3 $BaSO_4$ 181
A.4 Fly ash 182
A.5 China clay 182
A.6 Wollastonite 183
A.6.1 Coarse grade wollastonite 183
A.6.2 Fine grade wollastonite 183
APPENDIX B. Calibration of the abrasive belt rig **185**
B.1 Effect of normal load 185
B.2 Effect of sliding velocity 186
APPENDIX C. Principles of gloss measurement **187**
APPENDIX D. Mechanical test results **189**

CHAPTER I

INTRODUCTION

Polypropylene represents about 18% of the growing global demand for commodity polymers and has emerged as a true engineering material with a widening sphere of application. As Vogtländer pointed out, *"the future of polypropylene - and polyolefins in general is as promising as it has ever been in their history. Polyolefins stand on the edge of becoming one of man's fundamental materials for shaping the world around him. With its outstanding properties, wide application versatility, competitive cost performance, and environmental credentials polypropylene has gained an enviable reputation and continues to penetrate a wider range of application"*[1].

Polypropylene (PP) is well established in both the South African and international market areas of automobile applications, fibres and textiles, and packaging and containers[2,3]. It can be used in most thermoforming, blow moulding, and injection moulding processes. Furthermore, the attractive cost to performance ratio of polypropylene has led to its substitution in many applications previously dominated by other polymers[4-6].

Much of the recent research that has led to this growing market share for polypropylene has focused on the development of the polymerisation processes and the catalyst chemistry to further enhance the properties of the polymer. It is well documented that fillers and fibre reinforcement can influence the physical properties of a polymer. The mechanical properties, and in particular the strength and stiffness, are greatly affected by filler or fibre inclusions to the polymer matrix. In tribological applications the effect of the filler/fibre reinforcement is less defined. The wear behaviour of a polymer is not an intrinsic material property but depends both on the material and the

tribological system in which it functions. The research into polymer tribology has primarily centred on materials subjected to sliding wear and abrasive wear, and typically those polymers used in bearing applications. Of these materials, six polymers dominate the literature, *viz.*, polyamide, polyacetal, polytetrafluoroethylene, polyethylene, polyimide, and phenolics. Although the increasing world-wide demand for polypropylene continues, there is little information on the behaviour of this polymer under tribological conditions, and in particular its abrasive wear performance.

1.1 RESEARCH APPROACH

The present work focuses on the correlation between the mechanical properties and the abrasive wear performance of three homopolymer polypropylene materials, two of which have been reinforced with a selection of mineral fillers.

The specific aims of this project were:

i) to characterise the tensile behaviour of each polypropylene material as a function of filler content;

ii) to investigate the abrasive wear behaviour of polypropylene and the mineral-filled composites, as worn against Al_2O_3 abrasive counterfaces, and to correlate this performance with the mechanical behaviour;

iii) to determine the wear mechanisms responsible for material damage during abrasive wear through the use of optical and scanning electron microscopy techniques;

iv) to utilise a single-track scratch test as a model for abrasive wear deformation behaviour;

vi) to compare the tribological performance of polypropylene with other commodity polymers under conditions of bulk abrasive wear, single-point scratch tests, and scratch resistance, and,

v) to investigate the scratch resistance of polypropylene as a specific form of abrasive wear, and to determine the optimum polymer composite properties for applications where excellent visual appearance is paramount.

CHAPTER 2

LITERATURE REVIEW

2.1 POLYMER CONCEPTS

2.1.1 Introduction

Polypropylene is an aliphatic hydrocarbon of the type -(CH_2-$CHCH_3$)-. It is a thermoplastic and is semi-crystalline in nature. The microstructure of a crystalline polymer can be described as an ordered arrangement of molecules within the polymer. It is the microstructure and molecular make-up that has a wide influence on the physical, chemical, and mechanical properties of a polymer[7-9]. Furthermore, detailed knowledge of the morphology is required to understand the deformation behaviour of a polymer during tribological and mechanical processes. Semi-crystalline polymers, in fact, show ordering at a variety of dimensional levels. In this regard, it is important to develop some concepts of polymer crystal structure to elucidate the discussion of polymer morphology, the physical properties, and tribological performance.

2.1.2 Polymeric crystal structure

The ability of a polymer to crystallise depends primarily on the regularity of the macromolecular chains. In general terms, the more regular the polymer, the more likely it is to crystallise. A fundamental variable that can affect the molecular arrangement is the stereoregularity of the polymer chain. Polypropylene can exist in three spatially ordered arrangements according to the position and sequence of the -CH_3 group on the carbon chain. Atactic PP, which has a disordered sequence, is generally unable to crystallise. The

isotactic and syndiotactic forms of polypropylene are spatially ordered and are thus able to form a crystalline lattice. Typical crystallinity values for the syndiotactic form are 25 to 30%, while values of 50 to 70% are common for the isotactic form resulting in its enhanced mechanical properties. The production of polypropylene via stereospecific Ziegler-Natta and metallocene catalysts ensures a predominantly isotactic structure[10,11].

The packing arrangement of molecules in the crystal can be described in terms of the unit cell and its contents. Isotactic polypropylene can crystallise under normal conditions in three forms: monoclinic (α), hexagonal (β), and triclinic (γ)[12]. In melt-crystallised polypropylene the predominant crystal structure is the α-modification, though β-modification can occur under selective thermal conditions and by the inclusion of selective nucleating agents[13,14].

The chain configurations of an all-carbon backbone are based on the tetrahedral valence of the carbon atom. Furthermore, the conformation of the individual chains is bounded by minimising the internal energy of the C-C bond rotation. For polypropylene, this results in a stable helical chain configuration which maximises the packing density of the crystal[15,16]. The helical chain conformation of polypropylene is shown in Figure 2.1, as viewed parallel to the chain axis.

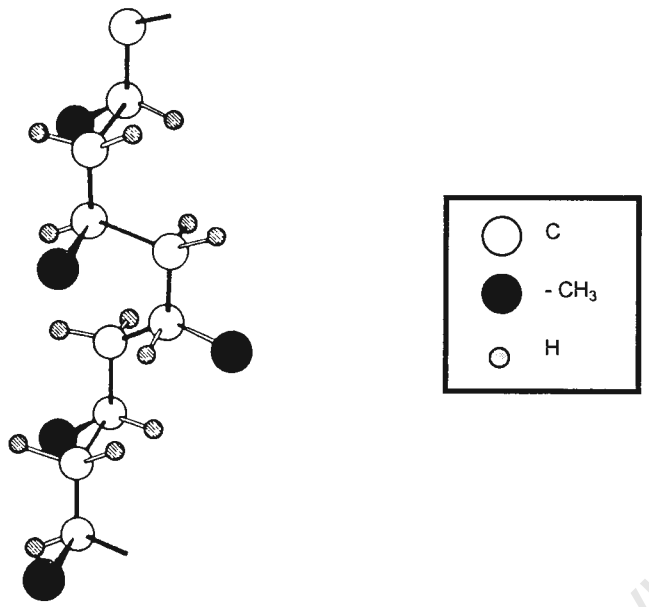

Figure 2.1: The helical conformation of polypropylene as viewed parallel to the chain-axis. [After Cowie[10]].

2.1.3 Polymer morphology

The bulk crystallisation of polymers from a melt is similar to that of the crystallisation of a single polymer crystal grown from a dilute solution. In the latter case, crystallisation of the molecules occurs in lamellae form. These lamellae are typically 10 to 20 nm thick and of the order of 1 μm wide[(9)]. X-ray diffraction studies indicate that the chains are oriented perpendicular to the plane of the lamellae. Since the length of a typical polymer chain is much greater than the dimensions of the lamellae, the chains must be folded back and forth on themselves[(17)]. This orientation in a typical crystal lamellae is shown for polyethylene in Figure 2.2.

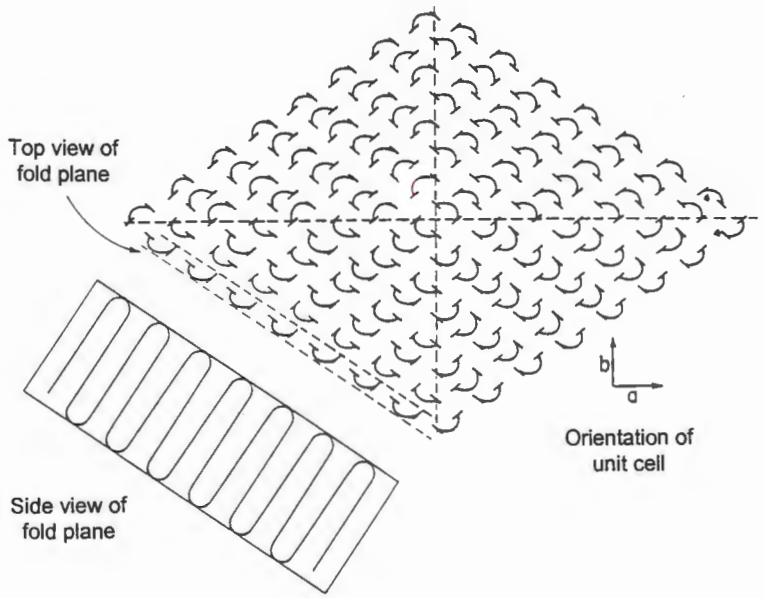

Figure 2.2: Fold packing in a single polyethylene crystal. [After Williams[17]].

The predominant morphology of polypropylene, as observed through a polarising microscope, is spherulitic in nature, the typical structure of which is shown in Figure 2.3. Spherulites are comprised of twisted chain folded lamellae which grow in all steric directions from a central nucleus, leaving non-crystallisable or amorphous material trapped between their fold surfaces and also between the spherulites themselves. Crystalline polymers are thus always partially crystalline as they contain both ordered and disordered material. Growth of the spherulites continues until the growth fronts of neighbouring structures impinge. The size and shape of the resulting spherulite structure depends on the thermal conditions of crystallisation and the presence of heterogeneous nucleating agents in the melt[(12)]. Spherulites can be considered to be radially symmetrical, optically uniaxial crystals. Examination of microtomed thin sections of polypropylene under polarised light show a Maltese Cross pattern indicative of the birefringent nature of the material.

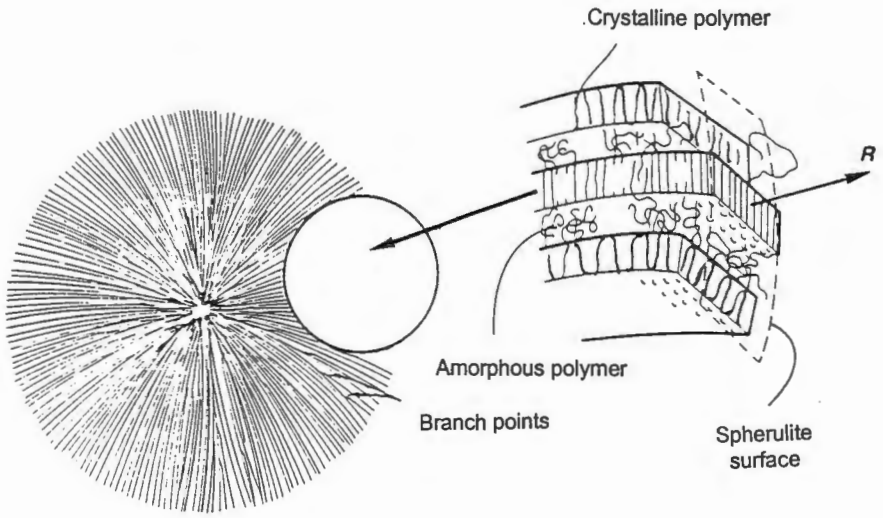

Figure 2.3: A typical polymer spherulite grown from the melt, showing a magnified view of the crystalline chain folded lamellae and the entrapped amorphous polymeric material. ***R*** indicates the spherulite radius direction. [After McCrum *et al.*[18]].

2.1.4 Molecular weight and distribution

One of the features that distinguishes synthetic high polymers from simple molecules is the existence of a distribution of chain lengths in the polymer[10,19]. This is due to the random nature of the polymerisation growth process. A polymer is thus best characterised by a molecular weight distribution and the associated average molar masses as shown in Figure 2.4. A colligative method, such as measurement of osmotic pressure, effectively counts the number of molecules present and defines a number average molar mass, M_n, as:

$$M_n = \Sigma n_i M_i / \Sigma n_i \qquad (2.1)$$

where n_i is the number of molecules with molecular weight M_i.

From light scattering measurements, an experimental method depending on the size of the molecules rather than their number, a weight average molar mass, M_w, is defined as:

$$M_w = \Sigma n_i M_i^2 / \Sigma n_i M_i \qquad (2.2)$$

The ratio M_w/M_n is known as the polydispersity and is an indication of the molecular weight distribution of the polymer.

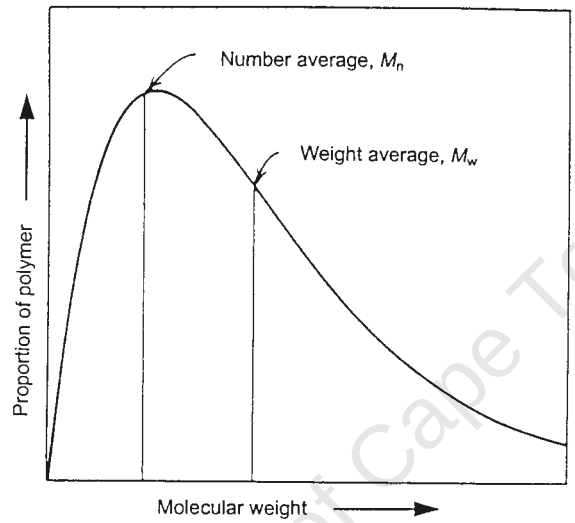

Figure 2.4: Typical distribution of molecular weights of a synthetic polymer. [After Billmeyer[19]].

2.2 MICROSTRUCTURE - PROPERTY RELATIONSHIPS

2.2.1 Introduction

Polypropylene and its filled composites have received much attention over the last decades as it has grown in importance as a commercial thermoplastic material. Advances in the polymerisation chemistry of polypropylene have resulted in materials with improved stereoregularity, molecular weight, and polydispersity control[11,20,21].

The purpose of this review is to examine some of the major works relating the polymer microstructure to the mechanical properties of polypropylene, which

will be pertinent to the understanding of the tribological behaviour of these materials.

2.2.2 Molecular weight and crystallinity

The most important factors which delineate the characteristic properties of polymers, and especially linear polymers such as polypropylene, are crystallinity and molecular weight. Most commercial processes for the production of polypropylene employ a Ziegler-Natta catalyst system. These catalysts have multiple reaction sites that differ in reactivity resulting in polymers with fairly broad molecular weight distributions (MWD). Typical values for the polydispersity range from 5 to 20[22]. The weight average molecular weight (M_w) for polypropylene is in the range from 3 x 10^5 to 7 x 10^5[23]. Metallocene catalysts can produce narrow MWD polypropylene with a typical polydispersity of 2[22].

A review of the literature reveals several papers that correlate molecular parameters with the physical and mechanical properties of polymers[24-26]. The review paper by Nunes *et al.*[27] highlights much of the work published in this regard from 1971 to 1982.

A molecular chain can exist in more than one lamellae and in more than one spherulite. The intercrystalline molecular segments are called tie molecules[12]. In rapidly crystallised linear polymers, such as polypropylene, the chains have less time to rearrange themselves from the disorganised arrangement, thus a strong interconnecting network is formed between crystalline entities. These tie molecules reinforce the significant amounts of amorphous material which accumulate at spherulite boundaries and are considered weak sites for fracture initiation[12,25].

For long-chain polymers, many mechanical properties can be improved by an increase in molecular weight. This effect reaches a limiting value at a

relatively high molecular weight after which no appreciable change in the property is apparent. Eventually, even with linear polymers, the molecular weight, and hence the melt viscosity, becomes so high that the polymers cannot be dissolved, worked mechanically, or be made to flow in the molten state. This critical condition usually sets in at a molecular weight above 10^7 g mol^{-1}[17]. Whereas the stress-strain behaviour of amorphous polymers is dependent on chain entanglements, and thus the molecular weight of the polymer, this influence of molecular weight is not as apparent for semi-crystalline polymers like polypropylene. This is due to the presence of crystallites which provide the strength capacity of the semi-crystalline polymer, much the same as chain entanglements do in amorphous polymers. It has been noted, however, that an increase in molecular weight can decrease the crystallinity of the polymer and hence produce a decrease in yield strength[27,28].

Strength and stiffness are closely related in theory but in practice a high modulus is not necessarily accompanied by a high strength[27,29]. High molecular weight polymers have longer polymer chains resulting in an increased tie molecule density and thus higher strengths. The modulus of a polymer is not strongly affected by molecular weight but is predominantly a function of the crystallinity. Increased crystallinity is associated with increased stiffness, however the work of Margolies[in 27] shows that increasing the molecular weight of linear polymers results in a deterioration in the crystallinity, and hence the stiffness of the polymer. The decrease in flexural stiffness reaches a critical point around a molecular weight of 1.75×10^6, above which no further significant decrease in evident The work of Phillips and co-workers[20] showed that in the absence of orientation, an increase in flexural modulus can be attributed to enhanced crystallinity.

2.2.3 Effect of strain rate on tensile properties

Hartmann *et al.*[30] performed uniaxial tensile tests on polypropylene at strain rates ranging from 0.02 to 8 min^{-1} at temperatures between 22 and 143 °C. Yield stress decreases with temperature but shows a linear increase when plotted against the logarithm of the strain rate. Young's Modulus decreases with temperature. At a fixed temperature of 22 °C, Young's Modulus is largely unaffected by an increase in strain rate.

Similar results were obtained by Tjong and co-workers[14] who compared the tensile behaviour of α-PP and the β-modified form of PP at strain rates between 0.02 and 7.69 min^{-1}. An increase in tensile yield stress with strain rate is observed. The α-PP showed an improvement in strength of ~10% over the β-PP. In contrast, β-PP showed much higher elongation at break at all strain rates; this implies that the addition of the β-nucleator is responsible for improved ductility. The ductility of both grades is found to be highly strain-rate dependent.

2.3 MECHANICAL PROPERTIES OF FILLED POLYPROPYLENE

2.3.1 Introduction

It is well documented in recent literature that the addition of inorganic fillers into polymeric matrices modifies the physical, mechanical, rheological, and thermal properties of the composite, as well as providing economic benefit[31,32]. In particular, the elastic modulus and the heat distortion temperature are enhanced by filler additions while tensile strength, impact strength, and elongation at break are adversely affected. Factors such as the filler type, content, shape, and size have considerable effect on the mechanical properties and several theoretical models have been proposed to predict composite behaviour[33-38]. Furthermore, it is known that the condition

of the filler-matrix interface is of prime importance in determining the mechanical response of these materials.

2.3.2 Theoretical models for mechanical behaviour

A brief overview of some of the theoretical models is given in this section. Most of the early models predicted mechanical behaviour of simple composite systems using spherical particulates in a polymeric matrix.

Kerner[33] deduced the shear modulus of a macroscopically isotropic and homogeneous composite in terms of the moduli and concentration of its components. The theory assumes that the included components can be analysed as spherical grains, and are uniformly distributed and suspended in a uniform medium. The Kerner equation is in the form:

$$E_c / E_m = 1 + [15\,(1-\nu_m) / (8-10\nu_m)]\,[V_f / (1-V_f)] \qquad (2.3)$$

where ν_m is Poisson's ratio for polypropylene.

Lewis and Nielsen modified the Kerner equation to include a factor (ϕ), based on the maximum volumetric packing fraction for spheres in a matrix (V_{max} = 0.64)[34]. They also stipulate that the condition $E_f / E_m >> 1$ must exist, where E_f and E_m are the elastic moduli of the filler and matrix, respectively. In their work Lewis and Nielsen measured the shear modulus for a glass sphere-epoxy system and modified the Kerner equation to the form:

$$E_c / E_m = (1 + A\,B\,V_f) / (1 - B\,\phi\,V_f) \qquad (2.4)$$

where $A = (7 - 5\nu_m) / (8 - 10\nu_m)$

and $B = [(E_f / E_m) - 1] / [(E_f / E_m) + A]$.

Similarly, in the Tsai-Halpin model[35], the Kerner equation is modified to include a parameter which takes into account the geometry of the reinforcing component. This geometry factor can be expressed in terms of the engineering elastic constants and differences in Poisson's ratio for the two components of the composite system. The Tsai-Halpin equations demonstrate the significant effect of particulate shape on the stiffness of a composite, specifically when comparing the properties of a sphere and a fibre filler.

In their work on glass bead-filled polyester resins, Leidner and Woodhams[36] developed a theoretical relationship linking the ultimate strength of a composite containing spherical fillers to the size, volume fraction, and surface adhesion of the dispersed phase. By assuming that the beads provided some load-bearing capabilities, a linear relationship between the strength of the composite and the volume fraction of filler is found to exist for composites with spherical filler particles. Furthermore, the strength of the composite is observed to be inversely proportional to the square root of the sphere diameter, indicating the detrimental effect of incorporating fillers of large particle size.

Ramsteiner and Theysohn[37] reviewed the existing simple models for predicting the Young's Modulus, tensile strength, and elongational viscosity for filled PP composites. They show that if shape factors are introduced, the models give good approximation to experimental results for Young's Modulus, not only for spherical fillers (shape factor = 2), but also for the fibrous wollastonite (factor = 7), and the platelet talc (factor = 16) fillers. In analysing the prediction of tensile yield strength, a better correlation with experimental data for spherical fillers was obtained using the following relationship based on the earlier work of Leidner and Woodhams[36].

$$\sigma_c = \sigma_m (1 - f V_f^{2/3}) \qquad (2.5)$$

where *f* is dependent on the volumetric packing of the filler.

In general, tensile yield stress of polymer composites is determined by two main factors, *i.e.* the decrease of effective load-bearing cross section of the matrix due to filler inclusions, and the matrix-filler interaction. These effects were studied by Turcsanyi and co-workers[38] who proposed a model for the yield stress in the form:

$$\sigma_c / \sigma_m = \{(1 - V_f) / (1+2.5V_f)\} \exp(BV_f) \qquad (2.6)$$

The factor *B* characterises the interfacial interaction and can be expressed as:

$$B = (1 + l A_f \rho_f) \ln (\sigma_i / \sigma_m) \qquad (2.7)$$

where: A_f = specific surface area of the filler
ρ_f = density of the filler
l = thickness of the interphase
σ_i = yield stress of interphase

2.3.3 Reported results on the mechanical behaviour of filled polypropylene

Much of the research effort to date in the area of the mechanical behaviour of polymers has focused on the more commonly used mineral fillers for thermoplastic compounding; *viz.* talc, $CaCO_3$, and $Mg(OH)_2$, and on the role of chemical surface treatments on the filler-matrix interface. Interfacial debonding is very often the first step of failure in both advanced fibre composites and particulate-filled polymers. The effect of these surface treatments and coupling agents is not fully understood and contradicting reports of their effect on the composite properties have been published[39-41]. In this section the influence of fillers on the tensile yield properties of

polypropylene will be highlighted as this has bearing on the tribological performance of these materials; other mechanical properties will be discussed where pertinent.

Jancar and co-workers[42-46] have published extensive research on the mechanical behaviour of filled polypropylene, correlating experimental results with the theoretical models. In particular, the influence of filler particle shape on the elastic moduli and yield behaviour of $CaCO_3$ and $Mg(OH)_2$ composites has been studied with reference to the characteristics of the interfacial adhesion between the matrix and the filler particles. Untreated filled composites show greater values of E_{mod} than the surface-treated composites due to the larger extent of polypropylene immobilisation in the interphase layer and in filler agglomerates[42]. A difference between theoretical prediction and experimental data is observed for the needle-shaped $Mg(OH)_2$ fillers: this is attributed to a decrease in aspect ratio of the particles through mechanical destruction during compounding.

Analysis of yield stress behaviour shows that a stearic-acid surface treatment lowers the yield strength of the filled composites by lowering the extent of polypropylene immobilisation. This, in turn, leads to a decrease in the filler content for the ductile-to-brittle transition point. The theory proposed by Turcsanyi *et al.*[38] was found to account for the effects of filler-matrix interaction. By introducing carboxyl groups onto polypropylene through the addition of maleic anhydride, the interfacial adhesion could be enhanced. This has a positive effect on the yield stress up to limiting value of 0.162 wt% COOH. A transition in fracture behaviour is associated with this carboxyl concentration. Below this concentration the filled composites exhibit ductile failure while above 0.162 wt% they behave in a quasi-brittle mode[44]. Furthermore, it was noted that the addition of maleated-PP increases the thickness of the interphase layer in comparison to that produced by the stearic-acid treatment which contributes to the enhanced yield strengths[46]. This increase in interphase-layer thickness is found to be closely related to

the length of the carbon chain of the coupling agent. This theory is substantiated by Harper *et al.*[47] in their measurements of the relative influence of various fatty acid surface treatments on the mechanical properties of polyethylene.

Maiti and co-workers[48,49] studied the tensile and impact properties of talc- and $CaCO_3$ filled polypropylene in the range of 0 to 60 wt% filler content. The effect of a titanate coupling agent on the behaviour was analysed. In both cases a significant increase in elastic modulus with increasing filler content is attributed to the mechanical restraint imposed on the polypropylene matrix by the filler particles. At the maximum filler content, the increase in Young's Modulus for the talc and $CaCO_3$ composites is 2.6 and 2.0 times that of the unfilled polypropylene, respectively, indicating the influence of filler particle shape on the behaviour. The addition of the titanate coupling agent further improves the stiffness of the composites as a result of possible chemical bonding and enhanced interaction.

The addition of the mineral fillers to the polypropylene matrix decreases the elongation at break and the tensile yield strength of the composites. The addition of the titanate coupling agent to the fillers, produces opposite trends however, and it is proposed by the authors, Maiti *et al.*[48, 49], that the varying filler shape has some influence in this regard. The surface-treated talc composites show improved yield strength, whereas the surface-treated $CaCO_3$ composites exhibit inferior properties to the untreated samples. It was also noted that the inclusion of the fillers results in a decrease in the crystallinity of the composite, a factor which is of primary importance for improved strength properties[32].

Similar results of mechanical behaviour were found by Chacko and co-workers who studied the morphology and tensile behaviour of $CaCO_3$ filled polyethylenes[39,40]. The incorporation of a titanate coupling agent improves dispersion of the $CaCO_3$ within the polymer matrix. This results in a greater

reduction of the load-bearing area and hence a lower yield stress as compared to the untreated $CaCO_3$ composites.

Liu and Gilbert[41] studied the effect of the level of phosphate coating on the structure and properties of 40 wt% talc filled polypropylene. It is observed that the talc and phosphate coating has a nucleating effect on the polypropylene promoting crystallinity which is mirrored by increases in the tensile yield strength of the composites.

Several workers[50,51] have studied the influence of $CaCO_3$ fillers on the impact fracture behaviour and toughness of polypropylene. Dongming and co-workers[50], using the *J*-integral method showed that the addition of $CaCO_3$ improves the fracture toughness of polypropylene. This is attributed to the microductility of the polymer matrix ahead of the propagating crack tip, caused by interfacial debonding at the filler-matrix interface. Maximum improvement is noted for 20 wt% filler and the presence of a coupling agent has no significant effect.

Jancar *et al.*[51] observed similar results, with maximum fracture toughness measured at 0.12 volume fraction filler. Above this value, the reduction of effective cross-section due to the filler becomes the controlling parameter and the fracture toughness decreases.

There has been much interest in $Mg(OH)_2$ as a filler for thermoplastic polymers as it is an effective filler for enhanced flame retardancy. Unlike organo-halogen type fire retardants, $Mg(OH)_2$ is halogen- and acid free and thus the combustion products of PP-$Mg(OH)_2$ composites are neither corrosive nor toxic[52].

Miyata *et al.*[53] reported the influence of $Mg(OH)_2$ particle size and a sodium-stearate coating on the mechanical properties and burning characteristics of polypropylene composites. Incorporation of not less than 57 wt% $Mg(OH)_2$

ensured nonflammability, however considerable reductions in impact and tensile strength are incurred at these levels. Impact strength increases with filler content to a maximum at around 30 wt% but decreases beyond this level to be lower than that of the unfilled polypropylene at high filler contents. These workers[53] observed that an average filler particle size of 2 μm produced the optimum filler dispersion and mechanical and rheological properties. The sodium-stearate surface treatment enhances the compatibility of the filler and polypropylene with slight improvements in tensile strength noted.

Harper and Cook[54] confirmed the enhancement of tensile properties with the addition of both stearic-acid and oleic-acid surface treatments to 60 wt%-PP copolymer systems. Optimum tensile and flexural behaviour is attained at small filler particle size (1 μm), whereas improved impact performance is noted for the larger 4 μm filled composites.

The increasing use of mica as a reinforcing filler for thermoplastics is highlighted by Busigin and co-workers[55] and Jarvela and Jarvela[56]. Busigin *et al.* showed that mica-reinforced polypropylenes achieve similar reinforcing performance to equivalent talc and short glass fibre PP composites but with favourable economic benefits. Measured tensile and flexural properties of 40 wt% mica composites show that while the flexural modulus is dependent on the aspect ratio of the mica particles, the tensile strength is primarily influenced by the mica particle size and shows no correlation with aspect ratio. Optimum tensile strength properties are observed for the smallest mica particles.

Jarvela and Jarvela[56] conducted mechanical tests on a series of multicomponent filled polypropylene samples, using mica, wollastonite fibres, and glass beads as the respective fillers. The mica and wollastonite fillers show improved stiffness as expected due to the filler shape factor. A combination of the two fillers produces superior stiffness properties over

those attained by the respective individual filled composites. This effect is attributed to the relative size difference in the two fillers with the smaller wollastonite particles (10 μm) able to situate themselves between the larger (40 μm) oriented mica platelets, making the polypropylene matrix more rigid. Optimum tensile strength is also achieved with this PP-mica-wollastonite system.

2.4 THE WEAR OF POLYMERS

2.4.1 Introduction

Tribology is the science and technology of interacting surfaces in relative motion. The word 'tribology' is derived from the Greek word *tribos* meaning the 'science of rubbing'[57]. It is an interdisciplinary subject encompassing friction, wear and lubrication. This review will be primarily concerned with the aspect of wear.

The wear performance of a material is not easily predicted as it is not an intrinsic material property but is influenced by the wear system in which it functions[58]. A tribosystem, as illustrated in Figure 2.5, can be depicted as an interaction of several factors which all contribute to the overall wear behaviour. These factors are, firstly, the internal properties or microstructure of the two contacting materials which can either be single or multiphase; and, secondly, the external factors which take into account the active wear mechanisms, the operating wear environment, and the counterface surface properties[58,59].

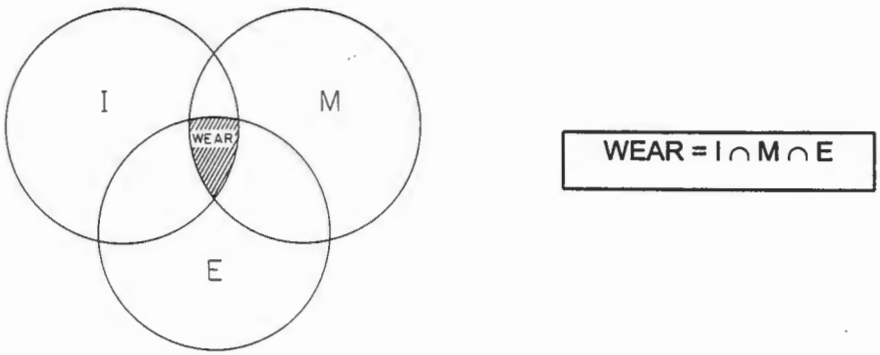

Figure 2.5: Wear as a system property. I = internal properties *i.e.* the microstructure of the polymer, M = the active wear mechanisms, E = external properties (operating conditions and counterface surface roughness). [After Friedrich[58]].

2.4.2 Wear mechanisms

Wear is defined as the progressive loss of material from the operating surface of a body occurring as a result of relative motion at the surface[(60)]. It can occur under conditions of rolling, sliding, rubbing, and impact of contacting surfaces. Evans and Lancaster[(61)] categorised four main groups of wear, *viz.* abrasion, adhesion, fatigue, and thermal/oxidative degradation. The difficulty in characterising wear in such broad terms is that in real situations failure does not occur via a single mechanism but through a combination of the various processes[(59)].

Briscoe[(62)] distinguishes two main classes of wear processes, namely cohesive wear and interfacial wear. Cohesive wear processes include those mechanisms which involve the dissipation of frictional work and its resultant damage in relatively large volumes adjacent to the contact interface through surface interaction. Abrasion and fatigue wear are typical of this process. The wear mechanism and the penetration of asperities is largely controlled by the cohesive strength or toughness of the polymer and wear rates can be correlated to bulk deformation experiments, such as uniaxial tensile tests.

Interfacial wear processes involve the dissipation of frictional work in much thinner regions at the contacting interface. The chemistry of the surfaces and the surface forces are the main influencing factors. Transfer or adhesive wear and chemical wear fall into this category.

A brief overview of adhesive and chemical wear will be given with a detailed review of the abrasive and fatigue wear mechanisms following.

2.4.2.1 Adhesive wear

When polymers slide repeatedly over themselves or very smooth metal counterfaces, adhesion or transfer wear becomes the dominant wear process. In these situations, bonding in the form of weak van der Waals forces, hydrogen, or chemical bonding can occur at the interface of the contacting surfaces. During sliding wear, the shear processes developed in the contact region cause rupture of the material. This rupture seldom occurs at the actual material interface but rather within the polymer itself. Thus a transfer layer of polymer builds-up on the counterface surface[62,63]. In semi-crystalline polymers like polypropylene, transfer fragments adhere to the smooth counterface as irregular films in the order of 0.1 to 1 μm thick and can lead to increased stress and wear[64]. Subsequent sliding motion will break up and remove this polymer transfer layer from the counterface as debris in the form of slivers, thin films, fibrils and aggregates[65]. The process continues as transfer layers are repeatedly deposited and removed and the polymer material is gradually worn away.

2.4.2.2 Chemical wear

In chemical/tribochemical wear the wear process is determined by the dynamic interactions between the material components and the environment. Chemical degradation is generally present in all wear processes, ranging from

mild chain scission to gross deformation of filled crosslinked resins under high loading. Furthermore, in coupled tribosystems, reaction products can cause increased wear and higher thermal conditions at the interface, leading to a change in the mechanical properties of the surface layer and a tendency for brittle fracture[60]. There is, however, doubt as to the precise role played by the chemical reactions in the overall wear process[62].

2.4.2.3 Abrasive and fatigue wear

Abrasive wear and fatigue wear are closely interrelated and the wear mode transition is generally governed by the material properties and the surface roughness of the contacting counterface. Fatigue wear deformation is largely elastic and is thus favoured in polymers with low moduli such as elastomers, as illustrated in Figure 2.6[61]. Fatigue wear is also important in harder polymers when sliding against smooth counterfaces with rounded asperities. Fatigue wear results in the formation of surface cracks which develop over a number of contact cycles. Particles of wear debris become removed by the growth and intersection of these cracks[66].

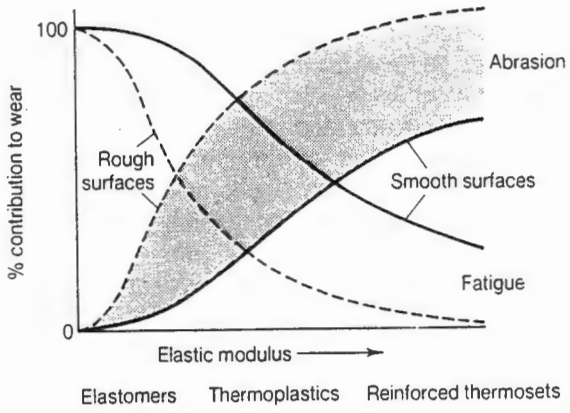

Figure 2.6: Schematic diagram showing the relationship between abrasive and fatigue wear in polymers. Fatigue wear is favoured for highly elastic polymers and against smooth counterfaces [After Evans and Lancaster[61]].

Abrasive wear can occur due to various mechanisms which cause surface destruction, such as cutting, scratching, and single and repeated plastic deformation[67]. The process is defined as "wear by displacement of material from surfaces in relative motion caused by the presence of hard protuberances, or by the presence of hard third body particles either between the surfaces or embedded in them"[68]. Thus an essential condition for abrasive wear is that the surface of the abrasive material must be harder than that of the wearing material.

Abrasive wear can be further characterised by either two-body or three-body wear as shown in Figure 2.7[66,69]. Two-body wear is caused by hard protuberances fixed on the abrasive counterface, encountered for instance when polymers slide against rough metal surfaces or abrasive papers[70]. In three-body wear the hard particles are loose and free to roll and slide between the two surfaces in motion. Wear rates for three-body abrasion are generally lower than those due to two-body abrasion[66].

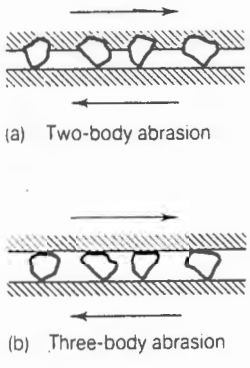

Figure 2.7: Illustration of the differences between (a) two-body abrasion and (b) three-body abrasion [After Hutchings[66]].

For rigid polymers, an ideal case of two-body abrasion can be considered in which a hard conical indentor penetrates and ploughs a groove in a softer material, removing material by shearing or cutting[70]. If the deformation is predominantly plastic it can be shown that[62,70]:

$$z = k\,(W / H)\tan\theta \qquad (2.8)$$

where:

H = indentation hardness

W = normal load

z = volume of material removed per unit sliding distance

k = the probability of the formation of a wear particle

θ = base angle of the cone, such that:

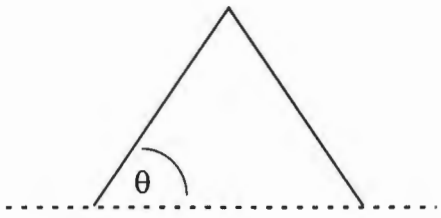

Lancaster[70] shows that for a simple cone model experiment, an elastic-plastic transition exists in the deformation mode of polymers. A soft metal (tin) and an amorphous polymer (PMMA) are compared with respect to the volume of material displaced as a function of the cone base angle (Figure 2.8).

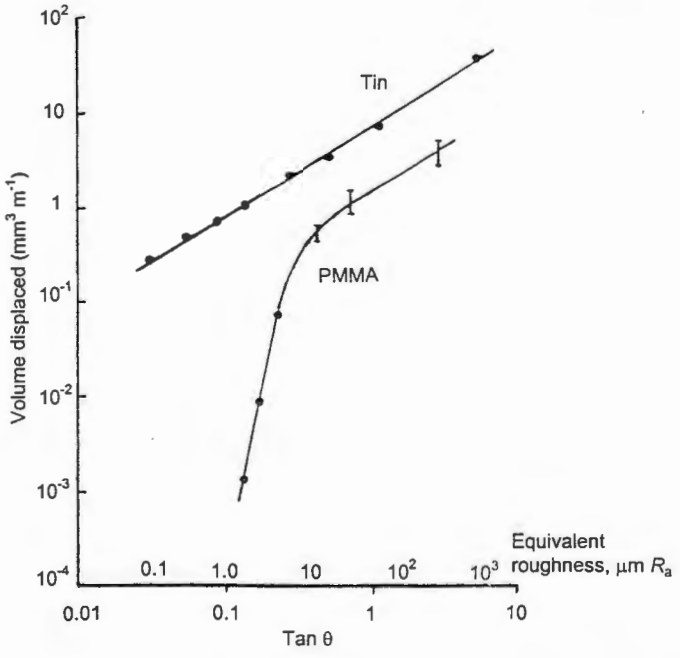

Figure 2.8: The relationship between volume of material displaced per unit sliding distance and the base angle of a conical indentor. [After Lancaster[70]].

With the soft metal, plastic deformation occurs at all cone angles. The PMMA, however, only shows a linear relationship between volume loss and tan θ when θ exceeds 30°. Thus with polymers, plastic deformation only becomes the dominant wear mode when the indentor is very sharp.

Further models for this elastic-plastic transition in polymers were given by Halliday[in ref. 61,70]:

$$\tan \theta = k\,(H / E)\,(1 - \nu^2) \qquad (2.9)$$

where: ν = Poisson's ratio

k = 0.8 for the onset of plasticity

k = 2 for full plasticity

and Greenwood and Williamson[71], who introduced the concept of the 'plasticity index' given by:

$$\psi = E / H\,(\delta / \beta)^{0.5} \qquad (2.10)$$

where: δ = standard deviation of the asperity heights

β = average radius of curvature of the asperities

Plastic deformation occurs when $\psi \geq 1$.

The cone model experiment can be extrapolated to show the equivalent surface roughness of a counterface corresponding to different cone angles. Evans and Lancaster show that plastic deformation will only occur when R_a = 12 μm[61].

2.4.3 Theories for abrasive wear

In abrasive wear, the product $\sigma\varepsilon$, which is essentially the area under the stress-strain curve, appears to become an important parameter influencing the wear behaviour prediction. Ratner *et al.*[72] developed a theory based on the single traversal of a polymer over a rough steel surface of the form:

$$W = k\mu / H\sigma\varepsilon \qquad (2.11)$$

This relationship is based on the consideration that there are three stages in the formation of a wear particle:

i) plastic deformation of the surface to an area of contact determined by the indentation hardness, H;
ii) relative motion opposed by the frictional force; and
iii) rupture of the polymer at the contact points involving an amount of work equal to the integral of the stress-strain relationship, which can be approximated by the product $\sigma\varepsilon$, where σ and ε are the fracture stress and fracture strain of the polymer respectively.

Lancaster[73] shows that for similar single traversals over steel counterfaces (R_a = 1.2 μm), a better relationship exists when only $1/\sigma\varepsilon$ is considered, as the hardness of polymers is more dependent on the elastic than the plastic deformation. This is illustrated in Figure 2.9 for eighteen engineering polymers.

Later work by Briscoe *et al.*[74] show that a better correlation exists when the wear rate is plotted against $1/\sigma^2\varepsilon$, where the additional stress term is included as a rough approximation to take into account the effect of surface hardness.

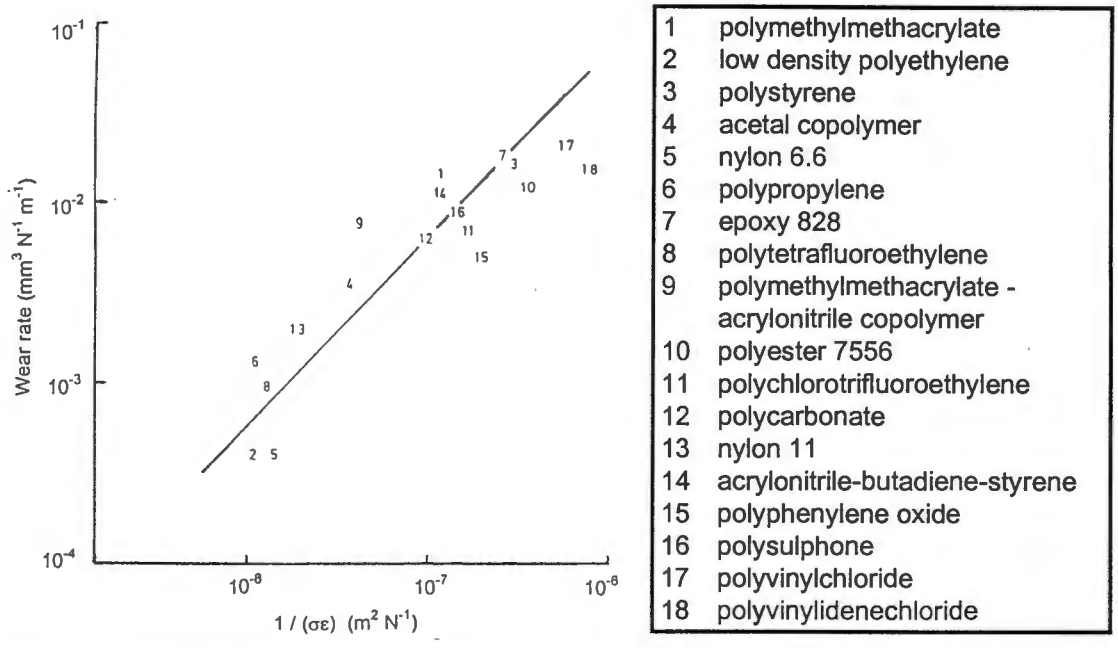

Figure 2.9: The Lancaster correlation between $1/\sigma\varepsilon$ and wear rate during single traversals of polymers over a rough steel counterface (R_a = 1.2 μm). The polymers in the inset refer to the numbers in the figure. [After Lancaster[69]].

The product $\sigma\varepsilon$ is related to the area under a stress-strain curve and hence is a measure of the toughness of the material. Ratner[(in 70)] attempted to correlate the abrasive wear performance with the notched impact strength of several polymers as the localised strain rates involved in the wear process approach those experienced during an impact test. These strain rates may be as high as 10^4 s^{-1}. The tensile tests from which $\sigma\varepsilon$ values are determined are carried out at typical strain rates of around 10^{-4} s^{-1}. Ratner's results proved inconclusive and exhibited variable scatter.

Giltrow[(75)] has shown that a correlation exists between the rate of abrasive wear of thermoplastic polymers and their cohesive energies. The cohesive energy is defined as the energy required to overcome all intermolecular contacts and thus refers to the dispersion forces between the polymer chains. The cohesive energy is calculated on the basis of the polymer's chemical structure, thus allowing the wear properties to be related to the chemical constitution of the polymer. Giltrow conducted abrasion tests of several

thermoplastic polymers against 100 and 600 grit SiC abrasive paper. A non-linear relationship is observed in which the abrasive wear rate for the 100 grit paper is shown to be inversely proportional to the square root of the cohesive energy of each polymer, as shown in Figure 2.10. The non-linearity of the relationship is attributed to the high rates of strain present during abrasive wear thus reducing the molecular mobility. Furthermore, the complex nature of the polymers influenced the results with no account made for variations in molecular weight, crystallinity, or chain branching of the respective polymers.

Against the 600 grit SiC paper, this cohesive energy correlation is no longer as defined, confirming Lancaster's view that very rough counterfaces are required to ensure that plastic deformation and microcutting are the dominant wear processes present[61].

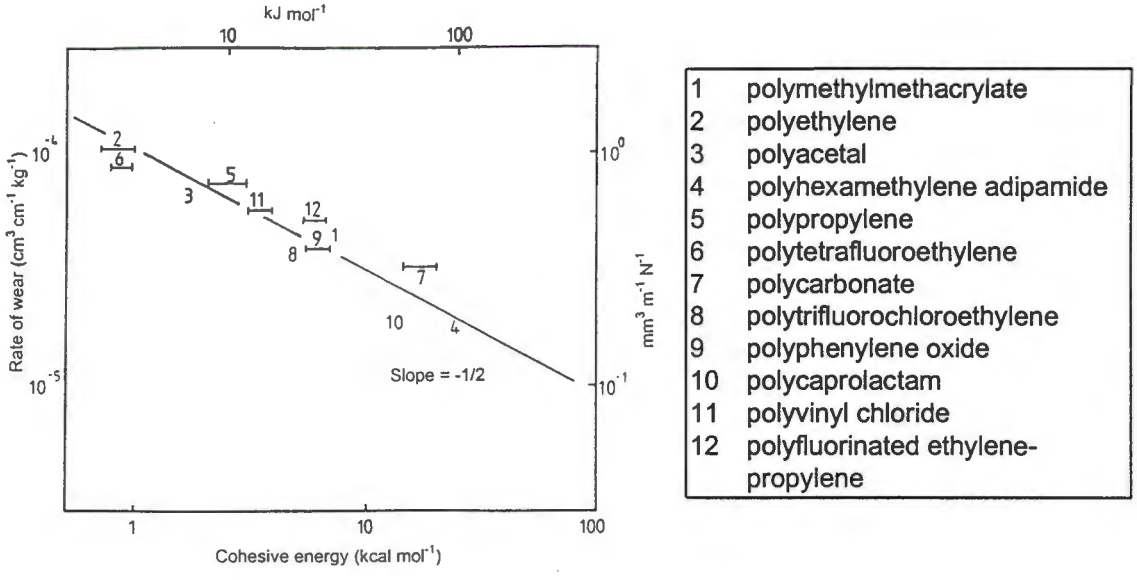

Figure 2.10: The relationship between abrasive wear and the cohesive energy of thermoplastic polymers. The polymers in the inset refer to the numbers in the figure. [After Giltrow[75]].

Based on Ratner's model, Vaziri and co-workers[76] studied the wear of several polymers against SiC abrasive papers, polished steel, and like polymer counterfaces. For wear against 600 and 800 grit SiC papers, correlation with Ratner's theory is observed though a better fit is obtained when using μ_p, the ploughing component of friction, rather than μ, the measured coefficient of friction in the Ratner equation. The model of Vaziri *et al.* did show some anomalies with PMMA deviating from this linear relationship. This is attributed to the properties of the polymer itself and, in particular, the low elongation to failure of PMMA during tensile testing.

Czichos[77] reported the results of multipass testing of a range of polymers against a steel counterface (R_a = 1 μm). A correlation between the wear rate and materials parameters such as the surface energy or the yield stress is established. This correlation is based on the assumption that the wear of the polymers is abrasive in nature. Santner and Czichos[78] noted from scanning electron microscopy (SEM) studies of worn polymer surfaces that surface roughness values of 0.8 to 1.0 μm of a hard sliding counterface will induce an abrasive wear process for unfilled polymers. The formation of a wear-debris particle can thus be related to the interfacial stress and the rupture stress for a given polymer.

Further correlation between the tribological and mechanical properties of polymers is observed by Bohm *et al.*[79]. An inverse relationship between wear resistance and hardness is found. Microtoughness, as indicated by the elongation to failure, is shown to be the dominant factor in abrasive and erosive wear resistance. However, interactions at a molecular level, such as molecular weight, crystallinity, and chain mobility, are considered influential.

Thorp[80] investigated the abrasive wear of commercial polymer-based bearing materials under multipass conditions. In contrast to single-pass testing, where the wear is solely dependent on the mechanical properties of

the polymer, in multipass testing the transfer film properties of the polymer become significant leading to the relationship:

$$\text{Average weight loss} = Dt^{c} \qquad (2.12)$$

where D and c are functions of the wear path diameter, and c is related to the film transfer capability of the polymer, and t = time.

2.4.4 Factors affecting the abrasive wear rate

2.4.4.1 Effect of operating parameters

Friedrich[58] performed tests to analyse the effect of load and velocity on abrasive wear behaviour. He shows that for a glass-fibre (GF) filled polyethyleneterephthalate (PET) single-pass tribosystem, an increase in load (contact pressure) results in a linear increase in wear rate. This result is in accordance with the simple Archard equation developed for abrasive wear[81]:

$$\text{Wear rate} = k\,W / H \qquad (2.13)$$

Similar relationships were obtained by Nathan and Jones[82] while investigating the role of operating parameters on the abrasion of soft metals[82], and by Misra and Finnie[83].

For the same GF-PET system Friedrich shows that at a given load, the dimensionless abrasive wear rate is independent of velocity over the range 100 to 500 mm min^{-1}. Again, good correlation is found between these results and those reported by Nathan and Jones for soft metals[82]. Cortellucci *et al.*[84] show that although the abrasive wear rate is independent of velocity, it is influenced by the properties of the polymer material itself. Three polymers differing in physical characteristics, *viz.* polytetrafluoroethylene (PTFE),

polymethylmethacrylate (PMMA) and a phenolic resin, were subjected to abrasion tests at two cutting rates. Whereas the PTFE and phenolic polymers show wear rates relatively unaffected by the abrasive cutting rate, noticeable differences are observed for the PMMA polymer. Increased wear rates noted at the higher cutting speeds are attributed to localised heating and melt flow as the glass transition temperature of the PMMA is exceeded.

2.4.4.2 Effect of counterface roughness and abrasive particle size

It is known that the wear rates of polymers are greatly influenced by the properties of the counterface and specifically the surface roughness. Hollander and Lancaster[85] obtained a relationship between the wear in a single pass abrasion test over an abraded steel counterface, and the ratio δ/β, where δ is the standard deviation of heights of the asperities, and β is the average radius of curvature of asperities. Tabor[86] has shown that the asperity slope may be estimated by the relationship:

$$\tan\theta \approx (\delta / 2\beta)^{0.5} \qquad (2.14)$$

Thus the wear rate increases with an increase in the calculated mean slope, as shown in Figure 2.11.

Lancaster[61,70] describes abrasive wear as the combination of the two extreme processes of cutting and fatigue. Cutting would be expected of rough surfaces with sharp asperities and fatigue of rough surfaces with rounded asperities.

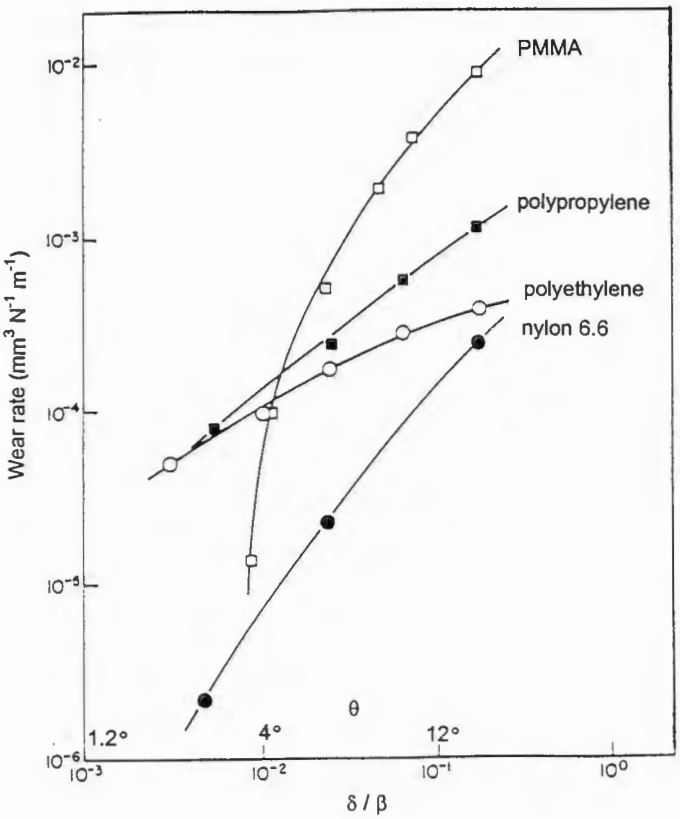

Figure 2.11: Single-pass wear rates of various polymers plotted against δ/β, showing a pronounced increase in wear rates with the calculated mean asperity slope, θ. The asperity slope is estimated from the relationship $\theta \approx (\delta / 2\beta)^{0.5}$. [After Briscoe[62], Tabor[86]].

In Figure 2.12 the wear rates of several polymers are charted as a function of counterface roughness in the transition range from fatigue to cutting wear. It is clear that the wear rates are very sensitive to changes in R_a. Moreover, there is a noticeable difference on the wear rate dependence on R_a for brittle, amorphous polymers like polystyrene (PS) and PMMA, than for the ductile polymers polyethylene (PE), polypropylene (PP), and PTFE. Lancaster's results were drawn from tests conducted during single-pass abrasion tests against steel counterfaces. In abrasion against SiC or Al_2O_3 abrasive papers the surface roughness' encountered are significantly higher. Although exact measurement of the roughness of these papers is difficult, estimated results show that $R_a \approx 6$ μm and $R_a \approx 38$ μm for SiC 600 grit and 100 grit papers, respectively[(61)].

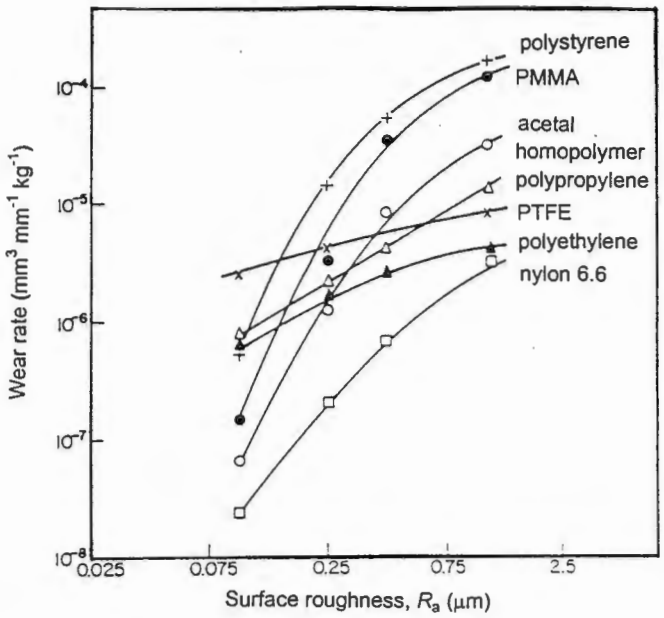

Figure 2.12: Abrasive wear rate as a function of surface roughness for various polymers in single-pass abrasive tests. The wear rates of the brittle, amorphous polymers show a marked dependence on the surface roughness in comparison to the more ductile polymers. [After Lancaster[69]].

Several authors have researched the effects of abrasive particle size on the wear behaviour of steels and soft metals[87-92]. Since many of the trends observed in these situations can be mirrored for polymeric wear, some of the pertinent findings are discussed here.

One of the interesting points to note is the existence of a 'critical diameter' of the abrasive particle. Above this diameter the wear rate is either independent of the abrasive particle size or increases marginally; below this value, the wear rate falls off rapidly with decreasing abrasive particle size. Larsen-Badse[87] reports a critical diameter value of 45 to 50 μm for materials such as NaCl, Pb, Sn, Zn, and Al, while Nathan and Jones[82] found a higher value of ~70 μm for tests performed at higher cutting speeds. Further work on copper shows that the critical particle size is proportional to the surface area of the specimen. This is attributed to the attrition of the abrasive paper by the copper specimen itself[88].

Date and Malkin[89] reported on multipass test results for metals and postulate that a lack of plastic contact with the specimen of the smaller abrasive particle sizes contributes to the decreased wear rates.

Misra and Finnie[83] observed that the particle-size effect for metals is not only prevalent for two-body abrasion but is also observed in both three-body abrasion and erosive studies. The particle size effect is illustrated in Figure 2.13. This effect is related to the surface properties of the material (in this case copper) and specifically to the presence of a higher flow stress in the surface layer in comparison to the bulk material.

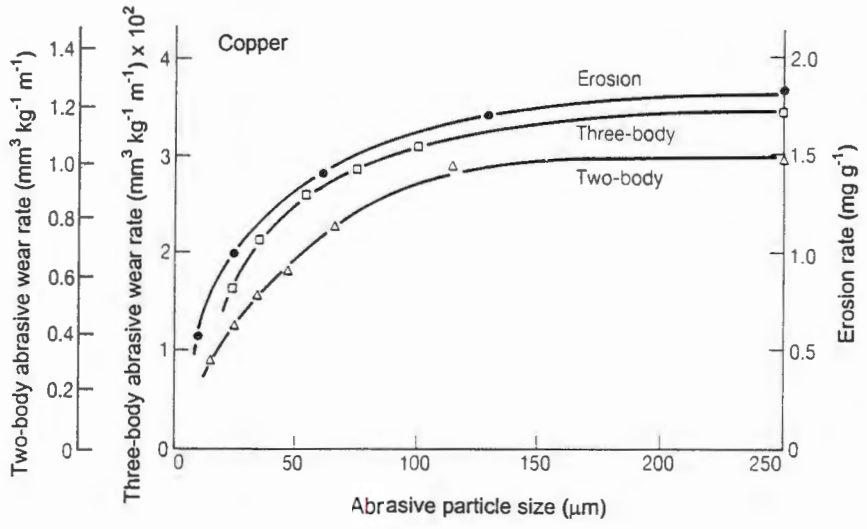

Figure 2.13: Wear rates of copper under conditions of two-body and three-body abrasion and erosion due to SiC particles of different sizes. [After Misra and Finnie[83]].

Friedrich and Cyffka[90] have reported on the single-pass abrasion of glass bead- and glass fibre-filled PET composites against abrasive papers of varying grit size and hardness. A linear increase in wear rate with increasing abrasive particle size over the range 7 to 100 μm is observed for GF-PET composites. No critical diameter is noted. The wear rates are found to be influenced by both the particle distribution densities of the respective abrasive counterfaces and the relative hardness of the different abrasives. Increased

wear rates observed for the harder abrasive particles are attributed to the increased number of cracking events of the brittle fillers.

Roberts and Chang[91] measured the single- and multipass wear rates of nylon (PA6,6) and polycarbonate (PC) against SiC abrasive particles in the size range 6 to 50 μm. The trend of increasing wear rate with increasing particle size is confirmed. A transition in wear mode, observed by SEM analysis of the worn polymer surfaces, was found to be associated with an average particle size of 10 μm. Roberts and Chang formulated an empirical relationship of the form:

$$\text{Wear rate} = (AP - B)^{0.2} \qquad (2.15)$$

where: P = particle size

A, B = constants

which holds true for abrasion in the particle size range from 6 to 40 μm.

2.4.4.3 Effect of fillers on the tribological behaviour of polymers

Most polymers used in commercial applications incorporate additives, fillers, and reinforcements, not only to improve the mechanical and thermal properties but also for enhanced processability and economic cost benefits[31,92]. Additives can be solid or liquid materials and are used primarily as stabilisers, UV absorbers, colourants, and lubricants.

Fibrous fillers, such as glass fibre and carbon fibre, are usually added to polymers for reinforcing effects while particulate inorganic fillers have been shown to modify properties such as stiffness, heat resistance, and thermal

stability. Metal powders are often used to improve thermal and electrical properties.

Much of the open literature has focused on the role of fillers incorporated into commercial polymer-based bearing materials, for instance, PTFE, high density polyethylene (HDPE), acetals (POM), and nylons[80,93-96]. Although these fillers can improve the mechanical properties of polymer significantly, it is not valid to assume that the tribological properties will be similarly influenced. In sliding wear applications, fillers such as metal powders (CuO, Pb_3O_4) can reduce wear by enhancing the adhesion of the polymer transfer layer to the counterface through chemical interactions. In contrast, other fillers, such as short glass fibres, can damage the counterface and can lead to an increase in wear rates[63,93].

Parameters such as filler content, aspect ratio, and filler size are known to be important, however the mechanism of filler action is not fully understood. The variability of polymer-filler interactions necessitates the need to investigate specific polymer-filler coupled systems and their predicted wear environment prior to application[93].

2.4.4.3.1 Fillers in abrasive wear

Under abrasive wear conditions where microcutting and ploughing mechanisms prevail, the effect of fillers and reinforcements on the wear rate is not always predictable. Fibre-reinforced composites have been the major focus of research by several authors[97-100]. Despite the increase in breaking strength σ, associated with the incorporated fibre content, the product $\sigma\varepsilon$ for a composite may be lower than the parent polymer due to the reduction in elongation at fracture.

Friedrich[58] has reported that the wear of thermoplastics is not improved by adding short fibres if the wear mechanism is highly abrasive in nature. In

contrast, continuous fibre reinforcement such as glass, carbon or aramid fibre, has proved beneficial in some abrasive wear conditions. However, the effective improvement in wear rate is strongly dependent on both the fibre orientation within the polymer matrix, and the specific polymer-fibre system[97-99].

There is comparatively less known about the role of particulate fillers in abrasive wear. Bijwe *et al.*[100] evaluated and compared MoS_2, graphite, bronze powder, and glass fibre as fillers for several thermoplastics under multipass abrasive conditions. The particulate fillers were more detrimental to the abrasive wear performance than the glass-fibre additions. The abrasive wear rates are again found to be specific to a filler-polymer couple.

2.4.5 Scratch resistance

2.4.5.1 Introduction

Tribology methodology seeks to simulate as closely as possible the service conditions that a material will encounter and to analyse the wear mechanisms accordingly.

The methods of measuring the abrasive wear performance of materials against rough counterfaces are well established. Pin-on-belt and pin-on-disc systems are most commonly used for evaluating the single-pass and multipass wear behaviour. The characterisation of scratch resistance, which can be viewed as a form of mild abrasive wear, is less well defined. This particular wear mechanism is of specific importance in applications where surface properties and visual appearance are key requirements.

2.4.5.2 Scratch testing

The material property of scratch resistance has received attention recently, most notably in the areas of protective coatings, transparent plastics, and the textured surfaces of interior car trim[101-103]. The ability of a material to scratch another originated as the basis for the Mohs scale of hardness[104]. Hardness can be defined as the ability of a material to resist indentation or abrasion by other bodies. Thus scratch resistance is often viewed as a controlled form of abrasion and a means of ranking materials as to their likely abrasion resistance in service[105]. In practice, the conditions encountered in typical scratch tests are far more severe than those in service and thus correlation is difficult. More often, scratch tests are used as qualitative techniques to compare the performances of relative materials, however they can give some indication of the wear mechanisms occurring. In particular, single-point scratch tests are used for modelling the effects of changing operating parameters such as load, velocity, and angle of attack in abrasive and erosive systems which can lead to transitions in the wear rates and mechanisms[106,107]. These transitions are easily represented in 'wear maps'. A typical wear map is shown in Figure 2.14, illustrating the wear transitions occurring for PMMA as a function of velocity and abrasive particle angle.

The establishment of an accepted standard qualitative scratch test for polymeric materials has proved difficult. The characterisation of scratch resistance has led to the development of specific tests, with different procedures, often for similar end-use applications. In the automotive industry for instance, scratch testing methods vary from polished spherical styli (1 mm to 7 mm diameter), to a row of 10 needle points, to wetted strips of specified abrasive paper[108-110]. Furthermore, methods of assessing the scratch damage are equally diverse. Image analysis is often used, however other methods include qualitative visual inspection and ranking and assessment of colour change or contrast[108,111]. In the case of transparent plastics and glossy paint films where good optical properties are essential, several

methods have been standardised which involve measurement of the haze change or specular gloss of the surface[112-115].

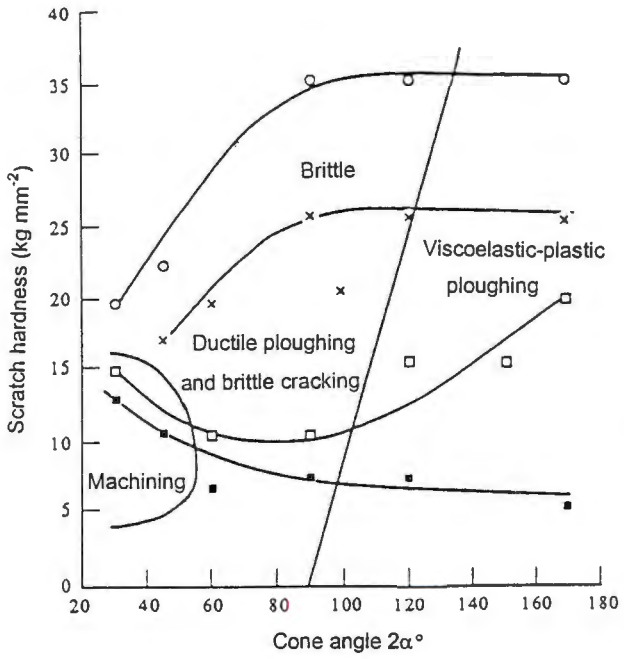

Figure 2.14: Typical wear map illustrating wear transitions for PMMA as a function of the included cone angle and scratch velocity. Scratch velocities are (m s^{-1}): ■ 1.2 x 10^{-7}, □ 2.1 x 10^{-6}, O 4.2 x 10^{-5}, × 4.2 x 10^{-4}. [After Briscoe *et al.*[107]].

2.4.5.3 Theory of single-point scratch testing

Early research in static single-point indentation techniques focused on brittle materials in an attempt to understand the initiation and propagation of microcracks and the associated stress fields in the material[116]. Subsequent studies expanded this concept to analyse the mechanisms of crack propagation beneath a moving sharp indentor[117-118]. The principles of indentation fracture and the importance of the stress systems occurring under sliding indentation experiments are paramount to understanding tribological processes such as abrasion, erosion, and machining.

Recently the scope of research has been extended to focus on rigid plastic solids and elastic-plastic deformation. Several analytical models have been

proposed to evaluate the point-contact deformation processes. Furthermore, the concept of scratch hardness has been developed and compared to standard indentation hardness values to understand the interrelationship between static- and dynamic-point loading[105,119,120].

Briscoe *et al.*[107] analysed the concept of scratch hardness under plastic and viscoelastic-plastic conditions using conical steel indentors with PMMA as the plastic solid. The indentation responses are shown in Figure 2.15. The effective normal hardness (static loading), H_n, can be defined as:

$$H_n = \text{load} / \text{projected contact area}$$

$$H_n = W / \pi(h \tan \alpha)^2 \qquad (2.16)$$

where: W = load on the indentor

h = indentation depth

α = included half-angle of cone, such that

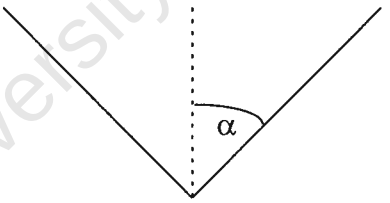

The scratch hardness can be defined in a similar manner, however the response of a plastic and viscoelastic-plastic material show some variation (Figures 2.15b,c).

In the case of a plastic response, as the indentor moves across the surface it will sink further into the material as a result of the loss of load-bearing capacity of the rear face of the indentor. The full load will thus be supported by the front face of the conical indentor. In this plastic condition, no recovery occurs in the width of the scratch track.

For the viscoelastic-plastic response to indentation, material recovery occurs in the depth of the groove behind the indentor with little change occurring in the width of the scratch track. Thus the rear face of the indentor is able to support part of the applied normal load. The sliding contact area, A_s, can be approximated to:

$$A_s = \pi d_s^2 / 4 \qquad (2.17)$$

where: d_s = the measured width of the scratch track

Thus by analogy with the static indentation hardness:

$$H_s = 4W / \pi d_s^2 \qquad \text{(viscoelastic-plastic response)} \qquad (2.18a)$$

and $$H_s = 8W / \pi d_s^2 \qquad \text{(plastic response)} \qquad (2.18b)$$

A general response for scratch hardness can be given in the form:

$$H_s = x\, 4W / \pi d_s^2 \qquad (2.19)$$

where: $x = 2$ for plastic
and $1 < x < 2$ for viscoelastic-plastic and is dependent on the material.

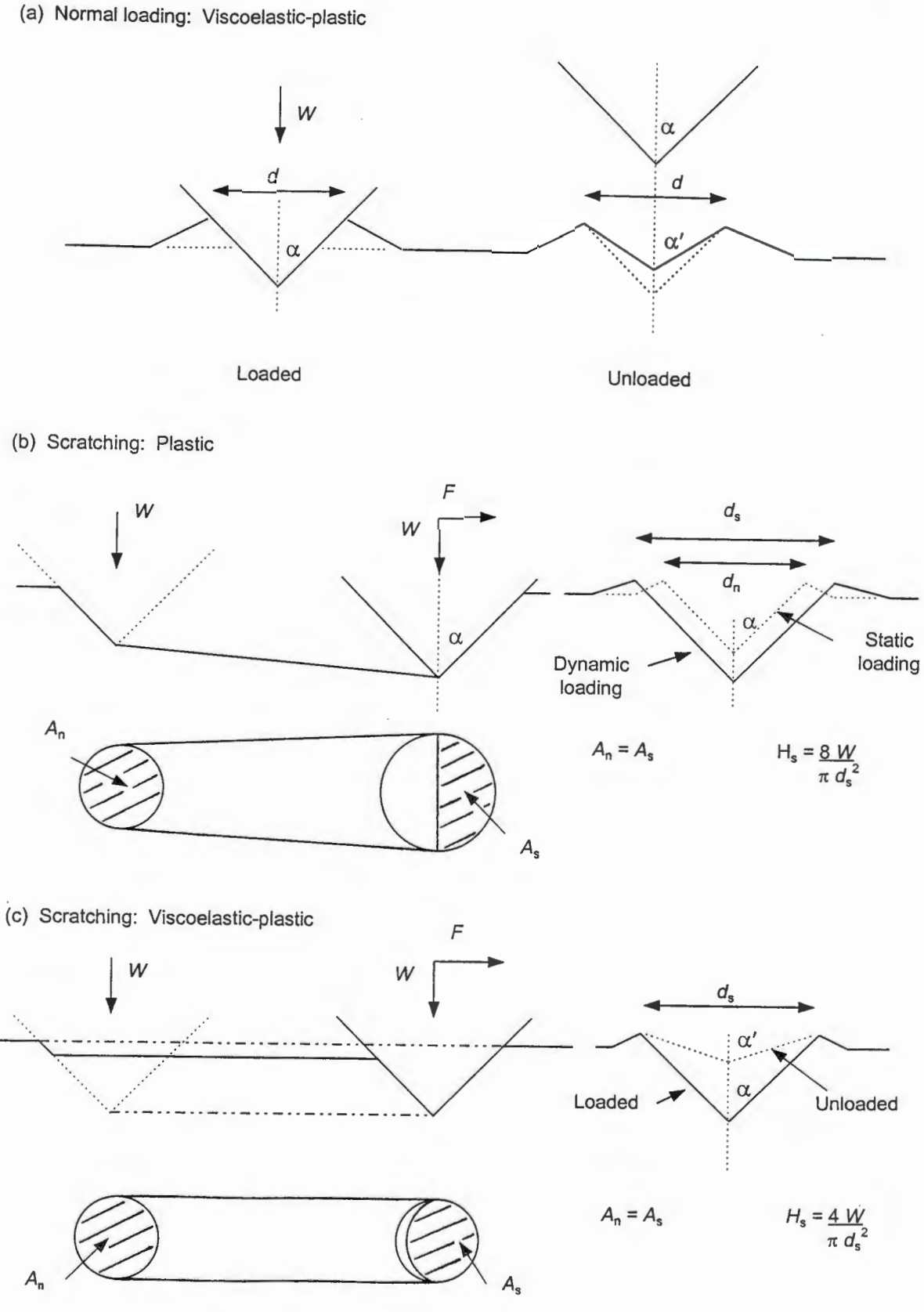

Figure 2.15: Schematic diagram showing the material response to normal hardness loading and scratch hardness loading under a moving indentor. Responses for both a plastic and a viscoelastic-plastic solid are illustrated. [After Briscoe *et al.*[107]].

2.4.5.4 Analysis of polymer scratch testing

Several authors have reported results of the scratch testing of polymeric materials. The common conclusion from these works is that for a specific polymer, one or more transition points exist for damage by different modes to occur.

Bethune[121] studied the material response of glassy polymers to scratch tests using steel ball-bearing indentors. At low applied loads no visible permanent damage to the polymer surface is observed. At higher loads, scratch tracks for polystyrene and PMMA are characterised by a series of parallel cracks oriented concavely to the direction of traversal. For polystyrene, the critical load for damage to occur was found to be proportional to the radius of the indentor.

Ni and Le Faou[122] confirmed the damage transitions occurring in polymers and classified the observed scratch morphologies into four regimes according to the main deformation mechanisms, *viz.*, surface shear yielding, surface cracking, subsurface yielding, and delamination. Combinations thereof can also occur. Furthermore, parameters such as scratching velocity, surface lubrication, and the geometry of the indentor influence the onset of wear damage transitions. These conclusions are in agreement with those of other authors[107,119].

Briscoe *et al.*'s[107] work on the scratch hardness and behaviour of PMMA highlights the elastic-to-plastic and brittle-to-ductile transitions in wear mechanisms. A critical indentor angle is found to occur for brittle debris chip formation.

Denape *et al.*[103] studied the scratch resistance of transparent polymers used in optical applications and evaluated several coating formulations for optimum performance. Wear and scratch damage was measured on a pin-on-disc

system and assessed with 3-D surface profilometry and SEM / optical microscopy observation. Three stages of surface damage are reported, *viz*., damage initiation (surface cracking) without material loss, particle detachment, and debris circulation and increased wear track depths. Colloidal silica coatings applied by a dipping technique are found to offer the optimum scratch resistance.

CHAPTER 3

MATERIALS AND EXPERIMENTAL APPROACH

3.1 MATERIALS

3.1.1 Polymers

The polymeric materials investigated in this study were three grades of homopolymer isotactic polypropylene (iPP), classified as Sasolen S1100L, Sasolen S1147H, and Novolen 1040K. The Sasolen grades were obtained from the supplier, Polifin Limited, South Africa, while the Novolen grade was obtained from BASF, Germany. The nomenclature of the three polymers refers to the additive content and melt flow index of each grade. The physical and mechanical properties of the materials, as supplied by the producer, appear in Table 3.1.

Table 3.1: Physical and mechanical properties of the three base polypropylene grades, as supplied by the producer.

		S1100L	S1147H	1040K
Physical property	Units			
Mass density	g cm^{-3}	0.908	0.91	0.91
Melting point	°C	162	162	165
Melt flow index	g / 10 min	5	2	3.5
Mechanical properties at 23 °C				
Tensile strength at yield	MPa	34	34	38
Elongation to break	%	> 100	> 50	20
Elastic modulus	GPa	1.4	1.5	1.9
Izod impact (notched)	kJ m^{-2}	3.0	8	
Ball indentation hardness	N mm^{-2}	76		100

In addition, several polymers were used in this study for comparative purposes. These are polymethylmethacrylate (PMMA), polycarbonate (PC), acrylonitrile-butadiene-styrene (ABS), and high density polyethylene (HDPE).

3.1.2 Fillers

In this study the effects of six filler types on the properties of polypropylene were studied. The fillers were two grades of talc, $CaCO_3$, $BaSO_4$, two different size grades of wollastonite, fly ash, and a china clay filler. The *Steaplast* talc and the *Polarite* china clay fillers are surface-treated materials; a silane coupling agent being added to the *Steaplast* talc filler, and the *Polarite* china clay modified with a polymer coating and a dispersion aid. The fillers are characterised in Table 3.2. These fillers were chosen as being typical mineral fillers used in thermoplastic compounding. The chosen materials also encompass a wide range of physical properties *i.e.* particle shape, size, and density. Details of the suppliers and further properties of each filler material are given in Appendix A.

Table 3.2: Physical properties of the mineral fillers.

	Physical property					
Filler	**Approximate chemical composition**	**Shape**	**Size (D50) (μm)**	**Density (g cm^{-3})**	**Hardness (Mohs)**	**Colour**
talc	(SiO_2 - MgO)	platelet	10	2.8	1	white
Steaplast talc	(SiO_2 - MgO)	platelet	2	2.8	1	white
$CaCO_3$	-	rhombehedral	5	2.7	3	white
$BaSO_4$	-	tabular	0.7	4.4	2.5 - 3.5	white
wollastonite	(CaO - SiO_2)	fibrous	~15; ~150	2.9	4.5	grey
fly ash	(Al_2O_3 - SiO_2)	spherical	~ 10	2.3	5	grey
china clay	(SiO_2 - Al_2O_3)	platelet	~ 4	2.5		natural

3.2 SAMPLE PREPARATION

3.2.1 Extrusion

The polypropylene composites were compounded and pelletised using a standard thermoplastic screw configuration on a Berstoff ZE-A twin screw extruder at the extrusion facility at MATTEK, Council for Scientific and Industrial Research, Pretoria. The extruder had a screw diameter of 33 mm and operated at speed of 200 rpm, producing an average polymer output of 40 to 50 kg h^{-1}. An operating temperature of 230 °C was kept constant along the length of the screw barrel through nine independent heaters. Table 3.3 details the range of polymer composite blends made from each base polypropylene grade and the respective fillers. The unfilled PP granules were also re-extruded so as to have the same thermal history as the blended pellets.

3.2.2 Injection moulding

The pelletised samples were injection moulded into standard mechanical test pieces at Plastamid (Pty) Ltd, Cape Town using an Arburg Allrounder (Model 221-75-350) moulder. Operating conditions are shown in Table 3.4. Prior to moulding each blend material was air dried at 70 to 100 °C to reduce the moisture content of the pellets to < 0.15 %.

Table 3.3: Experimental matrix showing the range of composite blends compounded from the base polypropylene grades and the respective fillers. The Novolen 1040K grade was tested in the unfilled condition only.

	Base polypropylene	
Filler	**S 1100L**	**S 1147H**
	Weight % filler in composite	
talc	10 20 40 60	
$CaCO_3$	10 20 30 40 50 60	
$BaSO_4$	10 20 30 40 50 60	
Steaplast talc (surface treated)	10 20 40	10 20 40
wollastonite fine / coarse grades (~ 15μm / ~ 150μm)	10 20 40	10 20 40
fly ash	10 20 40 60	
china clay (surface treated)	10 20 40	10 20 40

Table 3.4: Operating parameters for the injection moulding of the polypropylene test samples.

barrel temperature	210 °C
mould temperature	35 °C
screw speed	370 rpm
injection time	2.5 s
holding time	3.5 s
cooling time	25 s

3.3 SAMPLE ORIENTATION

3.3.1 Abrasive wear test sample

Samples were machined from the injection moulded flexural test bar as shown in Figure 3.1. The test face of each sample was machined with a tool steel fly-cutter to an average surface roughness of 0.70 μm and 1.10 μm in the parallel and transverse machining directions, respectively.

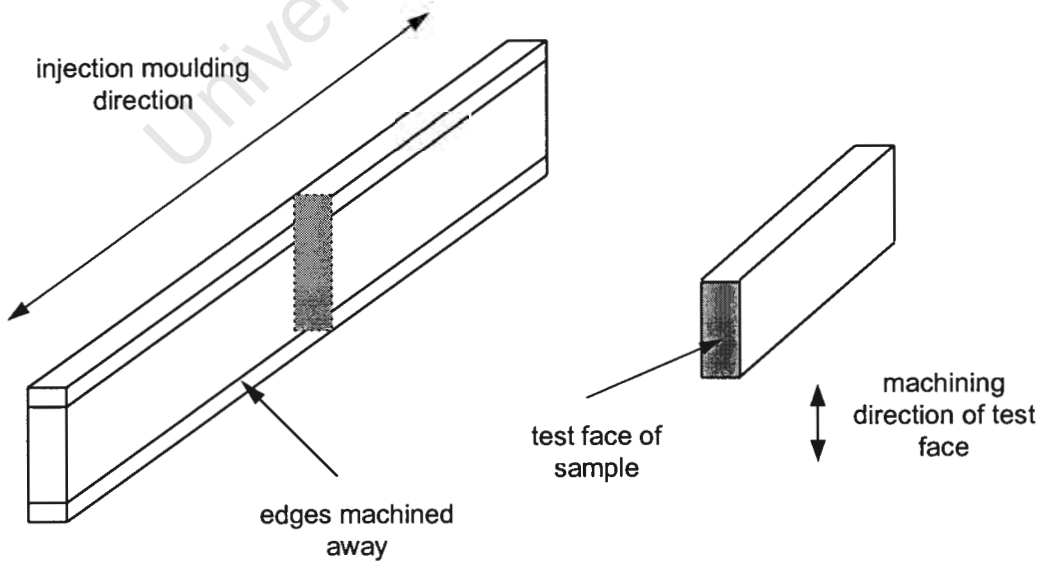

Figure 3.1: Schematic showing orientation of abrasive test sample cut from an injection moulded flexural test bar.

3.3.2 Scratch test sample

Test samples for the single-point scratch test and the abrasive scrub test were cut from the injection moulded dumbbell-shaped tensile test bar as shown in Figure 3.2.

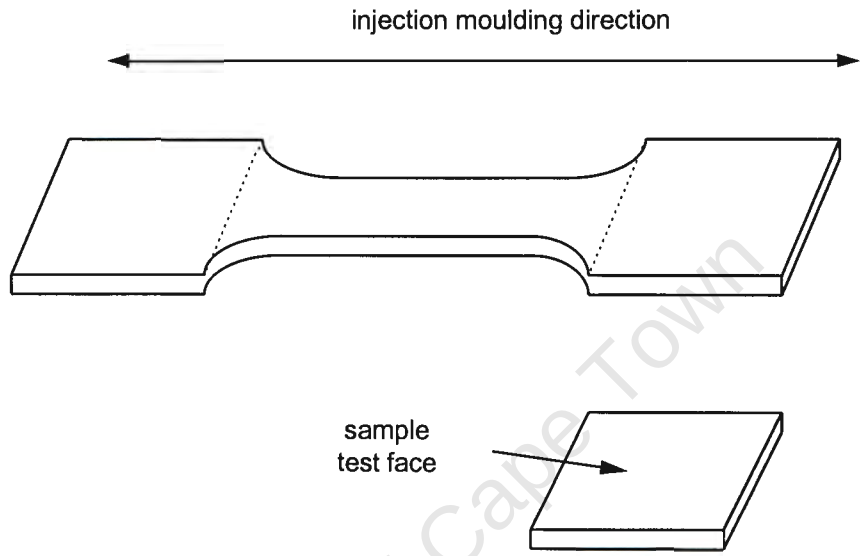

Figure 3.2: Schematic of the orientation of samples used for the single-point scratch and abrasive scrub tests.

3.4 MATERIALS CHARACTERISATION

3.4.1 Ash content tests

The weight fraction of filler in each polypropylene blend was verified using an ashing technique. For each blend, two weighed samples were placed in crucibles in an air furnace at a temperature of 550 °C. After complete burn-off of the polymeric material, the resulting weight difference could be attributed to the filler weight fraction in the blend.

3.4.2 Microscopy

3.4.2.1 Optical microscopy

Light microscopy was used in both the transmitted and reflected modes to study the microstructure of the polypropylene grades.

3.4.2.1.1 Polymer morphology

Morphology studies of the three unfilled polypropylene grades were performed using a polarised light mode on a Nikon Optiphot transmitted light microscope. Thin films of each parent polymer were melt pressed between a glass slide and coverslip at identical heating and cooling conditions. Although the resultant morphologies do not reflect the true polymer structure of an injection moulded sample due to the slower cooling rates used, they give a useful insight into the comparative morphologies of the three polypropylene grades.

3.4.2.1.2 Filler dispersion and orientation

Samples, cut in cross-section through an injection moulded tensile test bar, were cold mounted in an epoxy resin, mechanically ground down to 1200 grit on SiC abrasive pads, followed by diamond polishing to a 1 μm finish. A Reichert MeF3A metallurgical optical microscope was used to evaluate the filler dispersion and orientation within the polymer matrix.

3.4.2.2 Scanning electron microscopy

Extensive use of a scanning electron microscope was made to examine the worn surfaces after testing of the abrasive test samples, the abrasive scrub test samples, and the single-point scratch test samples. The SEM was also

used to analyse the condition of the filler-matrix interface in selected samples that had been cryogenically fractured in liquid nitrogen.

For all electron microscopy studies, the samples were mounted on aluminium stubs and sputter coated with a conductive gold/palladium layer prior to examination in a Cambridge Stereoscan 200 scanning electron microscope. The secondary electron signal was detected to produce images of the worn surfaces of the samples. An accelerating voltage of 10 keV was used to minimise radiation damage to the specimens.

3.4.3 Density measurements

The densities of the three polypropylene grades and their respective filled composites were calculated from measured mass and volume values. For each sample, an injection moulded flexural bar was machined to a standard dimension (error = ± 5 μm) and was weighed on a Sartorius R200D digital balance having a sensitivity of 0.01 mg. The sample dimensions were kept as large as possible to minimise the error in measuring the volume.

3.4.4 Differential scanning calorimetry

A Perkin-Elmer DSC2 differential scanning calorimeter (DSC) was used to determine the crystalline content of the three unfilled grades of polypropylene. The determination of the degree of crystallinity of a polymeric material is obtained from the measured heat of fusion (ΔH_f) and is based on calculating the area of a DSC melting peak relative to that of a standard material with a known value of $\Delta H_f^{(123)}$.

Samples of each polypropylene grade (~ 8 mg) were sliced from the injection moulded test pieces. A heating scan rate of 20 °C / min was used for each test. The percentage crystallinity (X_c) of polypropylene can be calculated from the equation:

$$X_c = (\Delta H_f / \Delta H_f^*) \times 100 \qquad (3.1)$$

where ΔHf^* is the heat of fusion of a 100% crystalline sample of iPP and is assumed to be 209 J g^{-1}[124].

3.5 MECHANICAL TESTS

3.5.1 Tensile tests

The tensile stress-strain behaviour of each composite material and the three unfilled polypropylene grades was determined by conducting uniaxial tensile tests to failure on a Zwick 1484 Universal Testing Machine. A strain rate of 8.33×10^{-3} s^{-1} was used and five samples of each material were tested.

Injection moulded test pieces conforming to the ASTM D638 standard were used. The gauge length of the specimen was parallel to the direction of injection of the polymer melt. Scanning electron microscopy was used to establish the tensile deformation behaviour and fracture modes of each sample.

3.5.2 Flexural bend tests

Centre-point bend tests, in accordance with the ASTM D790M-86 standard, were performed to determine the flexural modulus for each composite and the unfilled polypropylene grades. A Lloyds Instruments M5K tensometer was used for testing. Five samples of each composite were tested at a loading speed of 50 mm min^{-1}.

3.5.3 Hardness tests

3.5.3.1 Vickers microhardness

The Vickers microhardness, *HV*, of each unfilled polypropylene grade was measured using a load of $25g_f$ on a Matsuzawa MXT-α7 digital microhardness tester.

The Vickers microhardness was calculated from the formula:

$$HV = \text{load} / \text{area}$$
$$HV = 1.854\ W / d^2 \qquad (3.2)$$

where: W = load

d = length of indent diagonal

3.5.3.2 Shore D hardness

A hand-held Shore D hardness tester (ASTM D2240) was used to determine the bulk hardness of each filled composite sample. Ten readings were taken along the length of a flexural test bar for each material.

3.5.3.3 Ball indentor hardness tests

The bulk indentation hardness of the filled and unfilled polypropylenes, and the comparative polymers was measured on a Eseway SPVR-2 Hardness Tester using a 3 mm diameter steel ball indentor and a 30 kg load applied over a loading time of 10 s. For each sample five indents were made. The diameter of the indentations were measured using a Reichert MeF3A optical microscope as this offered improved clarity of the indent image.

As this was not a standard hardness test, but used for comparative purposes only, the average hardness value for each polymer was reported as:

$$H = 100\ (1 / \text{indent diameter}) \qquad (3.3)$$

3.6 TRIBOLOGY TESTS

3.6.1 Abrasion testing

Dry abrasion tests were performed on a modified Rockwell belt sanding machine (Figure 3.3) using alumina abrasive belts as the counterface. The sample is made to traverse normal to the direction of belt movement so that it always abrades against fresh abrasive. The samples were loaded perpendicularly (load = 4.9 N) on the cross-section face (3.2 mm x 9.8 mm) and were abraded over a total distance of 3.66 m at a speed of 200 mm s^{-1}. Three samples were tested for each material and the average mass loss was used to calculate the specific wear rate according to the formula:

$$\text{Specific wear rate } (mm^3\ N^{-1}\ m^{-1}) = \Delta\text{mass} / L\ W\ \rho \qquad (3.4)$$

where:

L = total distance travelled (m)

W = load (N)

ρ = density (g cm^{-3})

The wear rate for each material was determined using four different grades (80, 220, 400, 600 grit) of alumina abrasive belt. The average particle diameters and distribution densities were measured from scanning electron micrographs of the different abrasive belts. The average surface roughness, R_a of each belt was measured by surface profilometry. Scanning electron microscopy was also employed to characterise the material deformation and wear modes of the abraded surfaces of each material.

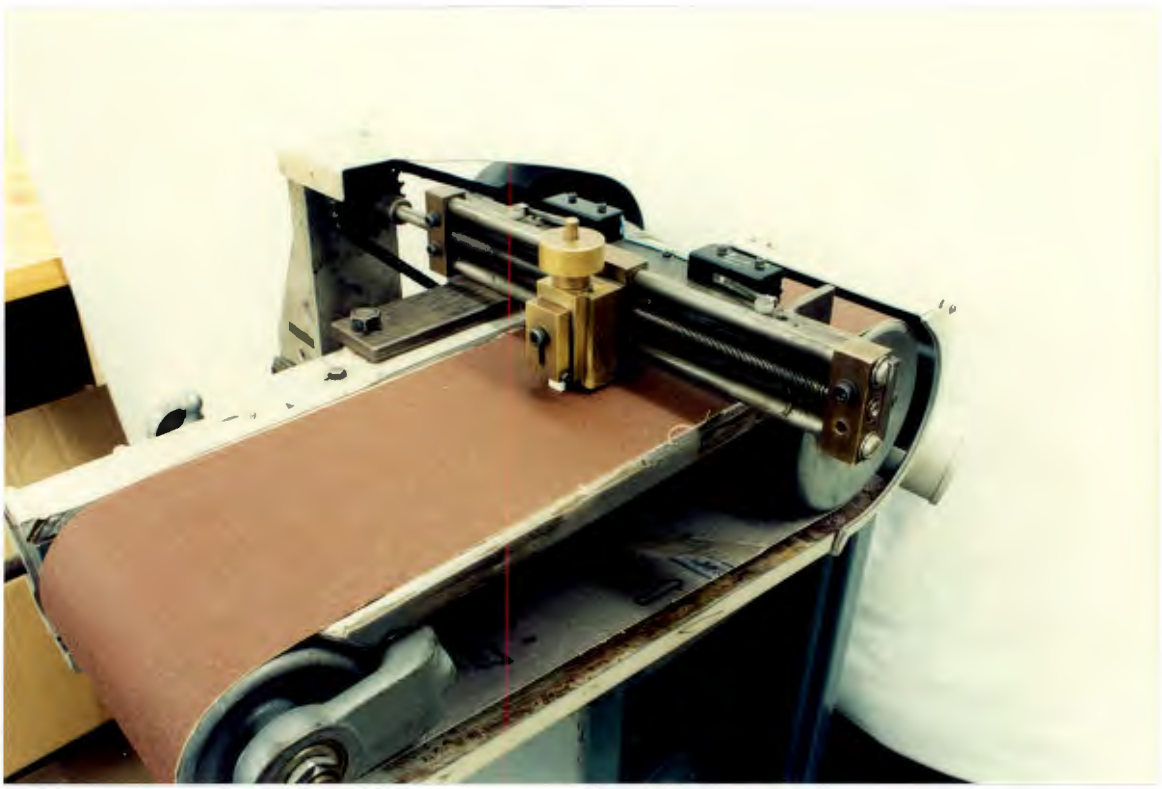

Figure 3.3: The modified Rockwell belt sanding machine used for each abrasive wear test. The sample is made to traverse normal to the direction of the belt movement ensuring that it abrades against fresh abrasive particles. The mass of the sample holder provides a normal constant load of 4.9 N.

3.6.1.1 Calibration of the abrasive belt rig

Samples of the PP grade 1040K were used for preliminary tests to determine the role of velocity and load on the abrasive wear rate. From these results the operating parameters for the tests were chosen. The preliminary tests were performed on Al_2O_3 220 grit abrasive belts and three samples were tested for each data point. The results of these calibration tests are shown in Appendix B.

3.6.2 Single-point scratch test

The test rig used for conducting single-track scratch tests is shown in Figure 3.4. Polymer samples, cleaned ultrasonically prior to testing, were clamped on a test table which was driven by a small electric motor. The scratch indentor was mounted, normal to the sample, under load at one end of a balanced beam. Sliding velocities of the sample between 9×10^{-6} and 1×10^{-4} m s^{-1} were achieved.

A Rockwell C diamond indentor was used to produce scratch tracks on the polymeric materials. For each sample, five scratch tracks 2 mm apart were made, corresponding to applied loads of 0.9 N, 2 N, 3 N, 5 N, and 10 N. The distance of traversal of each scratch was approximately 15 mm.

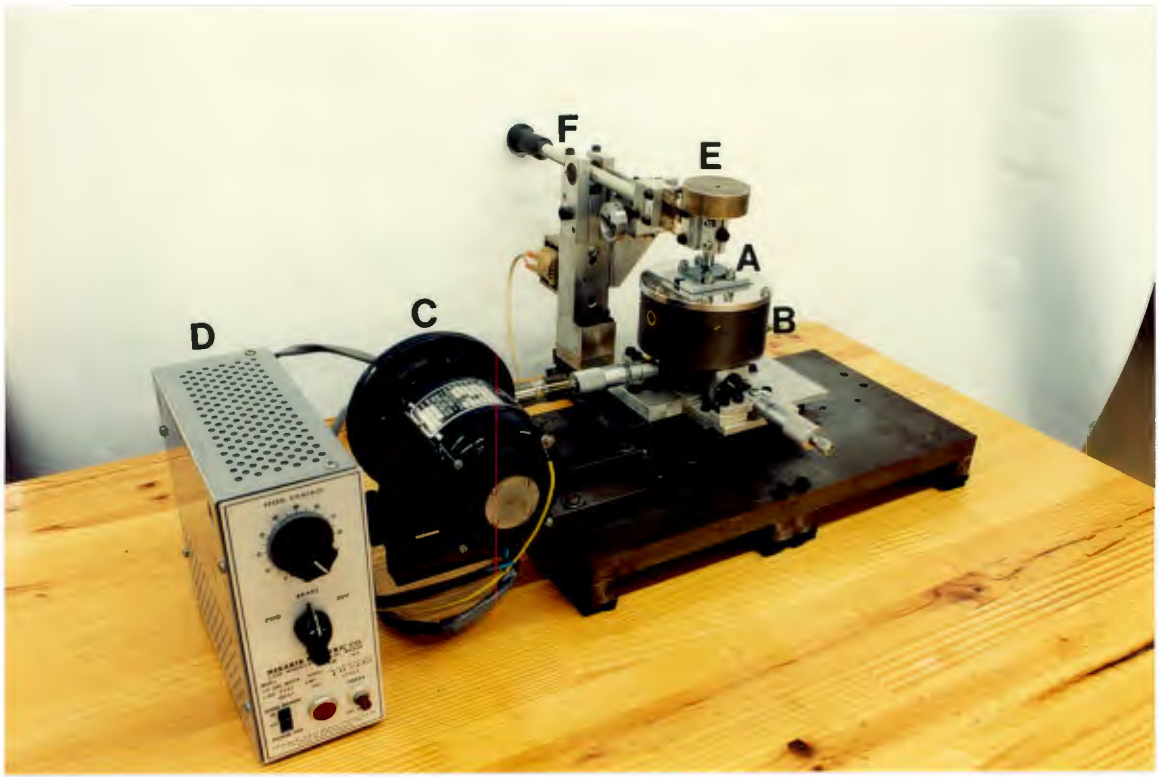

Figure 3.4: Test apparatus used for the single-point scratch tests. The sample (A) is clamped on the test table (B) which is driven by an electric motor (C) and speed controller (D). The scratch indentor (E) is mounted, under load, at the end of a balanced beam (F).

In separate experiments, a range of conical indentors manufactured from 431 stainless steel and having included cone angles (2α) in the range from 30° to 170° were used for scratch testing on the unfilled polypropylene grades, the comparative polymers, and several selected composite materials.

For all single-point scratch experiments, the width of each scratch track was measured, and the material deformation modes were evaluated using scanning electron microscopy. To allow for any elastic relaxation of the polymers to occur, track widths were measured approximately three hours after testing.

3.6.3 Abrasive scrub testing and gloss measurement

A commercially available test machine (Figure 3.5) was used to measure the abrasive scrub properties of the polypropylene samples. The test equipment was supplied by BYK Gardner Instruments. The test method (in accordance with ASTM D2486 and DIN 53778), has been developed to determine the 'washability', abrasion, and related properties of material surfaces.

The samples are clamped on a horizontal surface and subjected to a reciprocating sliding motion of an abrasive counterface over them. The supplied counterfaces, two nylon bristle brushes (ASTM D2486) are housed in brush holders suspended from the reciprocating carriage by cantilever arms. These brushes can be interchanged with other abrasive counterfaces or pads depending on the test material to be evaluated.

The reciprocating assembly is driven by an electric motor at a speed of ± 40 strokes per minute over a variable stroke length of 100 to 300 mm. The total sliding distance can be set by a 5-digit pre-set counter. A fluid reservoir can be attached to the test equipment if lubricated test conditions are required. Flow control of the fluid medium is controlled by a peristaltic pump.

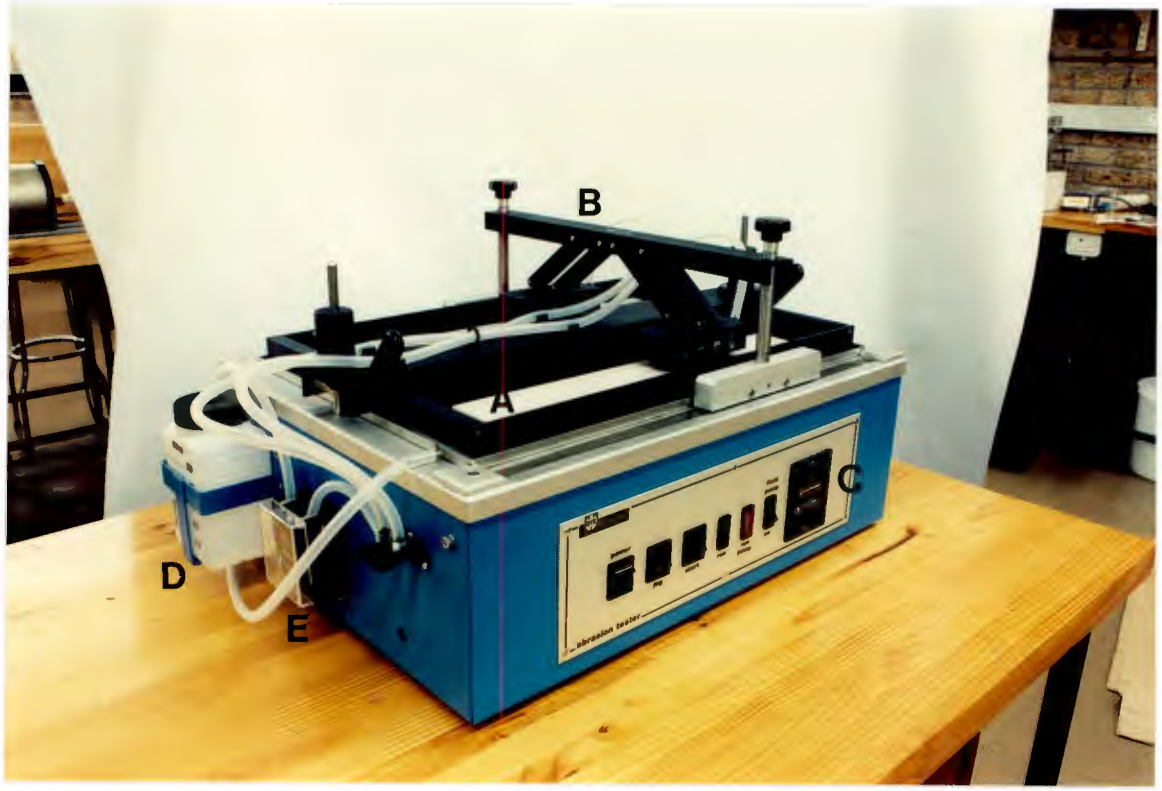

Figure 3.5: The abrasive scrub tester used in the 'washability' tests. The samples are subjected to a reciprocating abrasive action by abrasive counterfaces housed in holders suspended from cantilever arms.

A) Samples (attached to plastic panel) placed on flat glass test surface.
B) Reciprocating assembly incorporating the dual abrasive brush holders suspended from cantilever arms.
C) 5-digit pre-set counter to set the number of strokes per test.
D) Fluid reservoir for lubricated tests.
E) Peristaltic pump to control flow of liquid.

The test set-up allows the accelerated simulation of the surface abrasion and close repeatability of results from the two test heads. The assessment of a material's 'washability' or surface abrasion resistance is performed by measuring the reflectance of light from the test surface. This capacity of a surface to reflect directed light is known as the surface gloss. Appendix C details the principles of gloss measurement.

Gloss measurements from the test materials were made with a hand held Tri-micro glossmeter supplied by BYK Gardner Instruments. The glossmeter contains an automatic recalibration cell and can measure light reflection at three different geometries (20°, 60°, 85°) in accordance with ASTM D523 and DIN 67530.

3.6.3.1 Test procedure and operating parameters

Operating parameters are given in Table 3.5.

1.) Samples were cleaned ultrasonically, dried, and attached to a supplied black plastic panel with double-sided tape.
2.) The surface gloss of the samples prior to testing was measured, taking three readings for each sample.
3.) The plastic panel was clamped in place on the flat test surface of the abrasive scrub tester.
4.) The reciprocating assembly carrying the abrasive counterfaces/pads was attached to the supporting rods linking it to the electric motor.
5.) Tests were run for 10 000 strokes with intermediate gloss readings taken from the samples after 1000 and 5000 abrasive strokes.

Table 3.5: Operating parameters for the abrasive scrub tests.

Applied load (per brush holder)	250 g
Total number of strokes	10 000
Sliding speed	± 40 strokes min^{-1}
Stroke length	300 mm
Abrasive counterfaces	nylon bristle brush (ASTM D2486) commercial scouring pad commercial sponge pad
Environment	dry / wet

CHAPTER 4

RESULTS

The results of the materials characterisation and the mechanical tests are presented first and provide a background to the results of the tribology tests that are presented in later sections.

4.1 MATERIALS CHARACTERISATION

4.1.1 Polymer characterisation

Figures 4.1a-d show the typical variation in morphology of the S1100L, S1147H, and 1040K polypropylene grades, respectively. Under polarised light conditions, the spherulitic structure of the S1100L PP grade is observed. The Maltese-cross effect attests to the prevalence of birefringent units (Figure 4.1b).

The spherulitic morphology of the S1147H and 1040K grades is less distinct. These grades contain nucleating agents which allow a higher density of sites for spherulitic nucleation to occur. The resulting average spherulite size of these grades is thus greatly reduced in comparison to the S1100L polypropylene.

The results of the DSC analyses on the three unfilled polypropylene grades are detailed in Table 4.1. The two nucleated grades show expected increased melting points and higher crystallinities than the S1100L grade.

Table 4.1: DSC analysis of the unfilled polypropylene grades.

PP Homopolymer	Melting Point (°C)	X_c (%)
S1100L	158.5	46.6
S1147H	162.2	49.5
1040K	164.9	50.0

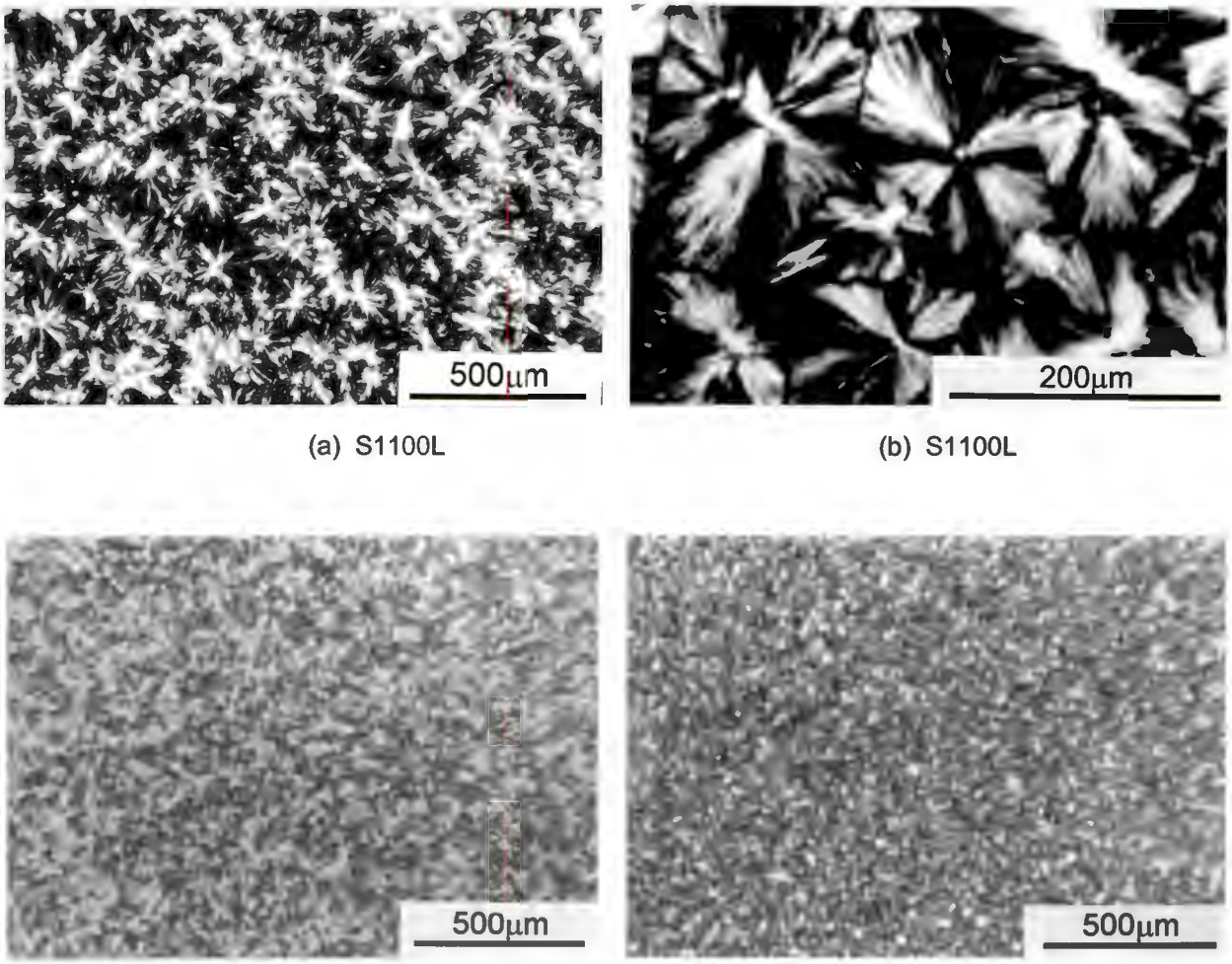

(a) S1100L (b) S1100L

(c) S1147H (d) 1040K

Figure 4.1: Optical micrographs highlighting the variation in morphology of the three unfilled polypropylene grades. The nucleated grades, (c) S1147H, and (d) 1040K, show reduced spherulite size in comparison to the unnucleated (a) S1100L grade. The high magnification of the S1100L grade (b) shows the Maltese-cross effect indicative of the birefringent nature of the polymer.

4.1.2 Filler characterisation

4.1.2.1 Weight fraction analysis

The results of the ashing procedure for the S1100L composite blends are shown in Table 4.2. The S1147H blends showed similar results. The values of filler weight % for each blend correlate favourably with the nominal values expected from the extrusion process. Due to differences in density of the fillers, the volume fraction, V_f, of filler in each blend varied. At 40 wt% for instance, the fillers with the highest and lowest densities, $BaSO_4$ and fly ash, had a V_f values 11.6% and 20.2%, respectively.

Table 4.2: Results of the ashing tests for the S1100L composites.

Sample	Nominal wt%	Actual wt%	Sample	Nominal wt%	Actual wt%
talc	10	11.1	fly ash	10	11.9
	20	21.8		20	22.1
	40	42.3		40	43.5
	60	63.8		60	61.4
$CaCO_3$	10	10.4	$BaSO_4$	10	10.8
	20	20.9		20	20.4
	30	33.0		30	30.5
	40	40.6		40	40.9
	50	51.9		50	50.8
	60	62.1		60	62.0
wollastonite	10	9.8	wollastonite	10	9.6
(coarse)	20	19.3	(fine)	20	19.3
	40	39.3		40	39.1
china clay	10	9.8			
	20	18.4			
	40	35.0			

4.1.2.2 Filler morphology

The scanning electron micrographs of the fillers (Figures 4.2a-g) show the typical morphologies and size range of the particles.

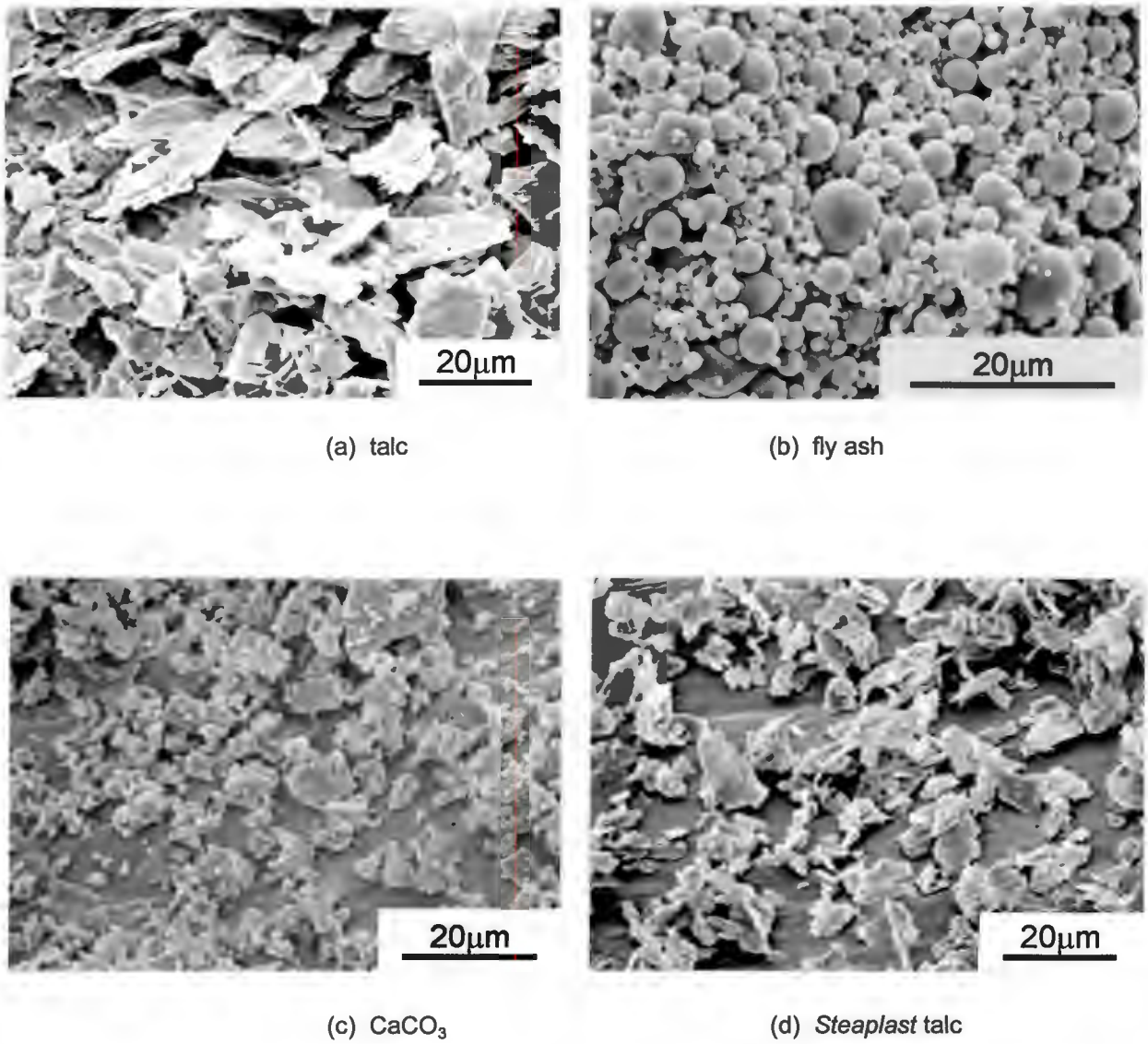

(a) talc (b) fly ash

(c) $CaCO_3$ (d) *Steaplast* talc

Figure 4.2: Scanning electron micrographs showing the variation in shape and size of the mineral fillers used in this study.

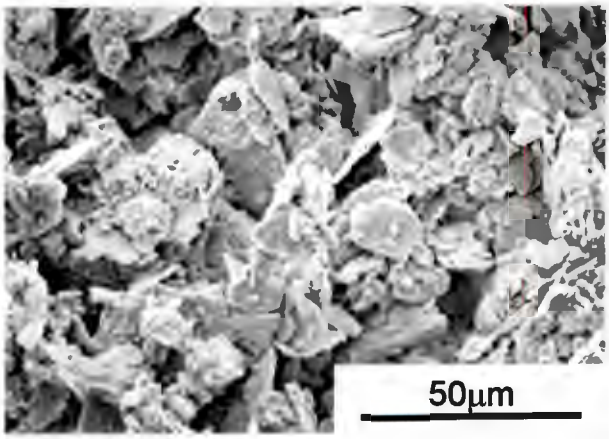

(e) china clay

(f) wollastonite (fine grade)

(g) wollastonite (coarse grade)

Figure 4.2 (cont.): Scanning electron micrographs showing the variation in shape and size of the mineral fillers used in this study.

4.1.2.3 Filler dispersion and orientation

The optical micrographs in Figure 4.3 show the distribution of filler particles in the polypropylene matrix for selected composite blends. The polished sections were cut transverse to the injection moulding direction of a tensile test bar. The fly ash sample (Figure 4.3a) contains 60 wt% filler which is distributed evenly across the specimen with no particle agglomeration evident. The 60 wt% talc sample (Figure 4.3b) also shows an even

distribution of the filler, however due to the platelet shape of the talc particles there is some orientation introduced from the injection moulding process.

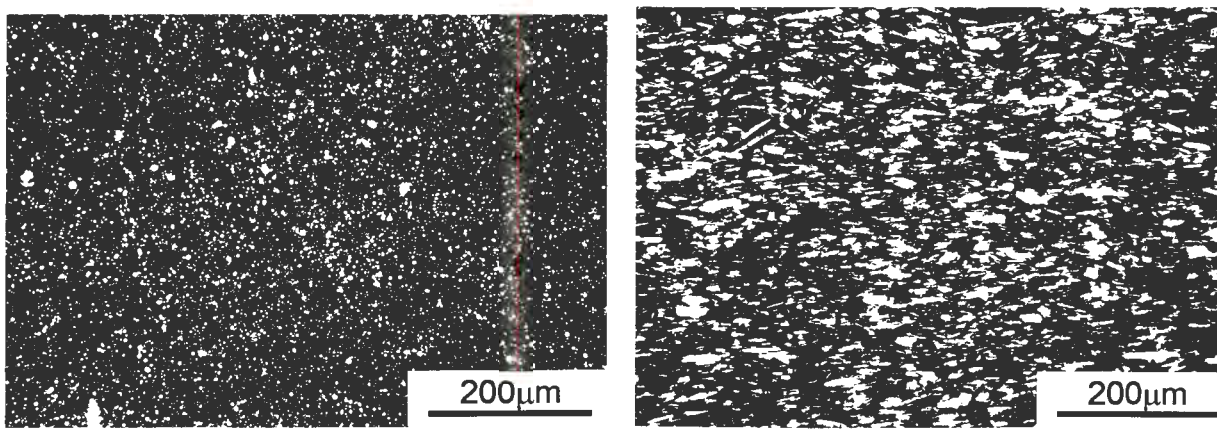

Figure 4.3: Optical micrographs showing the dispersion of filler particles in the polypropylene matrix: (a) spherical fly ash particles, and (b) platelet talc particles exhibiting some orientation effects due to the injection moulding process. The sections are cut transverse to the direction of injection moulding.

4.1.2.3.1 Nature of the filler - matrix interface

The scanning electron micrographs in Figure 4.4 show the surfaces of filled composites after cryogenic fracture in liquid nitrogen. The fly ash- and wollastonite-filled blends exhibit no interfacial adhesion between the filler particles and the polypropylene matrix (Figures 4.4a-b) as evident from the smooth surfaces of the filler particles and the polymer surface cavities. The platelet 40 wt% china clay filler (Figure 4.4c) shows improved adhesion but filler removal is still observed. As noted with the talc particles, there is a filler orientation effect present due to the injection moulding process. Interfacial adhesion is clearly noted on the fracture surface of the 40 wt% Steaplast talc sample (Figure 4.4d). Little filler removal is evident. There is also a noticeable lack of filler orientation present within the polypropylene matrix as was evident for the other platelet filler composites.

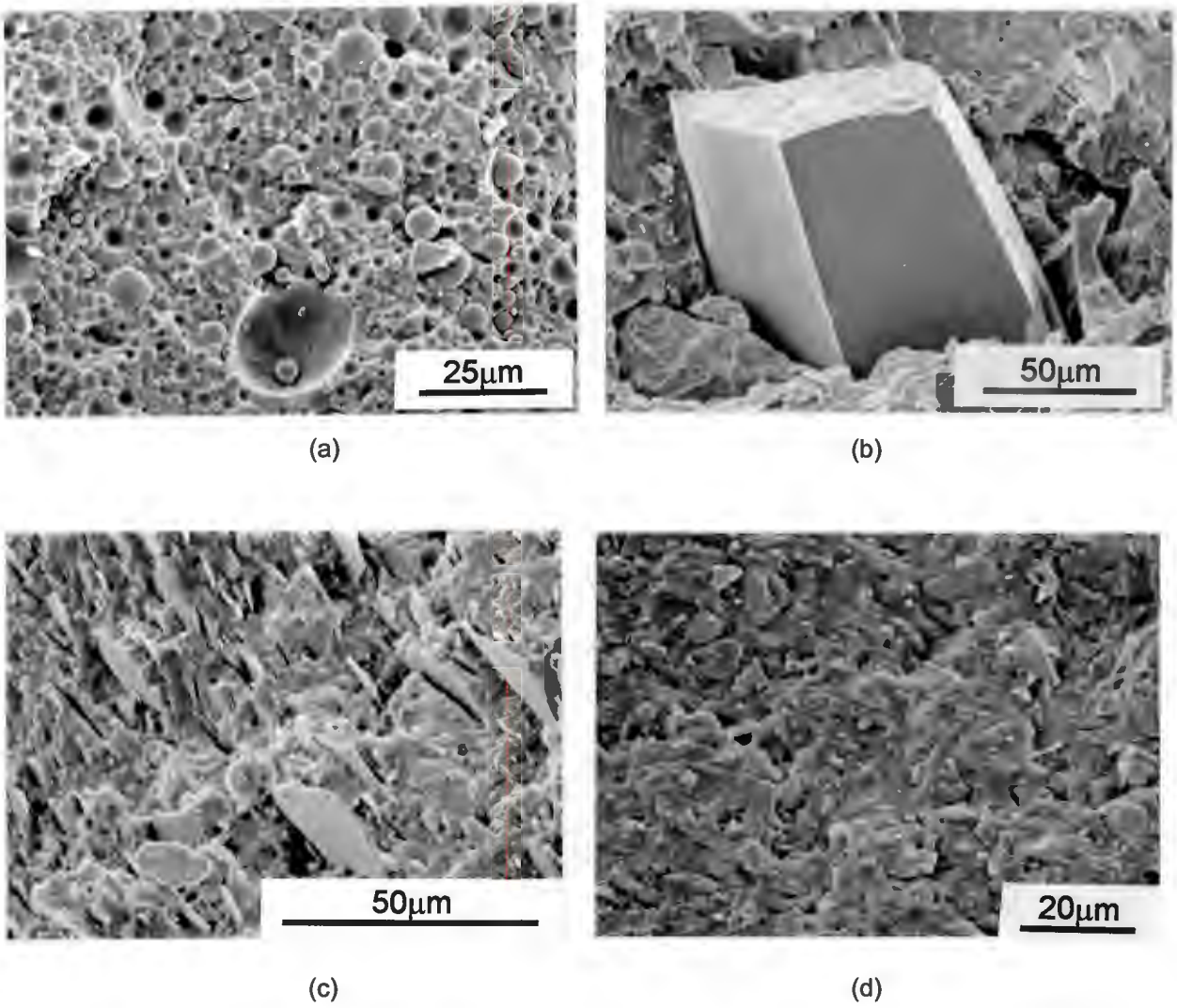

Figure 4.4: Scanning electron micrographs showing the degree of interfacial adhesion between filler particles and the polypropylene matrix. Little adhesion is evident for the (a) fly ash- and (b) wollastonite-filled composites. The fracture surface of the (c) 40 wt% china clay sample shows improved interfacial adhesion and filler orientation. Adhesion between filler and polymer is most pronounced in the (d) *Steaplast* talc composites.

4.2 MECHANICAL TESTING

4.2.1 Tensile tests

4.2.1.2 Effect of the base polypropylene homopolymer

The typical stress/strain curves for the unfilled polypropylene grades; S1100L, S1147H and 1040K, are shown in Figure 4.5, and the test results are summarised in Table 4.3.

The trends of the tensile properties of the three PP grades are in agreement with those supplied by the producer (Table 3.1). The values of tensile yield strength for all the grades are however slightly lower than expected. The two nucleated grades, S1147H and 1040K, show increased yield strength over the S1100L homopolymer. They exhibit similar elongation to failure of 20 to 40% which is considerably lower than the S1100L grade (> 150%).

Table 4.3: Tensile test results for the three homopolymer PP grades.

PP homopolymer	Yield stress (MPa)	Strain to failure (%)
S1100L	30.9	> 150
S1147H	35.0	39
1040K	34.3	23

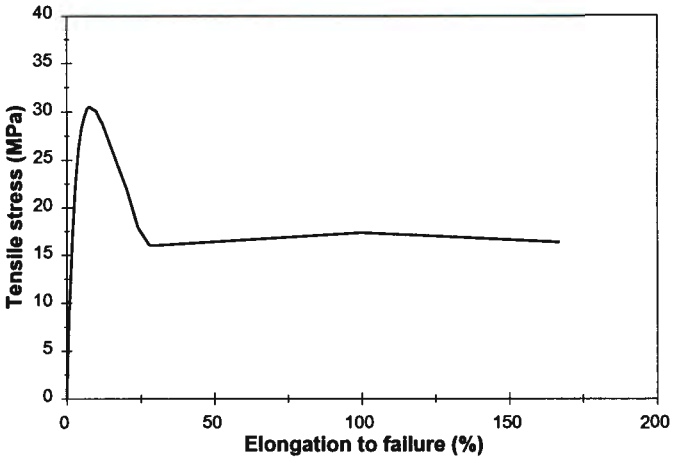

(a) S1100L

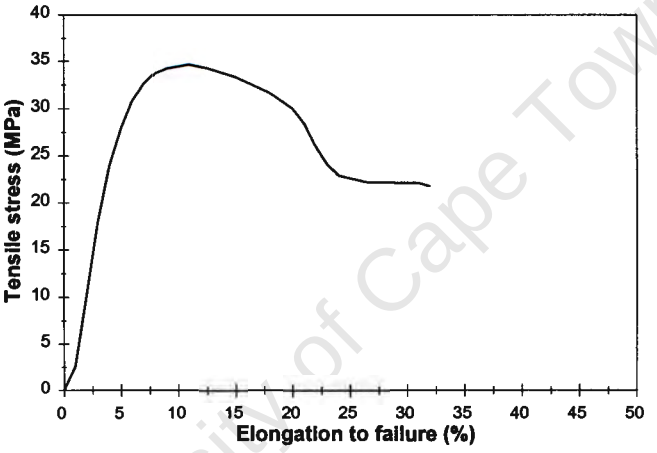

(b) S1147H

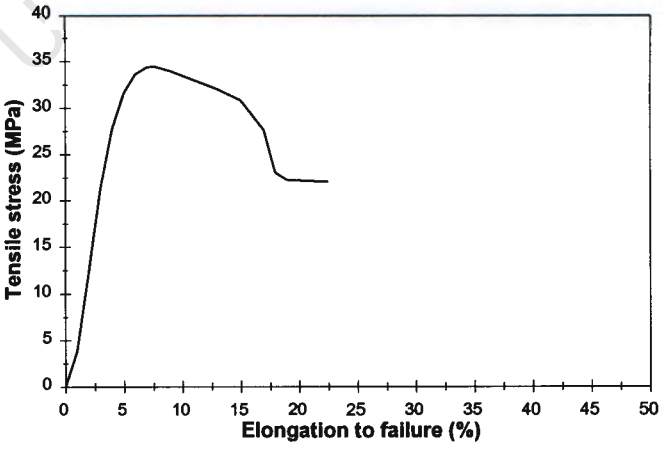

(c) 1040K

Figure 4.5: Tensile stress/strain curves for the unfilled polypropylene grades.

4.2.1.3 Effect of mineral fillers

The tensile test results for the filled PP composites compounded with the S1147H and S1100L polypropylene grades are summarised in Tables 4.4 and 4.5.

Table 4.4: Tensile test results for the S1147H filled composites.

PP homopolymer	Filler type	Filler content (wt%)	Yield stress (MPa)	Elongation to failure (%)
S1147H	*Steaplast* talc	10	32.5	34.4
		20	31.9	35.0
		40	30.4	28.6
	china clay	10	32.8	39.2
		20	32.3	31.0
		40	29.1	11.0
	wollastonite (fine)	10	32.5	27.6
		20	31.7	31.0
		40	28.6	24.2
	wollastonite (coarse)	10	32.2	21.2
		20	30.9	19.8
		40	27.8	16.6

The tensile yield strength and elongation to failure of each composite is reduced by the addition of the filler material, however differences are noted in the tensile behaviour of specific fillers. Figures 4.7 and 4.8 show the typical stress/strain curves obtained during testing of the two talc grades and the fly ash filled composites which illustrate this point. These filled composites were compounded with the S1100L base polypropylene grade. These curves will be discussed in detail in section 5.2.2.

Table 4.5: Tensile test results for the S1100L filled composites.

PP homopolymer	Filler type	Filler content (wt%)	Yield stress (MPa)	Elongation to failure (%)
S1100L	talc	10	35.0	15.5
		20	33.8	9.3
		40	32.4	3.8
		60	-	2.6
	fly ash	10	28.9	60.6
		20	26.2	45.1
		40	20.3	38.8
		60	17.1	27.8
	$CaCO_3$	10	29.5	96.4
		20	26.4	38.8
		30	24.3	27.8
		40	22.7	42.4
		50	19.8	28.9
		60	18.8	4.2
	$BaSO_4$	10	32.0	30.8
		20	30.0	27.6
		30	27.2	74.5
		40	25.6	66.1
		50	24.8	25.0
		60	24.7	1.2
	Steaplast talc	10	31.8	51.6
		20	31.8	28.4
		40	28.9	14.2
		60		
	china clay	10	30.6	49.6
		20	30.6	20.4
		40	30.2	9.2
	wollastonite (fine)	10	31.0	29.0
		20	29.4	28.2
		40	27.6	16.4
	wollastonite (coarse)	10	30.8	20.6
		20	29.8	18.8
		40	26.2	12.4

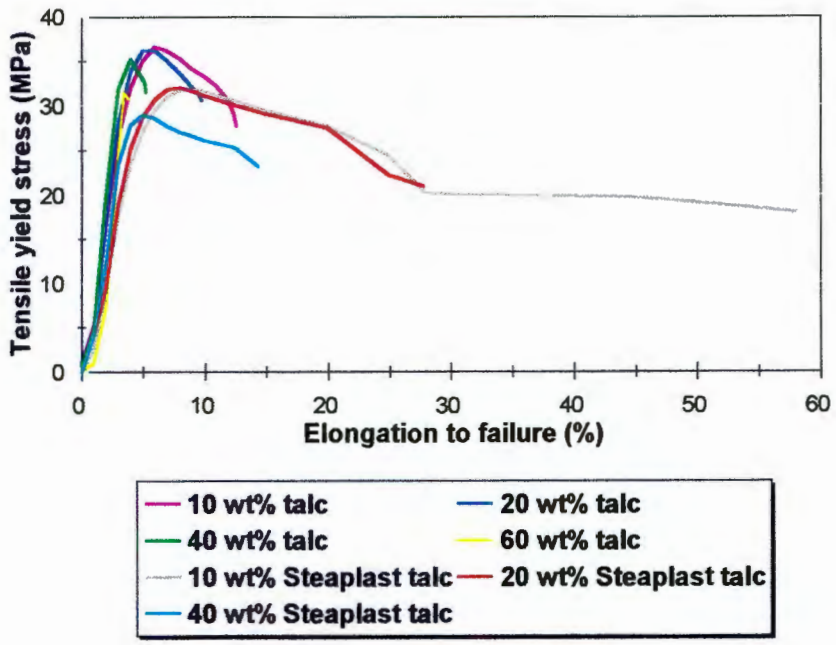

Figure 4.7: Tensile stress/strain curves for the S1100L PP composites of the two talc fillers. Differences in tensile behaviour between the two talc grades are noted and are influenced by the filler particle size.

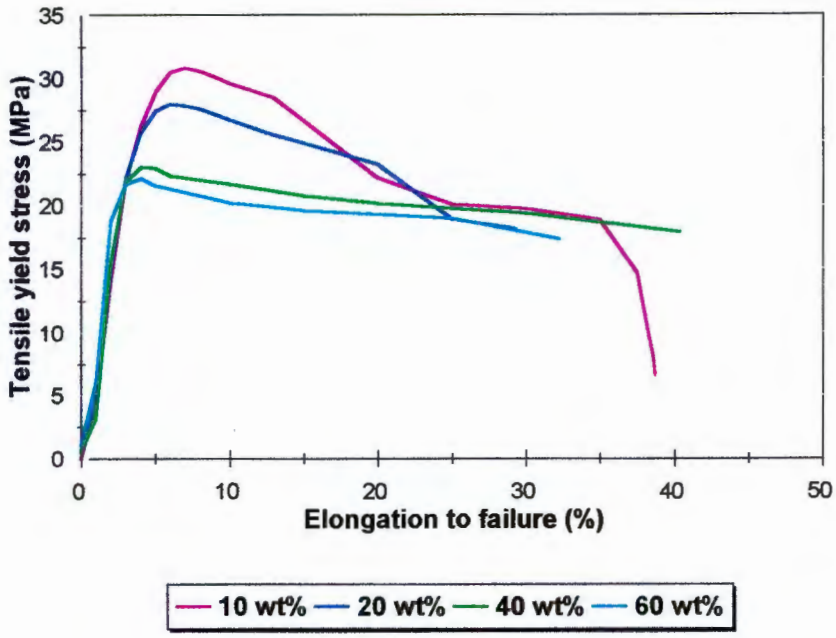

Figure 4.8: Tensile stress/strain curves for the S1100L - fly ash composites as a function of filler content. A decrease in tensile yield strength with increasing filler content is observed.

4.2.1.3.1 Effect of filler shape

Figure 4.9 shows the effect of the mineral fillers on the tensile yield stress of the S1100L composite materials. It is noted that although the fillers exhibit the same trend of decreasing tensile yield stress with increasing filler content, there are noticeable differences in their individual behaviour.

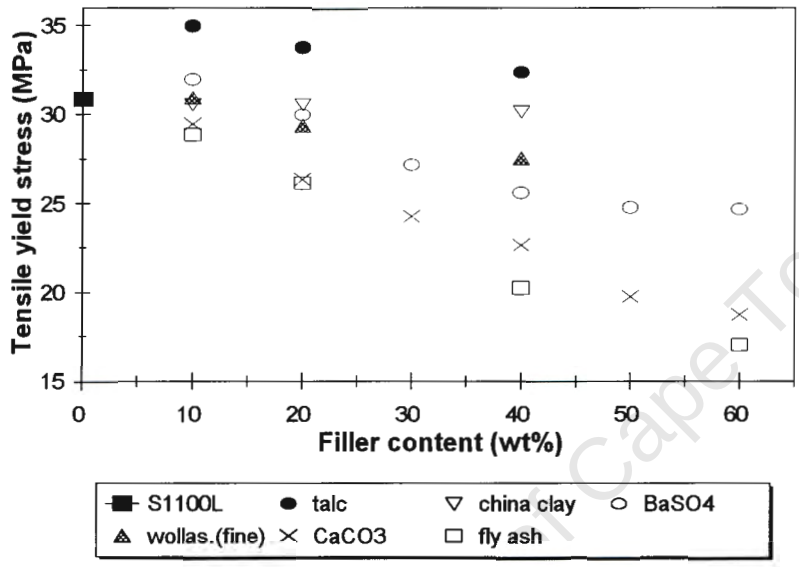

Figure 4.9: Plot of the tensile yield strength of the unfilled S1100L polypropylene grade and the mineral-filled composites as a function of filler content. A general trend of decreasing yield strength with increasing filler content is evident, although differences in individual filler behaviour are observed.

The platelet-shaped talc filler shows a significant improvement (13%) in yield strength over the unfilled polypropylene grade. Furthermore, the decrease in yield strength with increasing talc content is not as marked as for the other fillers and, even at 40 wt% loading the yield strength is higher than that of the unfilled grade. The platelet china clay-based composites have a slightly reduced reinforcing effect on the polypropylene matrix than the larger talc particles, but show little drop-off in yield strength when the filler content is increased from 10 to 40 wt%.

The fillers which have an aspect ratio close to unity, *i.e.* $BaSO_4$ and $CaCO_3$, show similar tensile behaviour, having large decreases in yield strength with increasing filler content. A slight improvement in yield strength over the unfilled S1100L polypropylene is seen for the $BaSO_4$ grades, though this is restricted to low filler contents (10 wt%). The large spherical fly ash-based composites exhibit the largest reduction in tensile properties of all the fillers.

The tensile properties of the wollastonite filler, which has a fibrous shape and an aspect ratio intermediate to that of the platelet and spherical fillers, follow a response that is midway between that of the reinforcing platelet fillers and the weakening 'spherical' fillers.

4.2.1.3.2 Effect of filler size

Figures 4.10 and 4.11 show the influence of filler particle size on the tensile behaviour of two fillers. The two grades of wollastonite, which have mean particle sizes of 15 μm and 150 μm respectively, have been compounded with the S1147H polypropylene grade (Figure 4.10). It is noted that the particle size difference has little effect on the tensile yield strength of the composites across the range of filler content (10 wt% to 40 wt%). The elongation to failure results are, however influenced by the particle size. The fine grade of wollastonite shows a 25 to 30 % improvement in ductility over the coarse grade at all levels of filler content. The deviation is most apparent at a filler loading of 20 wt% where the fine wollastonite grade exhibits an elongation to failure of 31%. This is an improvement over the 27.6% achieved at 10 wt% filler content for the same grade and is an anomaly in the general trend observed for all the filler materials.

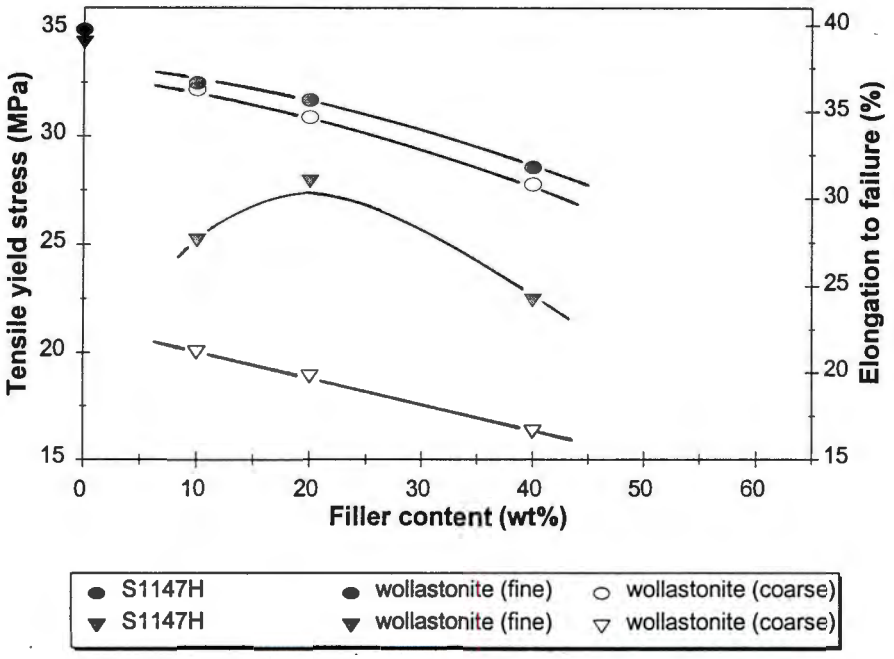

Figure 4.10: Tensile yield strength (circles) and ductility (triangles) of the wollastonite-filled composites illustrating the effect of filler particle size on the tensile properties.

Figure 4.11 shows the effect of particle size on the tensile properties of the two talc grades compounded with the S1100L polypropylene. The stress/strain curves of the materials are illustrated in Figure 4.7. The results for the elongation to failure follow a similar trend to those of the two wollastonite grades with the smaller particle size grade (*Steaplast* talc) showing better ductility at all levels of filler content. The improvement in ductility is more marked for these platelet fillers than for the fibrous wollastonite fillers. At a filler level of 10 wt% an almost threefold improvement in the ductility is noted for the *Steaplast* filler. At the higher filler loading of 20 wt% and 40 wt%, similar improvements are observed. The limited ductility of the large talc-based composites is emphasised in Figure 4.12 which shows the post fracture tensile samples of the range of filler contents tested. No necking or plastic deformation is observed.

The results of the tensile yield strengths for the talc fillers show contrasting behaviour to that observed for the fibrous wollastonite filler grades. Whereas the wollastonite filler particle size had little influence on the yield strength results of the composites, the pattern observed for the platelet talc fillers indicates that a larger particle size is beneficial to attaining a higher yield strength. Results for the large talc grade are consistently higher than those of the *Steaplast* grade over the range of filler loading.

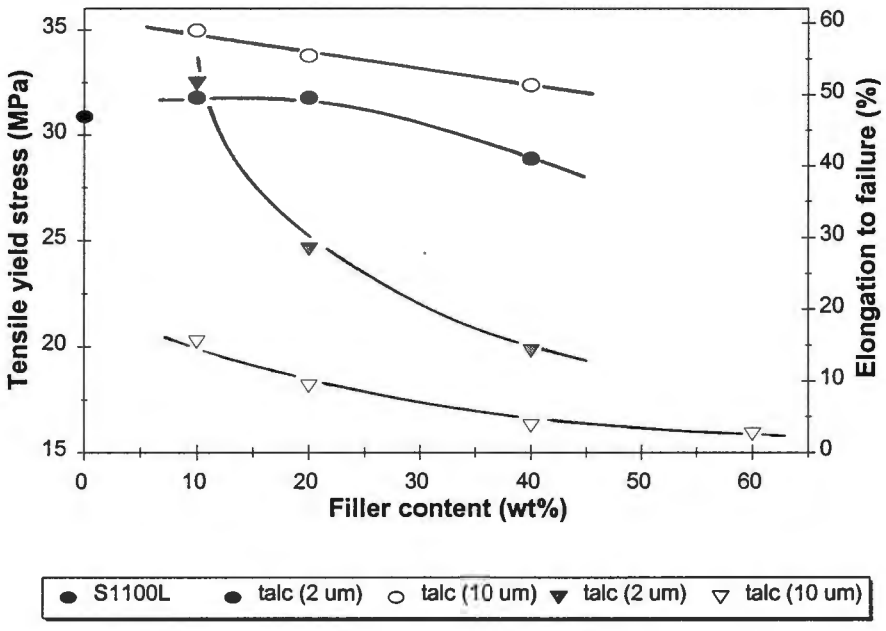

Figure 4.11: Tensile yield strength (circles) and ductility (triangles) of the two talc based composites showing the influence of filler particle size on the tensile properties. The elongation to failure of the base S1100L polypropylene grade is > 150%.

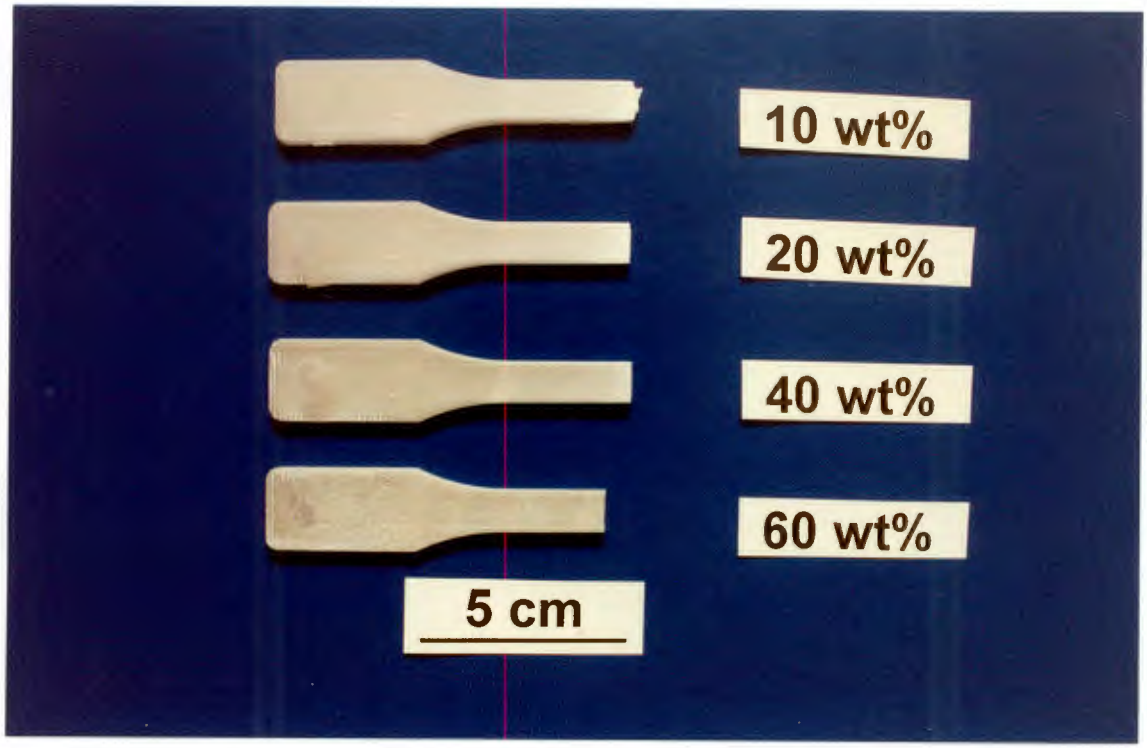

Figure 4.12: Post-fracture tensile samples of the range of talc-filled composites. Limited deformation can occur due to the alignment effect of the large talc platelets.

4.2.1.3.3 Effect of the base polypropylene grade

In comparing the tensile properties of those filled composites which have the same filler but have been compounded with both the S1100L and the S1147H polypropylene grades, several features can be noted.

The addition of the *Steaplast* talc filler to the S1100L PP grade, which has a yield strength of 30.9 MPa, produces an increase in yield strength to 31.8 MPa at 10 wt% loading. At the same filler loading for the S1147H based composite a decrease in yield strength from 35 MPa to 32.5 MPa is noted. Similar trends are observed for the wollastonite and china clay fillers.

The influence of the highly ductile (>150%), cold drawing S1100L polypropylene grade is also seen in the values attained for elongation to failure of the composites. At 10 wt% filler loading, the *Steaplast*-S1100L composite showed an average elongation at fracture of 51.6%, which represents a threefold decrease in ductility from the virgin polymer. In contrast, the 10 wt% *Steaplast*-S1147H composite, although having a lower average ductility (34.4%), only decreased the ductility of the unfilled S1147H polymer (39%) by ~ 12%.

4.2.1.4 SEM analysis of tensile fracture samples

With the exception of the large talc filler-based samples, the tensile fracture surfaces of the other filled composites can be divided into two classes according to the distinguishing fracture features present. These are: fracture at low wt% filler, and fracture at high wt% filler.

The large particle talc-based composites show little difference in fracture surface appearance with varying filler content. The fracture surfaces are characteristically brittle with the regular alignment of the large talc platelets hindering the deformation of the ductile polypropylene matrix. This is seen in Figure 4.13 which shows the fracture surface of a 60 wt% talc sample.

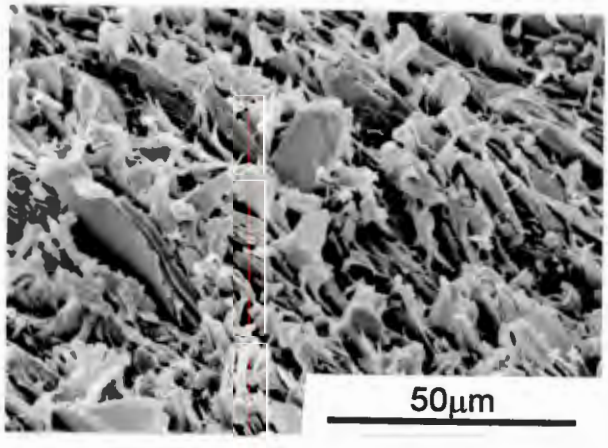

Figure 4.13: Tensile fracture surface of a 60 wt% talc-S1100L composite. The alignment of the large talc platelets can be seen restricting the plastic deformation of the polypropylene matrix.

4.2.1.4.1 Tensile fracture at low filler content

The filled composites containing 10 to 20 wt% filler exhibit necking and elongation of the gauge length. Stress whitening along the sample length is observed (Figure 4.16 of the fly ash-filled composites) and this is associated with microvoid formation in the bulk polymer (Figure 4.14). Distinctive ductile plastic deformation features and void formation are characteristic of the tensile fracture surfaces of the filled polypropylene composites, and are shown in Figure 4.15.

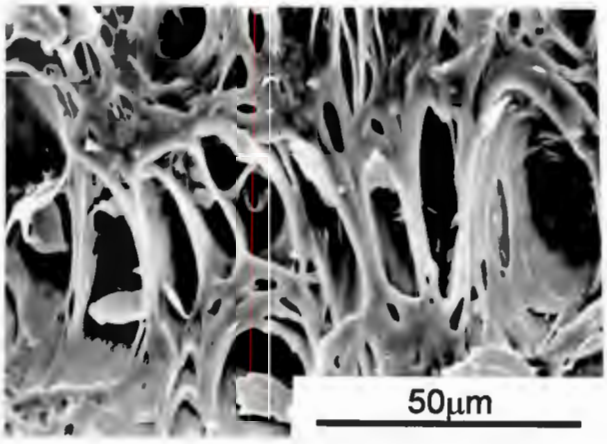

Figure 4.14: Microvoid formation during tensile deformation of S1100L composite. The filler particles can act as initiation sites for voids to form.

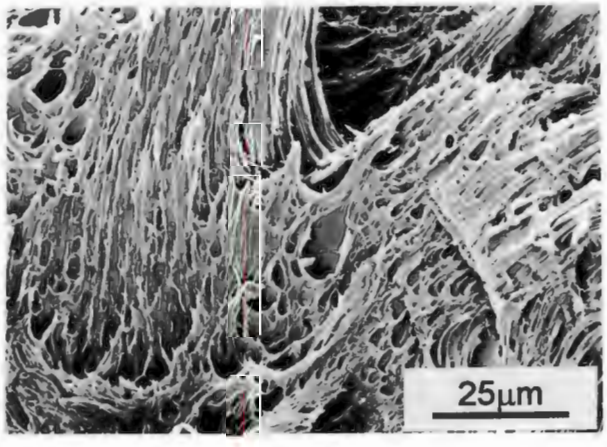

Figure 4.15: Typical ductile deformation features present during the fracture of low filler cortent composites.

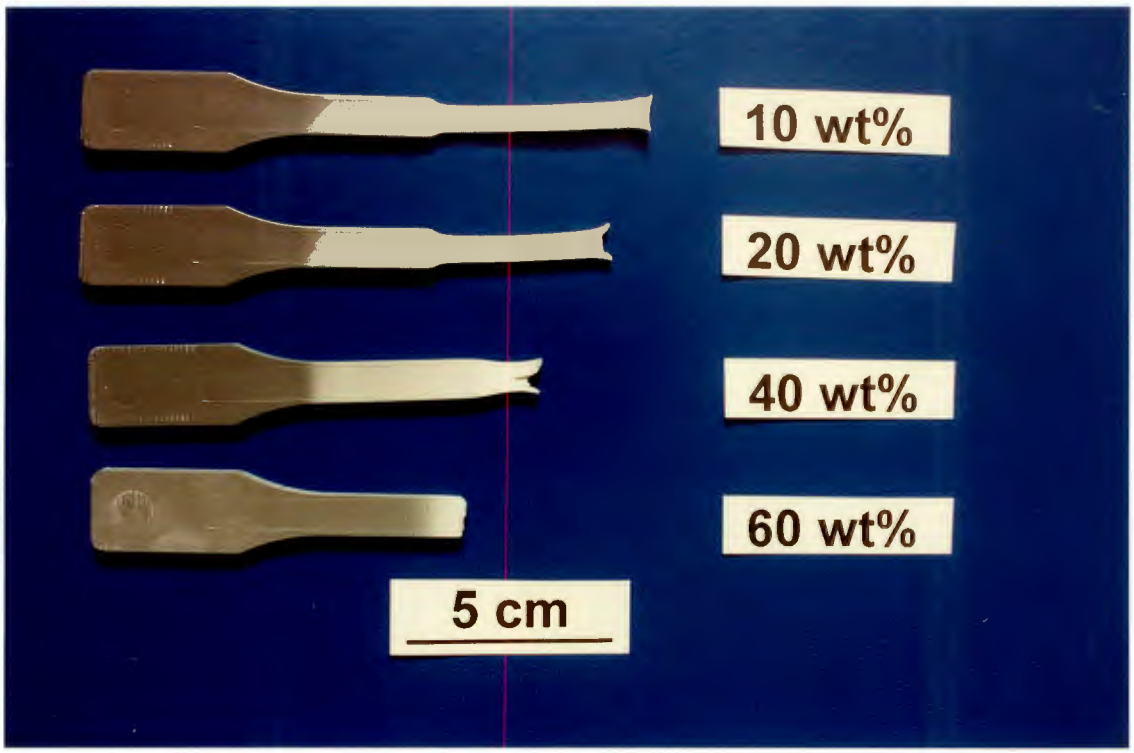

Figure 4.16: Post-fracture tensile samples of the range of fly ash-filled composites. At low filler content, the samples exhibit increased ductility and stress whitening along the gauge length; at high filler content, deformation is restricted.

4.2.1.4.2 Tensile fracture at high filler content

The fracture surfaces of samples containing 40 to 60 wt% filler show two distinct regions as illustrated in the schematic of Figure 4.17 and in the scanning electron micrograph of Figure 4.18.

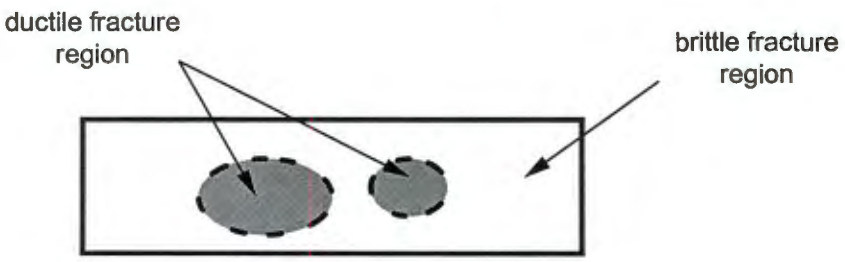

Figure 4.17: Schematic of a typical tensile fracture surface of a high filler content composite.

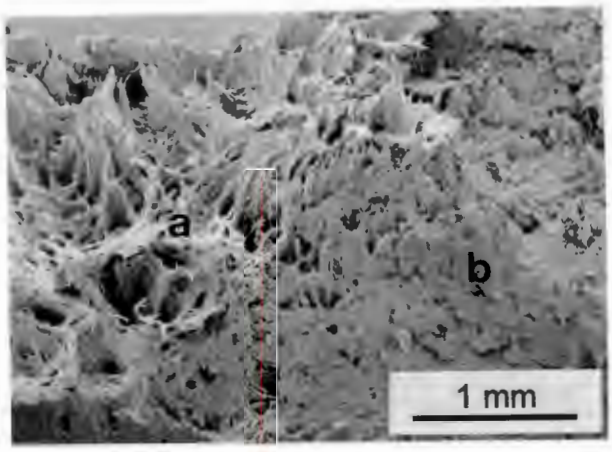

Figure 4.18: Fracture surface of a 40 wt% wollastonite-S1147H composite. Two regions of fracture are noted: (a) ductile tearing, and (b) brittle fracture.

The central core of each sample shows typical features of ductile deformation with fibrils of deformed polypropylene diverging from the centre (Figure 4.19). The outer area of the fracture surface is characteristically brittle as evident from the respective micrographs of the fly ash and wollastonite composites shown in Figure 4.20. This deformation behaviour and characteristic fracture surface appearance of the filled composites, is analogous to the 'cup-and cone' tensile fractures in steel specimens. In this case, necking and ductile void formation in the centre regions of steel tensile specimens occurs as a result of constraint set up by the triaxial stress system. Rapid brittle shear occurs in the outer areas of the fracture surface.

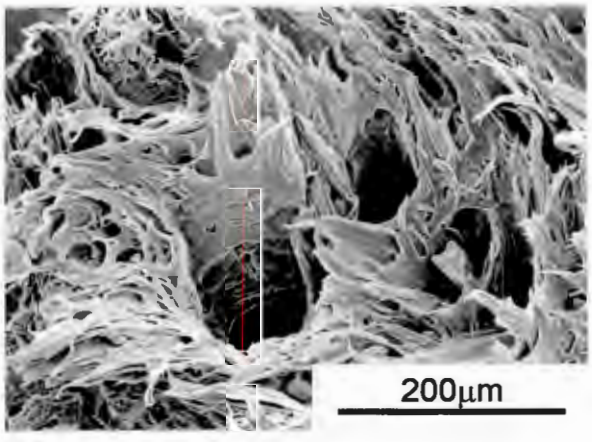

Figure 4.19: Ductile features in the core of a 40 wt% wollastonite-S1100L tensile specimen exhibit divergent tearing behaviour. Fibre pullout has occurred during fracture.

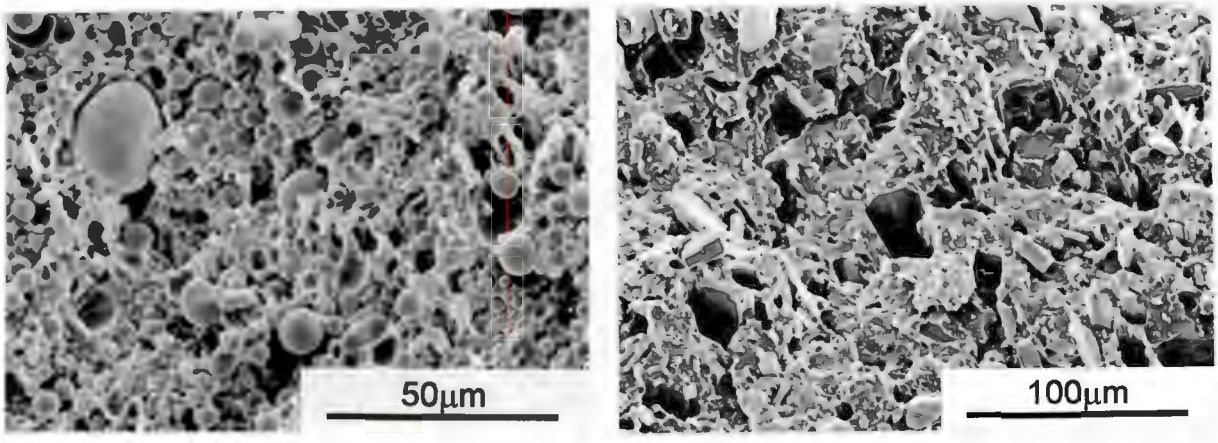

(a) (b)

Figure 4.20: Brittle outer fracture regions of (a) fly ash and (b) wollastonite tensile samples. Note the lack of bonding between the filler particles and the polypropylene matrix, leading to decreased interfacial strength.

In contrast to the large talc grades, where the platelet alignment prevented deformation from occurring, there is little obstruction to polymer deformation for the other filled grades. Figure 4.21 shows the side view of a 40 wt% fly ash tensile sample in the region just below the fracture surface. Ductile fibrils of deformed polypropylene are evident.

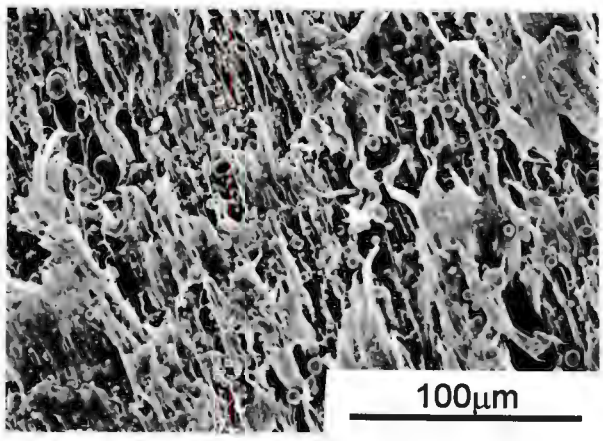

Figure 4.21: Scanning electron micrograph of the side view of a 40 wt% fly ash-S1100L tensile sample. The deformation of the polypropylene matrix is unrestricted by the spherical fly ash particles.

4.2.2 Flexural tests

Figure 4.22 shows the variation in flexural stiffness observed for the three grades of unfilled polypropylene. The nucleated grades, S1147H and particularly 1040K, showed improved stiffness over the S1100L homopolymer. The results of the flexural 3-point bend tests on the filled polypropylene composites are summarised in Table 4.6.

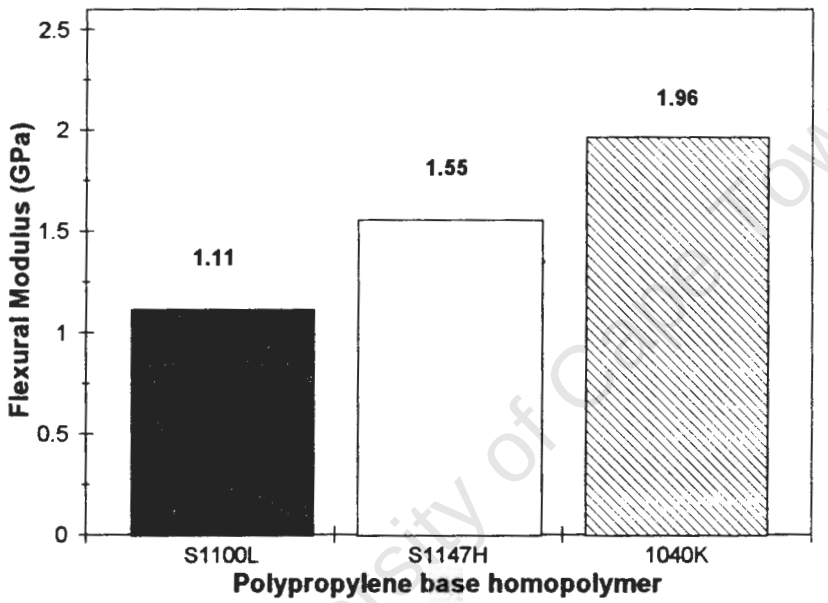

Figure 4.22: Flexural modulus values for the three unfilled grades of polypropylene showing the improvement in stiffness achieved by the nucleated homopolymers, S1147H and 1040K.

Table 4.6: 3-point flexural test results for the filled polypropylene composites.

Filler type	Filler content (wt%)	Flexural modulus (GPa)	
		S1100L	S1147H
talc	10	1.79	
	20	2.22	
	40	3.58	
	60	8.73	
fly ash	10	1.38	
	20	1.55	
	40	2.32	
	60	4.70	
$CaCO_3$	10	1.34	
	20	1.52	
	40	2.26	
	60	4.04	
$BaSO_4$	10	1.38	
	20	1.49	
	30	1.62	
	40	1.83	
	50	2.15	
	60	2.77	
Steaplast talc	10	1.75	1.85
	20	1.89	2.00
	40	3.16	3.08
china clay	10	1.74	1.84
	20	2.01	2.26
	40	3.61	3.27
wollastonite (fine)	10	1.60	1.76
	20	2.02	2.11
	40	3.16	2.96
wollastonite (coarse)	10	1.61	1.65
	20	1.66	2.07
	40	2.56	2.78

4.2.2.1 Effect of mineral fillers

A general trend of increasing flexural stiffness of the polymer composite with increasing filler content is observed in Figure 4.23 which shows the 3-point bend test results for the unfilled S1100L polypropylene sample and selected filled composites. As with the tensile yield strength results, a variation in behaviour of the individual filler composites is seen.

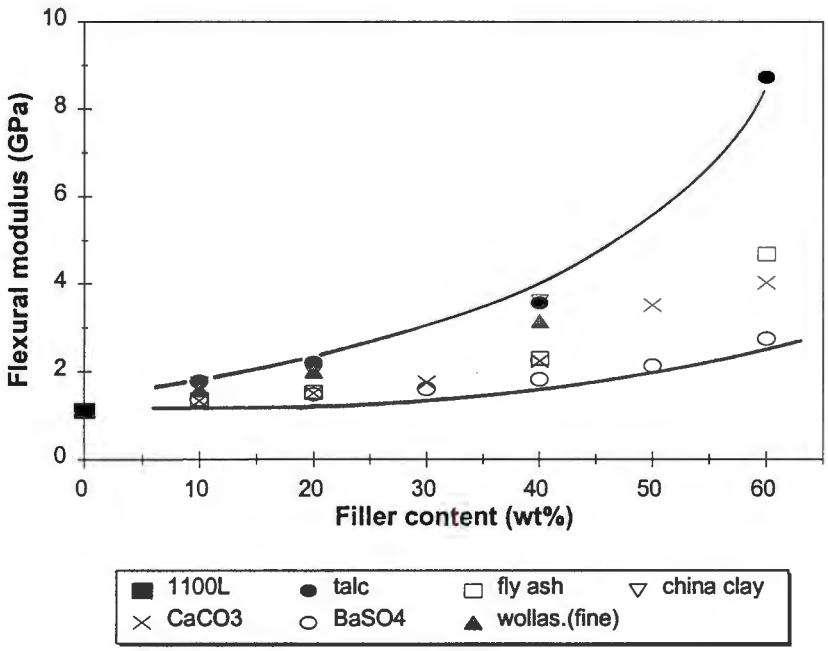

Figure 4.23: Influence of increasing filler content on the flexural modulus of S1100L polypropylene. The platelet-shaped fillers, talc and china clay, offer the most significant improvement in stiffness.

4.2.2.1.1 Effect of filler shape

From Figure 4.23 it is noted that there is a marked dependence of the stiffness of a polymer composite on the shape of the mineral filler. The platelet-shaped fillers, talc and china clay, offer the strongest reinforcement to the polypropylene matrix, most significantly at high filler loading where the 60 wt% talc-filled sample rendered a flexural modulus of over 8 GPa. The

$BaSO_4$ filler had little effect on the flexural properties of the polypropylene, even at a high filler loading of 60 wt%. The $CaCO_3$, fly ash, and wollastonite fillers all exhibit similar reinforcing effects on the polypropylene matrix, intermediate between those of the platelet fillers and the $BaSO_4$ filler. It is noted that the spherical fly ash particles, which yielded the largest reduction in tensile strength of the filled composites, have a significant stiffening effect under flexural conditions.

4.2.2.1.2 Effect of filler size

Figures 4.24 and 4.25 illustrate the influence of filler size on the flexural behaviour of the polypropylene composites using the wollastonite and talc fillers as contrasting examples.

At low filler loading, the two wollastonite fillers show equivalent flexural properties. As the filler content is increased the results for the two grades deviate, with the fine particle sized grade (15 μm) displaying an improved stiffness of around 20% over that of the coarse particle sized (150 μm) filler (Figure 4.24).

In contrast, the two talc fillers exhibit the reverse trend, with the smaller particle sized grade (*Steaplast* talc) contributing to the reinforcing of the polypropylene matrix to a lesser degree than the larger particle sized grade. This is shown in Figure 4.25.

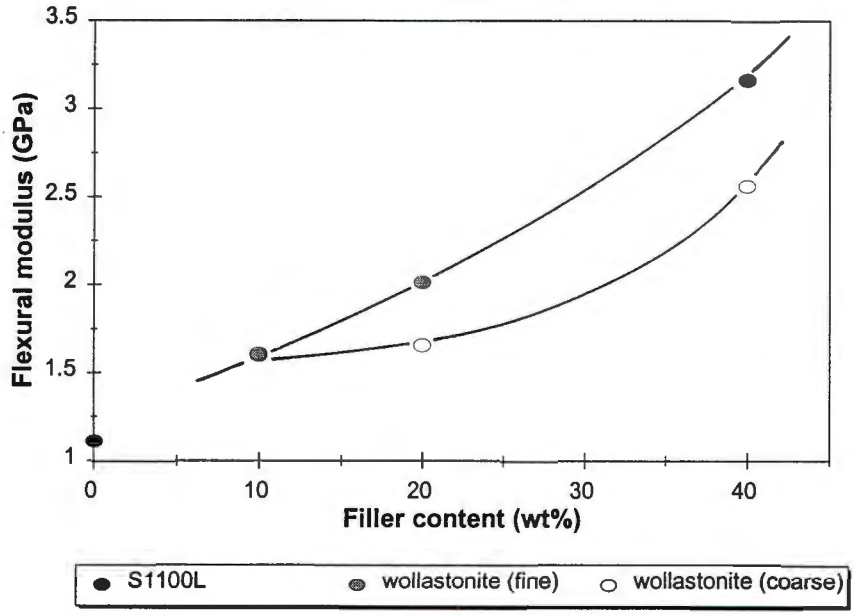

Figure 4.24: Influence of wollastonite particle size on the flexural modulus of S1100L polypropylene.

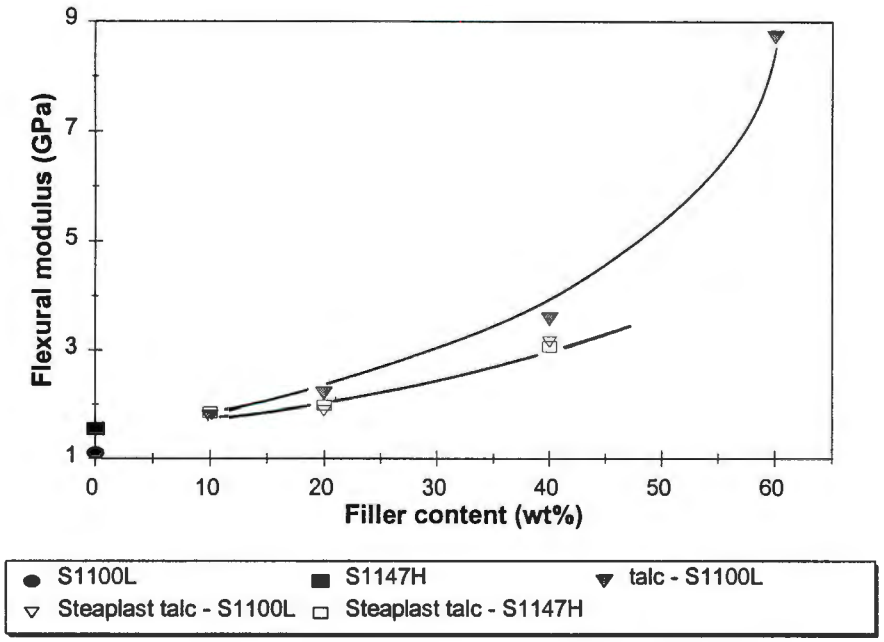

Figure 4.25: Influence of talc particle size on the flexural properties of S1100L polypropylene. The results for the *Steaplast* talc composites compounded with the S1147H polymer are also included, showing the minor influence of the base polypropylene grade on the flexural properties of these talc-based composites.

4.2.3 Hardness tests

4.2.3.1 Vickers microhardness tests

The results of the Vickers microhardness tests for the three unfilled polypropylene grades are detailed in Table 4.7. The increased crystallinity of the two nucleated grades has no effect on the microhardness of the polymer.

Table 4.7: Results of Vickers microhardness for the three unfilled PP grades.

Polypropylene homopolymer	Vickers microhardness (50 g_f) (kg mm^{-2})	Standard deviation
S1100L	7.56	0.15
S1147H	7.66	0.27
1040K	7.44	0.29

4.2.3.2 Shore D hardness tests

The results of the Shore D hardness measurements for the unfilled polypropylene grades, the comparative polymers, and the filled composite samples are shown in Table D.1, Appendix D. There is little variation in the results for the individual fillers with a general trend of increasing hardness with increasing filler content being observed. An increase in filler content from 10 wt% to 40 wt% increases the hardness by 5 to 7%.

4.2.3.3 Ball indentation hardness tests

The results of the bulk indentation tests of the respective filled and unfilled polymers are given in Table D.2, Appendix D. The results follow a similar pattern to those measured using the Shore D method, with an increase in relative hardness observed with increasing filler content for the filled polypropylene composites.

4.3 TRIBOLOGY TEST RESULTS

4.3.1 Abrasive wear tests

The surface morphologies of the four grades of Al_2O_3 abrasive belt used in this study are shown in Figure 4.26. The measured average particle size, distribution density, and surface roughness, R_a, of the belts are detailed in Table 4.8.

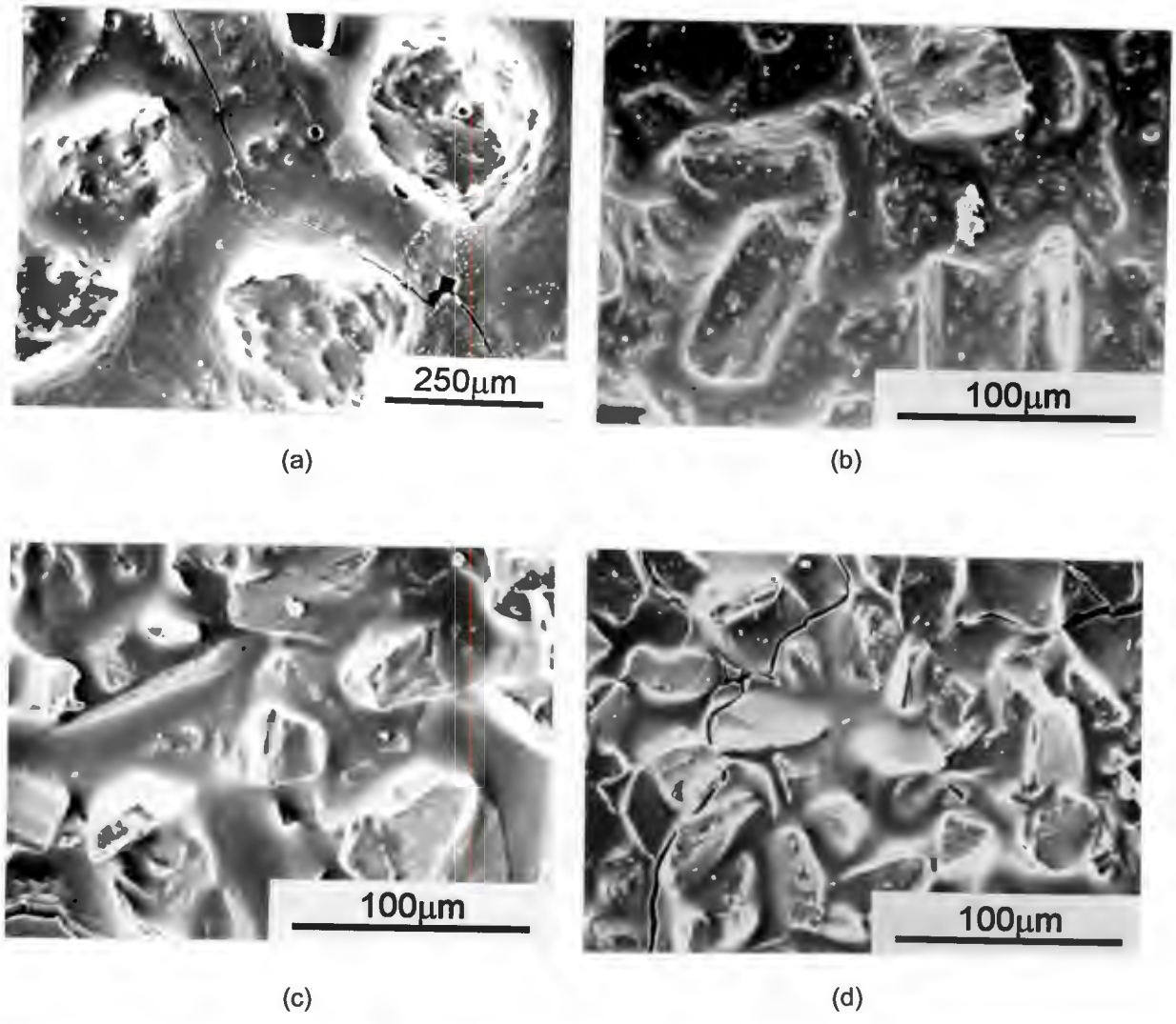

Figure 4.26: Surface morphologies of the four grades of alumina abrasive belt. (a) 80 grade, (b) 220 grade, (c) 400 grade, and (d) 600 grade.

Table 4.8: Average abrasive particle sizes, particle distribution densities, and the surface roughness for each grade of Al_2O_3 abrasive belt.

Abrasive belt grade	80	220	400	600
Average particle diameter (μm)	260	70	30	15
Distribution density (particles mm^{-2})	7	163	375	650
Surface roughness, R_a (μm)	21.6	18.1	12.9	8.4

4.3.1.1 Effect of the base PP polymer

The abrasive wear rates for the three unfilled polypropylene grades are graphically illustrated in Figure 4.27. The 1040K grade shows some improvement in abrasion resistance compared to the S1100L and the S1147H grades. This is particularly evident when the polymers are worn against the large sized Al_2O_3 abrasive belt, the 1040K grade displaying a 20% decrease in wear rate compared to the S1100L grade. With abrasion against the smaller grit size belts (220 and 400), this improvement in wear resistance is less distinct. A 9% increase in wear resistance is noted in this instance for the 1040K grade over the S1100L polymer. Results for the tests conducted on the fine 600 grade Al_2O_3 belt show no variation in the wear performance of the three PP grades.

The scanning electron micrographs of Figures 4.28 and 4.29 indicate the typical ductile wear modes prevalent for polypropylene during abrasion. The development of the wear surfaces is dominated by the ductile deformation of the material, characterised by a microploughing process. As polymer material comes into contact with the abrasive belt, the hard alumina particles are able to penetrate into the softer polymer, forming a series of grooves as material is forced up in ridges to the front and to the side of the abrasive particle (Figure 4.28a). After successive traverses of the sample across the abrasive belt, wear debris is produced and removed from the polymer surface.

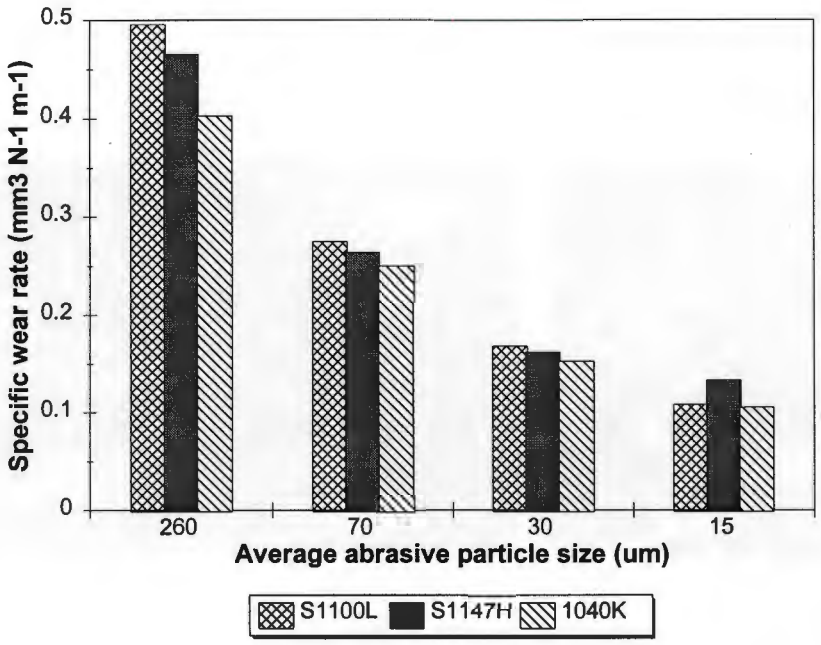

Figure 4.27: Abrasive wear results for the unfilled polypropylene grades as a function of the abrasive belt particle size. Against the coarse abrasive belt, the 1040K polypropylene grade shows an improvement in wear resistance of ~20% over the S1100L material. This improvement in wear resistance is less distinct against the smaller particle sized abrasive belts.

Figure 4.28b is a micrograph of wear debris on a 220 Al_2O_3 belt after testing. The degree of deformation of the polymer is a function of the size of abrasive particle. Abrasion against the coarse abrasive belt (Figure 4.29a) results in severe material deformation and the formation of large grooves on the wear surface. These grooves are approximately 100 μm wide. The wear surface resulting from abrasion against the finer grit belts shows less severe material deformation and a decrease in the average groove width produced by the alumina particles (Figure 4.29b).

Table 4.9: Specific wear rates measured against the four different sizes of alumina abrasive belt for the comparative polymers. Polypropylene (S1100L) values are included for comparison.

Polymer	Specific wear rate ($mm^3 N^{-1} m^{-1}$)			
	80 (260μm)	**220 (70μm)**	**400 (30μm)**	**600 (15μm)**
S1100L	0.495	0.28	0.17	0.11
PMMA	0.57	0.53	0.36	0.21
PC	0.51	0.35	0.20	0.13
ABS	1.32	0.94	0.53	0.37
HDPE	0.35	0.15	0.07	0.09

HDPE shows the best wear resistance of the five polymers and is also the only polymer to have superior wear behaviour compared to the polypropylene grades. The wear surface morphology of the HDPE is very similar to that of the PP with extensive ductile ploughing of the material and groove formation (Figure 4.30a). The other three polymers all exhibit brittle wear modes as observed in Figures 4.30b-d. These brittle wear modes are associated with higher material loss and increased wear rates. The wear rate of the ABS is considerably higher than PMMA and PC against all the abrasive belt grit sizes.

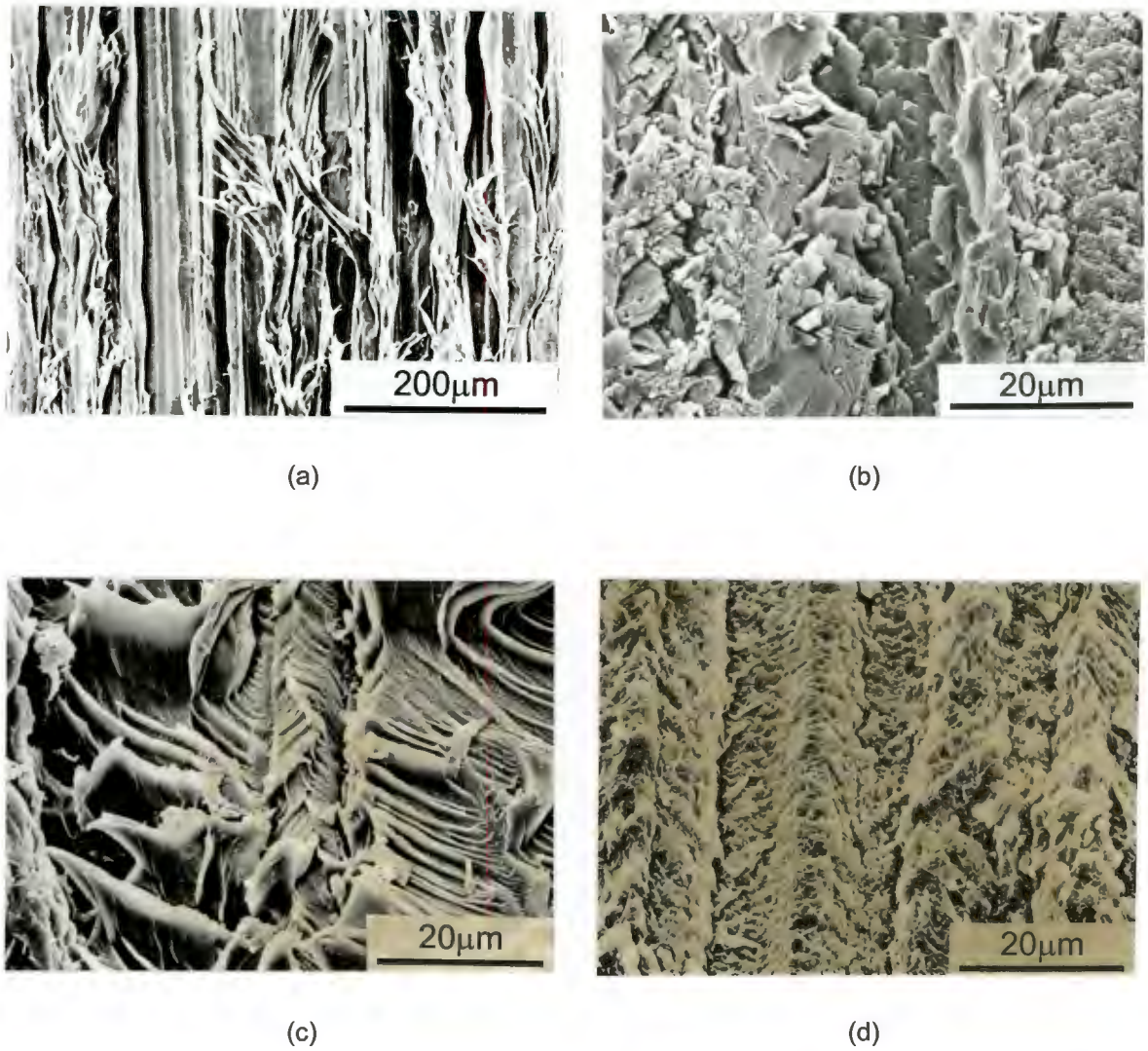

Figure 4.30: Scanning electron micrographs of the wear surfaces of the four comparative polymers as worn against a 220 grit Al_2O_3 belt. (a) HDPE exhibits typical ductile deformation while brittle wear modes are observed for (b) PMMA, (c) PC, and (d) ABS.

4.3.1.3 Effect of filler addition on the abrasive wear rate

Tables 4.10 and 4.11 display the abrasive wear results of the S1100L and the S1147H filled composites, respectively. The wear data of selected fillers are highlighted in Figures 4.31 and 4.32, showing the influence of filler content on the wear rate for abrasion against both a coarse particle size belt (260 μm) and a fine particle size belt (30 μm).

Table 4.10: Abrasive wear results for the filled composites compounded with the base polypropylene, S1100L.

Filler type	Filler content (wt%)	Abrasive belt			
		80 (260 μm)	220 (70 μm)	400 (30 μm)	600 (15 μm)
		Specific wear rate ($mm^3 N^{-1} m^{-1}$)			
talc	10	0.53	0.30	0.15	0.11
	20	0.58	0.35	0.17	0.12
	40	0.72	0.45	0.21	0.13
	60	1.28	0.64	0.33	0.22
fly ash	10	0.58	0.29	0.18	0.11
	20	0.66	0.32	0.19	0.14
	40	0.87	0.42	0.26	0.21
	60	1.38	0.59	0.37	0.26
$CaCO_3$	10	0.54	0.30	0.19	0.12
	20	0.50	0.33	0.22	0.13
	40	0.77	0.38	0.24	0.18
	60	1.27	0.55	0.33	0.20
$BaSO_4$	10	0.54	0.29	0.15	0.10
	20	0.56	0.29	0.19	0.16
	40	0.73	0.38	0.23	0.17
	60	1.04	0.50	0.32	0.19
Steaplast talc	10	0.58	0.30	0.20	0.09
	20	0.71	0.32	0.18	0.10
	40	0.79	0.34	0.22	0.13
china clay	10	0.74	0.30	0.18	0.13
	20	0.60	0.35	0.19	0.14
	40	0.78	0.39	0.23	0.16
wollastonite (fine)	10	0.57	0.30	0.18	0.14
	20	0.67	0.33	0.17	0.13
	40	0.97	0.36	0.22	0.15
wollastonite (coarse)	10	0.67	0.28	0.17	0.11
	20	0.76	0.32	0.21	0.12
	40	0.81	0.30	0.23	0.13

Table 4.11: Abrasive wear results for the filled composites compounded with the base polypropylene, S1147H.

Filler type	Filler content (wt%)	Abrasive belt			
		80 (260 μm)	220 (70 μm)	400 (30 μm)	600 (15 μm)
		Specific wear rate ($mm^3 N^{-1} m^{-1}$)			
Steaplast talc	10	0.64	0.30	0.19	0.13
	20	0.49	0.28	0.18	0.13
	40	0.65	0.37	0.23	0.16
china clay	10	0.50	0.29	0.16	0.12
	20	0.49	0.27	0.17	0.14
	40	0.71	0.33	0.22	0.14
wollastonite (fine)	10	0.64	0.27	0.17	0.12
	20	0.56	0.30	0.19	0.12
	40	0.76	0.34	0.19	0.15
wollastonite (coarse)	10	0.58	0.27	0.17	0.12
	20	0.65	0.27	0.17	0.12
	40	0.85	0.34	0.19	0.12

Overall, the addition of the mineral fillers to the polypropylene matrix results in a deterioration of the wear performance of the filled composites, as measured by the volume loss of material.

Although a decrease in abrasive particle size on the Al_2O_3 abrasive belt results in a decrease in material loss from the sample, there is no distinct improvement in wear behaviour compared to the unfilled polypropylene grades worn against the respective abrasive counterfaces. This lack of pattern is illustrated in Tables 4.12 and 4.13 and Figures 4.33 and 4.34 which show values of composite abrasion rates calculated relative to those of the S1100L and S1147H polypropylene grades, respectively, for each abrasive grit size.

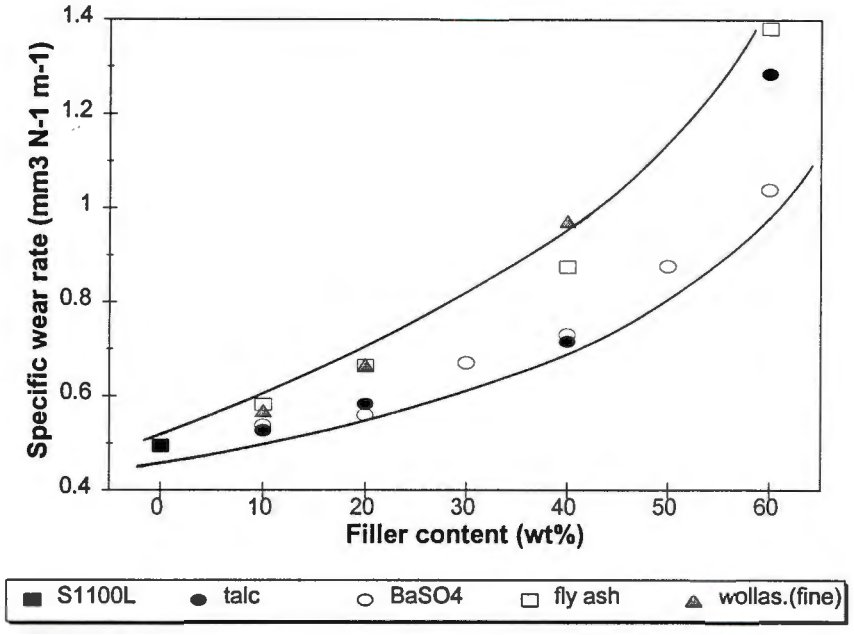

Figure 4.31: Variation in specific wear rate with filler content for tests performed against the coarse abrasive belt (260 μm). Results for selected fillers compounded with the S1100L base PP grade are shown.

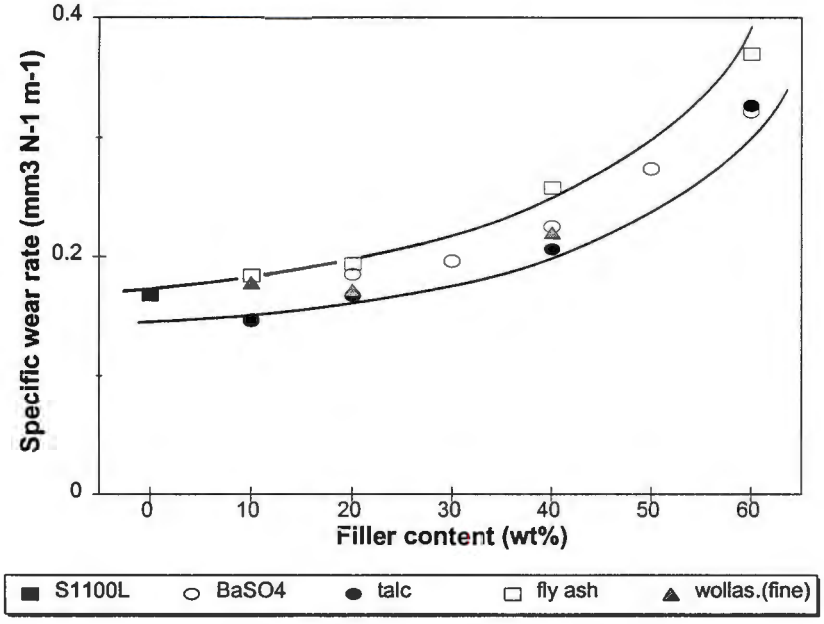

Figure 4.32: Variation in specific wear rate with filler content for tests performed against the 400 grade abrasive belt (30 μm). Results for selected fillers compounded with the S1100L base PP grade are shown.

The four filled S1100L composites shown in Figure 4.33 display the varying trends of abrasion rate relative to the unfilled S1100L polypropylene. The fly

ash and $BaSO_4$ blends show higher relative abrasion against the coarse 80 grade and the ultra fine 600 grade belts than against the 220 and 400 grade Al_2O_3 belts.

An opposing trend is highlighted by the 20 wt% *Steaplast* talc and coarse wollastonite samples. In this case, a progressive improvement in relative abrasion with decreasing abrasive particle size is observed.

Similar variances are observed for selected S1147H composites shown in Figure 4.34. The china clay and *Steaplast* talc composites show little change in relative abrasion for all abrasive particle sizes. In contrast, the two wollastonite grades (10 and 40 wt%) show the same trend of decreasing relative abrasion rate with decreasing abrasive particle size. It is noted that under conditions of very mild abrasion produced by the 600 grade Al_2O_3 belt, the wear rates of both these wollastonite composites is less than that of the unfilled S1147H polypropylene grade. It is also seen that the influence of high filler content on the abrasion rate is strong, most notably when the composites are abraded against the coarse 80 Al_2O_3 belt. From Table 4.12 this influence of filler content is clearly apparent for all the high filler content composites. At low filler additions of 10 to 20 wt%, and for some fillers at 40 wt%, a relative abrasion rate compared to the unfilled polypropylene grades of around 1.3 is common. At higher loading, especially at 60 wt% filler addition, there is a marked increase in the relative abrasion rate, with values approaching 2. The 60 wt% fly ash and $CaCO_3$ composites have normalised values of 2.76 and 2.54, respectively.

Table 4.12: Normalised abrasive wear rates of the filled composites relative to the base polymer, S1100L.

Filler type	Filler content (wt%)	Abrasive belt			
		80 (260 μm)	220 (70 μm)	400 (30 μm)	600 (15 μm)
		Normalised wear rate			
talc	10	1.06	1.09	0.89	1.01
	20	1.16	1.27	1.01	1.11
	40	1.44	1.64	1.25	1.20
	60	2.56	2.32	1.96	2.03
fly ash	10	1.16	1.05	1.07	1.02
	20	1.32	1.16	1.13	1.30
	40	1.74	1.53	1.55	1.94
	60	2.76	2.15	2.02	2.41
$CaCO_3$	10	1.08	1.09	1.13	1.11
	20	1.0	1.20	1.31	1.20
	40	1.54	1.38	1.43	1.67
	60	2.54	2.0	1.96	1.85
$BaSO_4$	10	1.08	1.05	0.89	0.93
	20	1.12	1.05	1.13	1.48
	40	1.46	1.38	1.37	1.57
	60	2.08	1.82	1.91	1.76
Steaplast talc	10	1.16	1.09	1.19	0.83
	20	1.42	1.16	1.07	0.93
	40	1.58	1.24	1.31	1.20
china clay	10	1.48	1.09	1.07	1.20
	20	1.20	1.27	1.13	1.30
	40	1.56	1.42	1.37	1.48
wollastonite (fine)	10	1.14	1.09	1.07	1.30
	20	1.34	1.20	1.01	1.20
	40	1.94	1.31	1.31	1.39
wollastonite (coarse)	10	1.34	1.02	1.01	1.02
	20	1.52	1.16	1.25	1.11
	40	1.62	1.09	1.37	1.20

Table 4.13: Normalised abrasive wear rates for the filled composites relative to the base polymer, S1147H.

Filler type	Filler content (wt%)	Abrasive belt			
		80 (260 μm)	220 (70 μm)	400 (30 μm)	600 (15 μm)
		Normalised wear rate			
Steaplast talc	10	1.37	1.13	1.17	0.98
	20	1.05	1.06	1.11	0.98
	40	1.40	1.40	1.42	1.20
china clay	10	1.08	1.10	0.99	0.90
	20	1.05	1.02	1.05	1.05
	40	1.53	1.25	1.36	1.05
wollastonite (fine)	10	1.37	1.02	1.05	0.90
	20	1.20	1.13	1.17	1.90
	40	1.63	1.29	1.17	1.13
wollastonite (coarse)	10	1.25	1.02	1.05	0.90
	20	1.40	1.02	1.05	0.90
	40	1.83	1.29	1.17	0.90

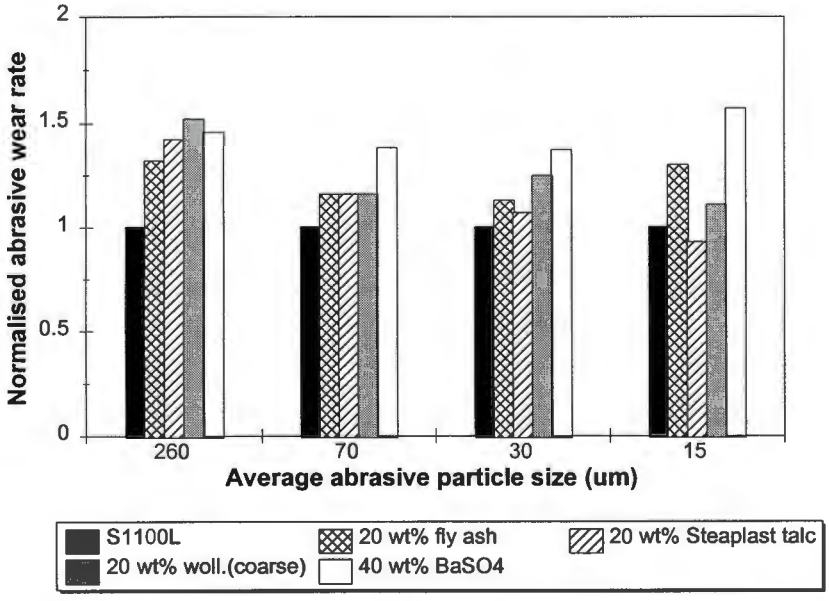

Figure 4.33: Abrasive wear rates of selected filled composites relative to the base polymer S1100L as a function of abrasive particle size.

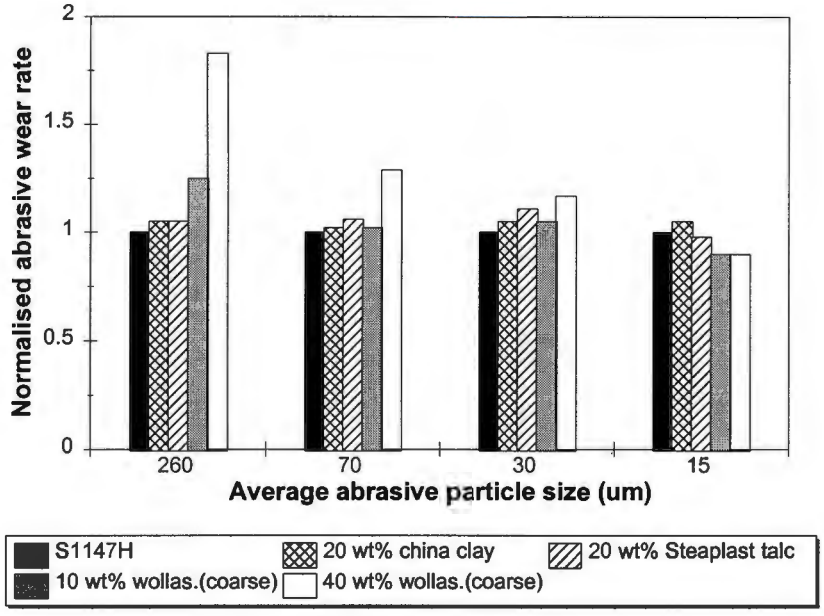

Figure 4.34: Abrasive wear rates of selected filled composites relative to the base polymer S1147H as a function of abrasive particle size.

Although the filled polypropylene composites show wear rates of a similar order of magnitude at equivalent filler content, there are some aspects of this behaviour to note. As with the tensile properties of the studied composites there appears to be some dependence, though it is not as well defined, of the abrasive wear resistance of the materials on the physical properties of the included fillers.

4.3.1.3.1 Effect of filler particle shape and size

Under mild abrasive conditions (400 and 600 belts), the talc and $BaSO_4$ filled composites show the best wear resistance and at low filler loading (10 to 20 wt%) outperform the unfilled S1100L polypropylene grade. The large spherical fly ash-filled composites show the most pronounced decrease in abrasive wear resistance of all the fillers against both the coarse and fine abrasive belts. The results of the abrasive tests for a 60 wt% fly ash-filled sample worn against the 80 grade Al_2O_3 belt reflect an almost threefold increase in wear rate over that of the base S1100L polypropylene sample.

Examination of the wear surfaces of the filled composites by scanning electron microscopy highlighted differences in the material deformation behaviour of the various fillers.

The development of the abraded surfaces of the filled composites is similar to that of the unfilled polypropylene materials where ductile deformation is the dominant wear mode. Figures 4.35a and b show the wear surfaces of a 40 wt% talc composite that have been abraded against coarse 80 grade and fine 400 grade Al_2O_3 belts, respectively. As with the unfilled samples there is a difference in the wear groove width produced on the surface by the abrasive particles. Although this microploughing process is the dominant deformation mechanism of all the composites investigated, higher magnification viewing of the abraded surfaces show there to be different micro-deformation and micro-fracture mechanisms operating when the filler shape and size is varied. This is illustrated in Figure 4.36 which compares the worn surfaces of a 40 wt% talc sample and a 40 wt% fly ash sample, both abraded under identical conditions.

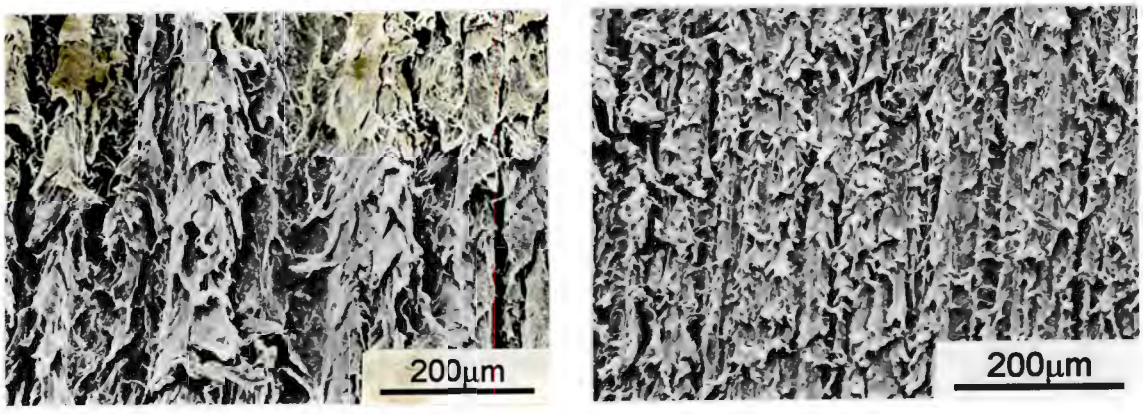

(a) (b)

Figure 4.35: Scanning electron micrographs of a 40 wt% talc-filled composite after abrasion by the (a) coarse 80 grade (260 µm) and (b) the fine 400 grade (30 µm) Al_2O_3 abrasive belts. The wear surfaces emphasise the mode of ductile deformation occurring during abrasion of the filled composites. The other filled blends showed similar appearances.

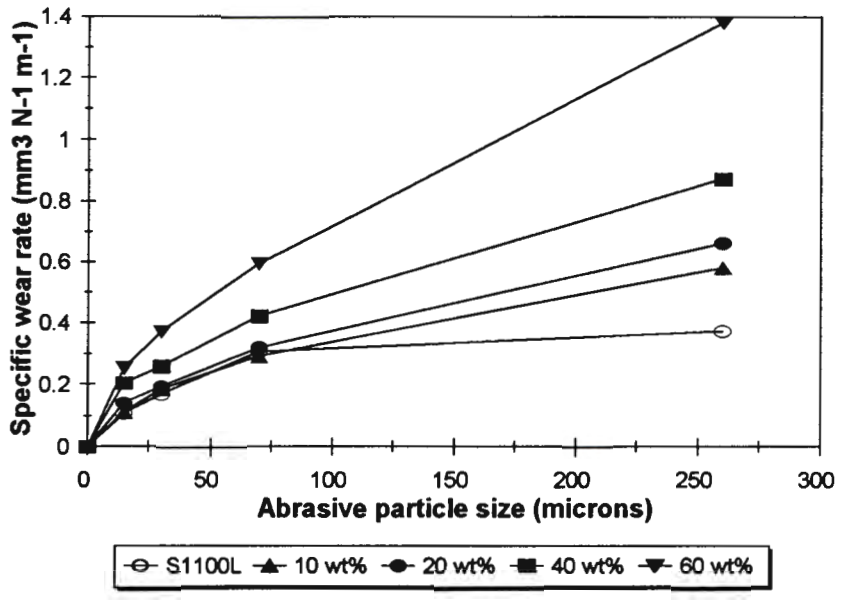

Figure 4.37: Variation of specific wear rate with abrasive particle size for the fly ash composites as a function of filler content.

For most of the samples, increasing the counterface particle size from 15 μm to 30 μm results in a wear rate increase of approximately 1.5 times. A further increase in particle size to 70 μm (220 belt) imparts an increasing wear rate factor of 1.5 to 1.8. The change from the 220 belt to the 80 grade belt (260 μm), a fourfold increase in Al_2O_3 particle size, results in a twofold increase in wear rate.

4.3.2 Single-point scratch tests

4.3.2.1 Rockwell C Diamond indentor tests

The scratch track widths of the three polypropylene grades and the comparative polymers, as measured for each test load, are detailed in Table 4.14. The widths of the scratches were essentially constant along the length of the scratch. Reported values are an average of five measurements per scratch.

Table 4.14: Measured scratch track widths at each test load for the polypropylene grades and the comparative polymers.

Polymer	Scratch track width at normal test load (μm)				
	0.9N	2N	3N	5N	10N
S1100L	96	154	192	250	346
S1147H	96	144	183	231	327
1040K	86	144	183	240	346
PMMA	-	77	106	144	212
PC	96	134	164	222	308
ABS	96	144	173	240	335
HDPE	144	202	240	308	450

The three polypropylene grades show little variation in scratch width across the range of test loads. Noticeable differences are observed for the four other polymers. The PMMA exhibits the most marked resistance to the scratch indentor, with narrower track widths measured at all test loads. The HDPE sample, at the other extreme, has the least resistance to scratch indentation. The PC and ABS polymers show similar scratch values at test loads below 3 N. At the higher loads of 5 N and 10 N, polycarbonate displays improved scratch resistance over ABS.

Figure 4.38 shows a plot of the results of Table 4.14. It is noted that the individual polymers all have different responses to scratch indentation.

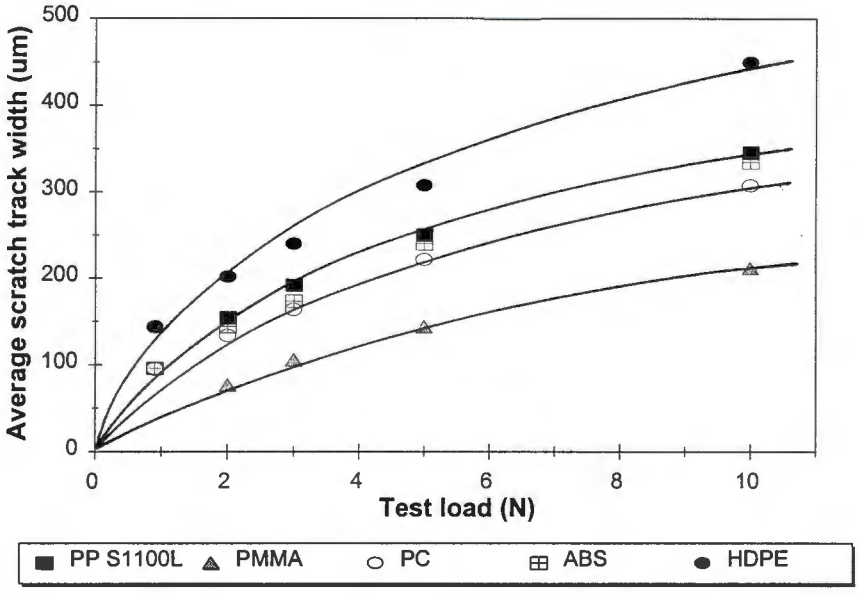

Figure 4.38: Variation in scratch track width with test load for the polypropylene grade S1100L and the four comparative polymers.

Electron microscopy analysis of the polymer scratch tracks shows several variations of scratch morphology for the respective polymers. The tracks shown in Figure 4.39 are all from tests performed using a 10 N test load. The most scratch-resistant polymers, PMMA and PC, show featureless clear scratch tracks with shoulders on both sides. The ABS track shows some deformation bands and fracture of the polymer concave to the sliding direction. The HDPE sample shows no ridging on the track edge but grooving of the polymer surface in the track itself is observed. The three polypropylene samples have similar track morphologies, characterised by deformation bands that are oriented convexly with respect to the sliding direction. No fracture of any of the polypropylene grades is observed, however high magnification viewing of the scratch track shows localised melting and roll formation of the PP polymer occurring at the track centre (Figure 4.39b).

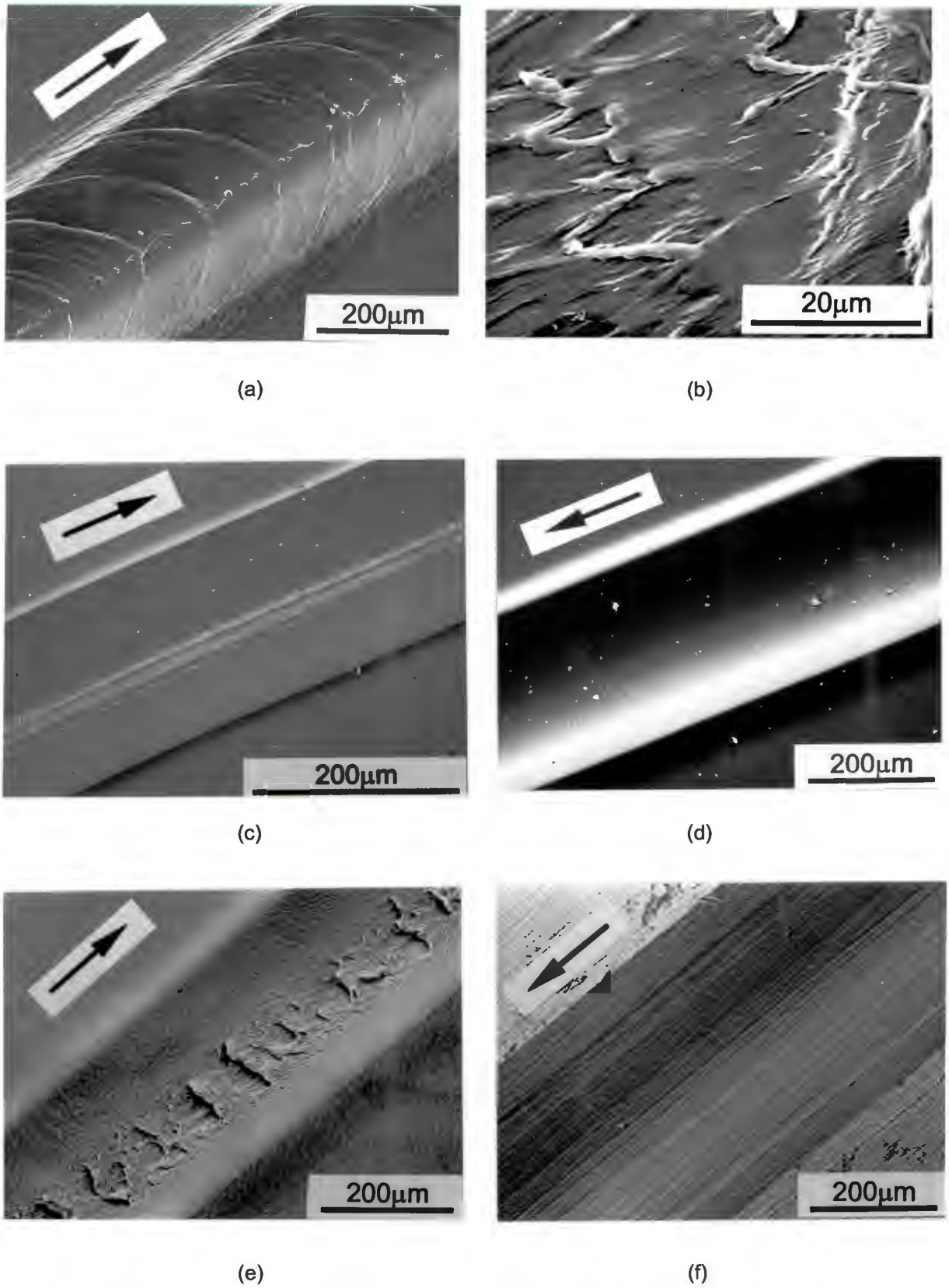

Figure 4.39: Scanning electron micrographs showing the variation in scratch track morphology of the polymers. The tracks were all produced using a 10 N test load. (a) S1100L PP, (b) roll formation in PP track, (c) PMMA, (d) PC, (e) ABS, (f) HDPE. The arrows indicate the direction of scratching.

4.3.2.1.1 The effect of fillers on the scratch behaviour

The influence of the addition of mineral fillers is not as marked for scratch indentation as it is for general abrasion resistance. Table 4.15 shows the average scratch track widths for a range of selected filled composites. There is little difference in the scratch track dimensions of the filled and unfilled polypropylenes at loads less than 3 N. At the higher loads of 5 N and 10 N the filled composites exhibit wider scratch tracks than the unfilled parent polymer, and enhanced material damage.

Table 4.15: Average scratch track widths (μm) for each test load for selected filled polypropylene composites. Track widths were measured from scanning electron micrographs.

	Load on Rockwell C diamond indentor (N)				
Filled PP composite	**0.9 N**	**2 N**	**3 N**	**5 N**	**10 N**
PP S1100L	96	154	192	250	346
fly ash 10 wt%	106	170	200	290	420
fly ash 60 wt%	96	157	190	260	340
talc 10 wt%	96	180	195	250	390
talc 60 wt%	100	~200	~250	~340	~450
wollas. 10 wt% (coarse)		~150	~190	265	390
wollas. 40 wt% (coarse)		~160	~210	280	390
Steaplast talc 10 wt%		~170	~210	280	395
Steaplast talc 40 wt%		~140	~200	265	400

There are no definite trends observed from the reported results. What is evident is that each filler shows individual trends and characteristic track morphologies.

The *Steaplast* talc- and wollastonite-filled composites show very similar scratch behaviour. There is no influence of filler content on the scratch performance with both the 10 wt% and 40 wt% composites having equivalent scratch widths. SEM micrographs of the respective scratch tracks (at 10 N load), show both composites to exhibit a 'stick-slip' deformation mechanism, which is more pronounced at higher filler contents (Figure 4.40). The wollastonite composite, in Figure 4.40b, shows exposure of the large filler particles within the scratch track. This is not evident for the *Steaplast* talc composites due the fine nature of the filler particles and the enhanced adhesion between the polypropylene and the talc.

The fly ash composites of 10 wt% and 60 wt% filler content show deformation bands occurring in the scratch track, but no 'stick-slip' or tearing mechanism is observed (Figure 4.41). Furthermore, it is noted that the 60 wt% composite shows improved scratch performance over the 10 wt% grade. This difference is emphasised at higher test loads.

Contrary to the results of the fly ash composites, the talc composite of 10 wt% filler has better scratch resistance than the corresponding 60 wt% grade. The 60 wt% talc composite, in fact, shows the poorest scratch performance of all the filled grades. The SEM micrographs of the talc composites show gross deformation and damage of the scratch track. Delamination is evident as material is pulled away from the surface after contact with the diamond indentor (Figure 4.41c).

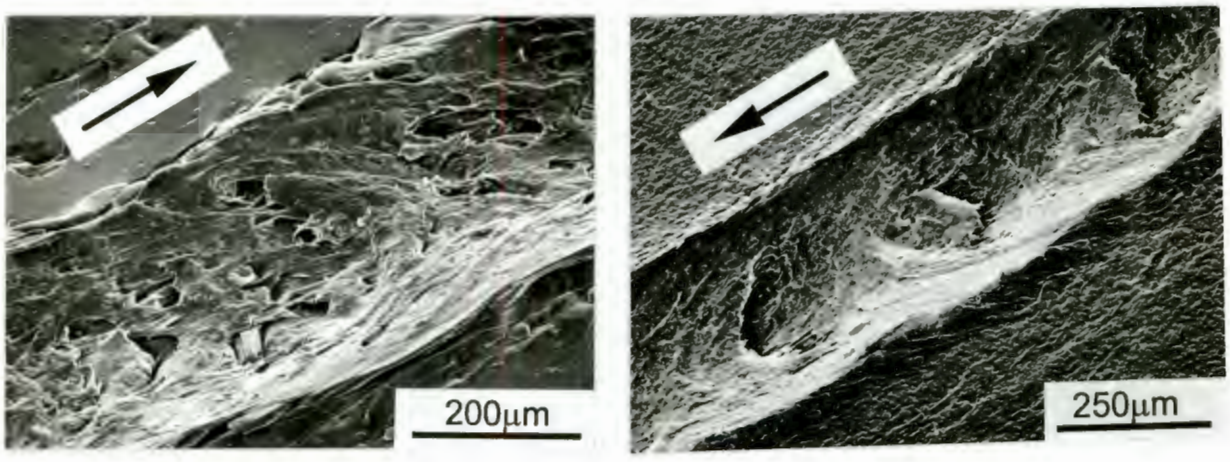

(a) (b)

Figure 4.40: Scanning electron micrographs of the scratch tracks of the filled PP composites measured under a test load of 10 N: (a) 40 wt% coarse wollastonite and (b) 40 wt% *Steaplast* talc showing a 'stick-slip' deformation mechanism. Sliding direction is indicated by the arrow.

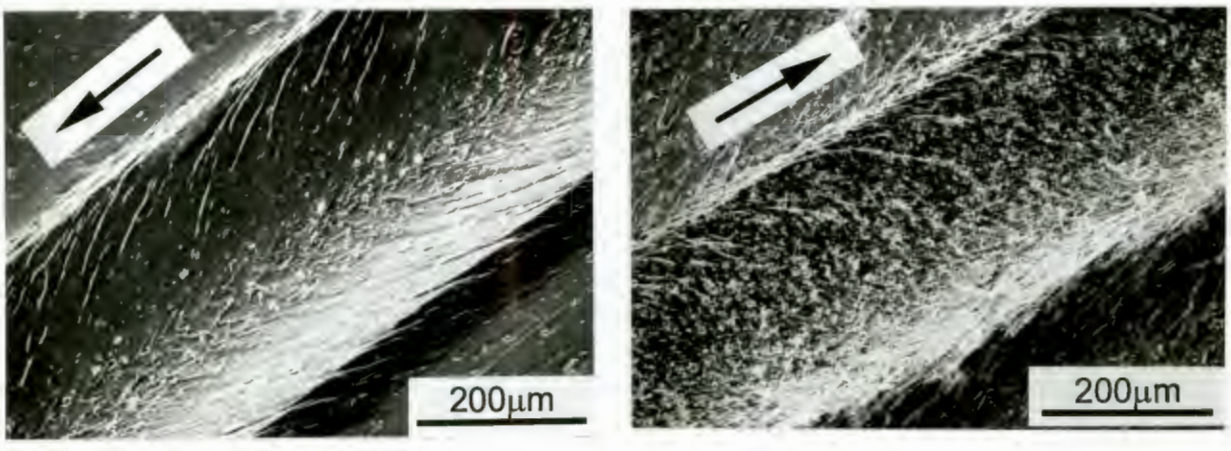

(a) (b)

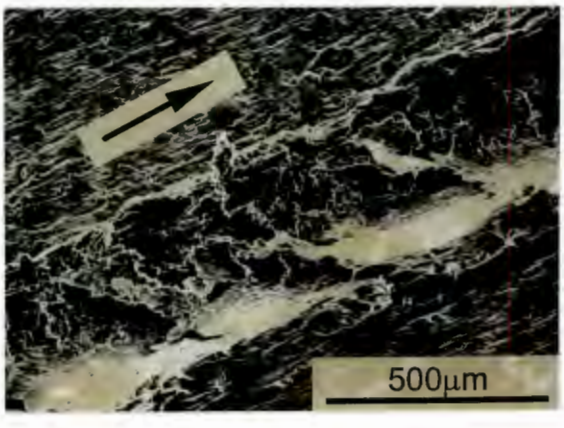

(c)

Figure 4.41: (a) 10 wt% and (b) 60 wt% fly ash composites. The deformation bands and the sliding direction are indicated on the scratch tracks. (c) 60 wt% talc composite showing severe material damage and delamination of the polymer within the track.

4.3.2.2 Variable included angle scratch tests

The results for the scratch tests performed on the polymeric materials using stainless-steel indentors with included half-angles ranging from 15° to 85° are detailed in Table 4.16. The results are given both in terms of the width of the resultant scratch track and the mode of material deformation. In some cases, the scratch track was not visible on the polymer surface due to elastic relaxation. Three different scratch morphologies, as illustrated in the schematic of Figure 4.42, were identified and are discussed in the following section. For all the polymers tested, there is a transition in scratch deformation mode with the variation in indentor angle.

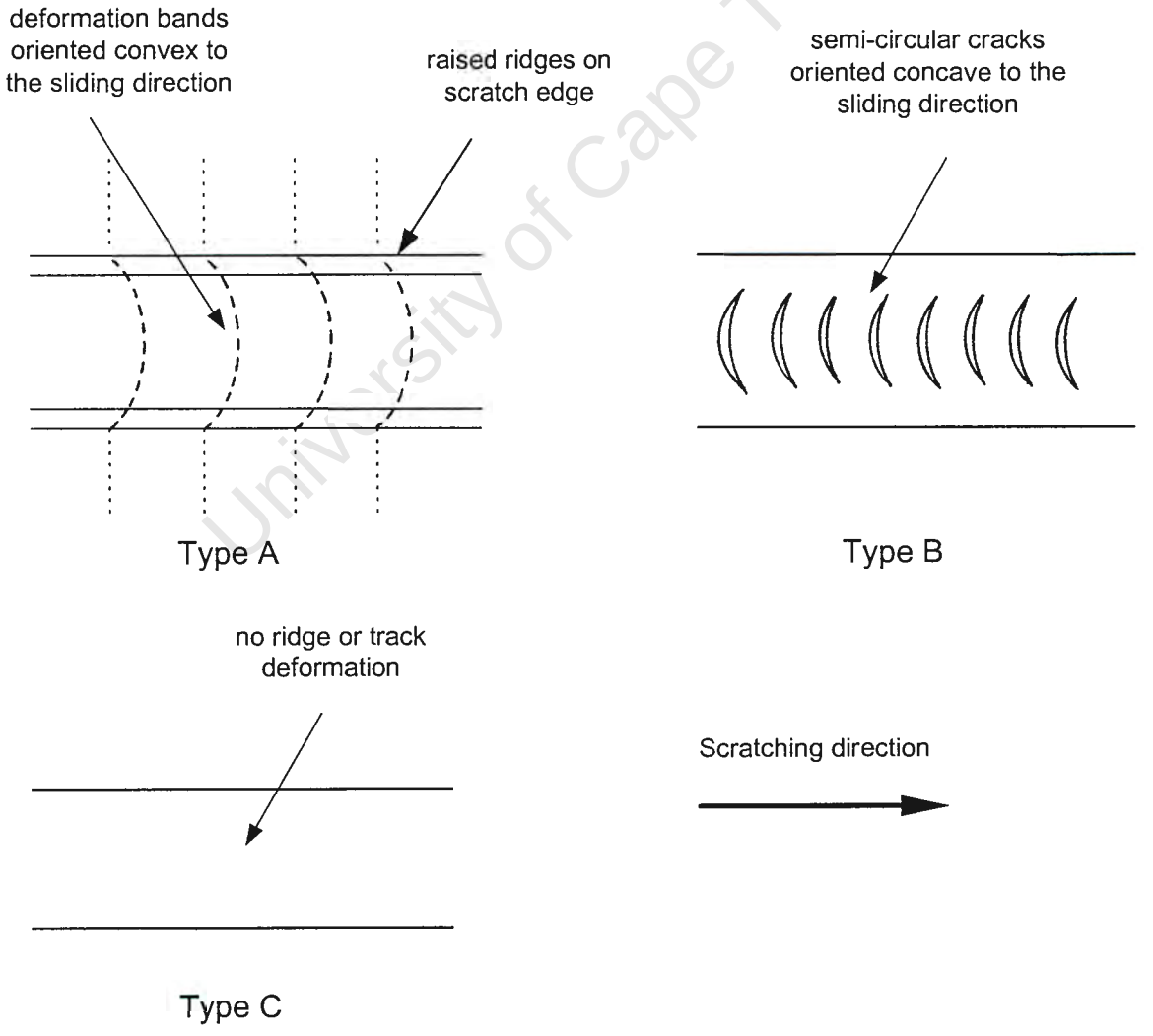

Figure 4.42: Schematic illustrating the three different scratch morphologies identified.

Table 4.16: Scratch track widths (μm) and deformation mechanisms for selected filled and unfilled polypropylenes and the comparative polymers. Values are measured using a 2 N test load.

Polymer	Indentor included half-angle					
	15°	**30°**	**45°**	**60°**	**75°**	**85°**
S1100L	113 cutting	125 cutting	170 type A	175 type C	255 type C	445 type C
1147H	120 cutting	120 cutting	170 type C	170 type C	246 type C	400 type C
PMMA	87 cutting	110 cutting	106 type B	-	-	-
PC	100 cutting	120 type B	150 type B	-	-	-
ABS	145 cutting	130 type B	200 type A	type C	-	-
HDPE	110 grooving	135 type A	163 type C	166 type C	244 type C	-
talc 60 wt%	200 cutting	210 cutting	190 ploughing	200 type A	-	-
fly ash 60 wt%	208 cutting	217 cutting	175 ploughing	-	-	-
Steaplast talc 40 wt%	193 cutting	155 cutting	155 ploughing	172 type C	-	-
wollas. (coarse) 40 wt%	160 cutting	145 cutting	170 ploughing	-	-	-

4.3.2.2.1 Polypropylene and the comparative polymers

The unfilled polypropylene grades exhibited a ductile cutting deformation mode at small included indentor angles. This cutting process is characterised by raised scratch track ridges and the formation and detachment of polymer chips, as shown in Figure 4.43a. At higher indentor angles, two different scratch morphologies were observed. Type A scratches show deformation bands running convex to the sliding direction and raised track edges are

visible (Figure 4.43c). Type C scratches show no ridge deformation and smooth track surfaces (Figure 4.43d).

The comparative polymers display a variety of scratch transition modes. The PMMA, PC, and ABS polymers all show a similar cutting mode for the 15° track, with severe material damage and polymer chip removal from the surface, as shown in Figure 4.43b. The deformation in this case is brittle in nature. In contrast, the scratch damage of HDPE is characterised by deep grooving of the material with limited ridging occurring and no evidence of material chip formation or detachment (Figure 4.43g).

At higher angles, the mechanisms of deformation for each polymer differ. PMMA shows a brittle cutting process at angles of 15° and 30° with the average scratch width markedly narrower than for other polymers. A transition to a type B scratch is observed for the 45° track. This scratch is characterised by no deformation banding but surface cracking occurs concave to the sliding direction (Figure 4.43e). At higher indentor angles the scratches are no longer visible due to elastic relaxation effects.

The PC sample exhibits a similar transition from a brittle cutting mode to typical type B scratches though this transition occurs for the 30° track in comparison to the 45° for the PMMA sample. ABS shows a full transition from cutting and surface cracking, as shown in Figure 4.43f, to deformation banding (type A) and clear scratch tracks (type C) at higher indentor angles. The HDPE sample also goes through a transition from the groove formation to deformation bands occurring, to typical type C scratches at high angles.

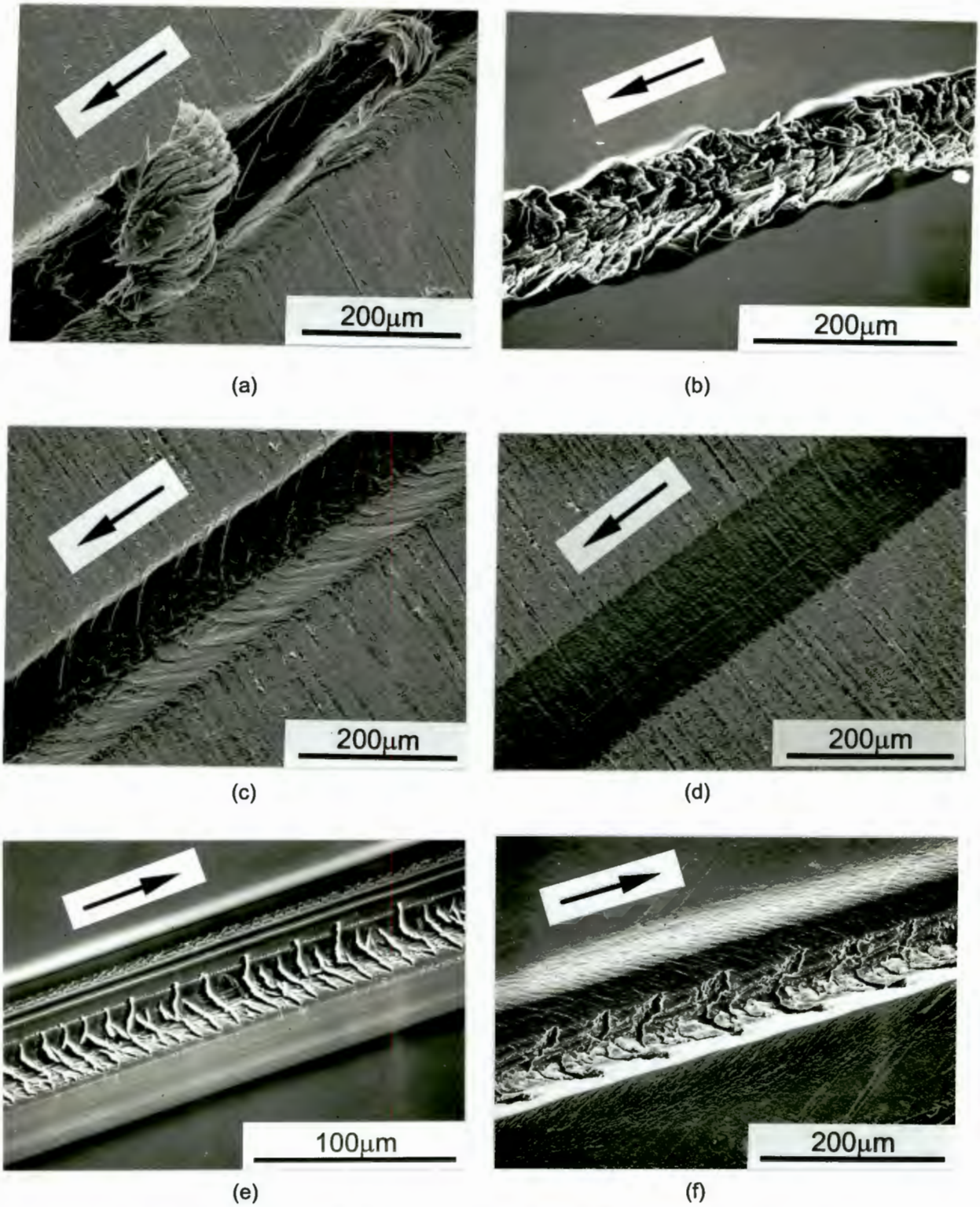

Figure 4.43: Scanning electron micrographs illustrating the different scratch morphologies. (a) ductile cutting in PP (15° included indentor half-angle), (b) brittle cutting in PMMA (30° indentor), (c) Type A scratch showing deformation banding in PP (45° indentor), (d) type C scratch with no ridge or track deformation in PP (60° indentor), (e) type B scratches showing the semi-circular cracks oriented concave to the sliding direction in PMMA (45° indentor) and (f) ABS (30° indentor).

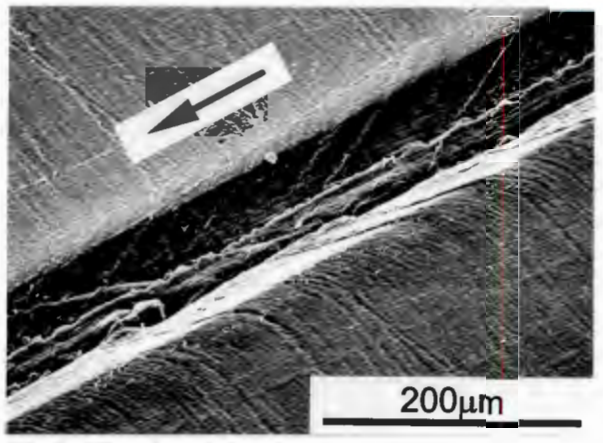

(g)

Figure 4.43 cont.: Groove track morphology of HDPE (15° indentor), There is no evidence of polymer chip formation or removal.

4.3.2.2.2 The effect of the fillers on the variable included angle scratch behaviour

The filled polypropylene composites reveal similar scratch morphologies to the unfilled PP samples at small included indentor angles where a ductile cutting mode is evident. The scratch widths measured for these filled samples are wider than the unfilled grades and show enhanced ridging and material deformation. In particular, the talc-filled composites show increased material deformation and wear debris formation in comparison to the other filled composites, as shown in Figure 4.44a and b. Furthermore, there is a noticeable increase in the level of stress whitening occurring in the deformation regions on the track ridges of the talc samples.

At 45°, the scratch tracks on the filled composite specimens are characterised by ductile ploughing of the polymer and ridging on the track edge (Figure 4.44c). No deformation banding is observed. At higher included angles type C scratches are evident.

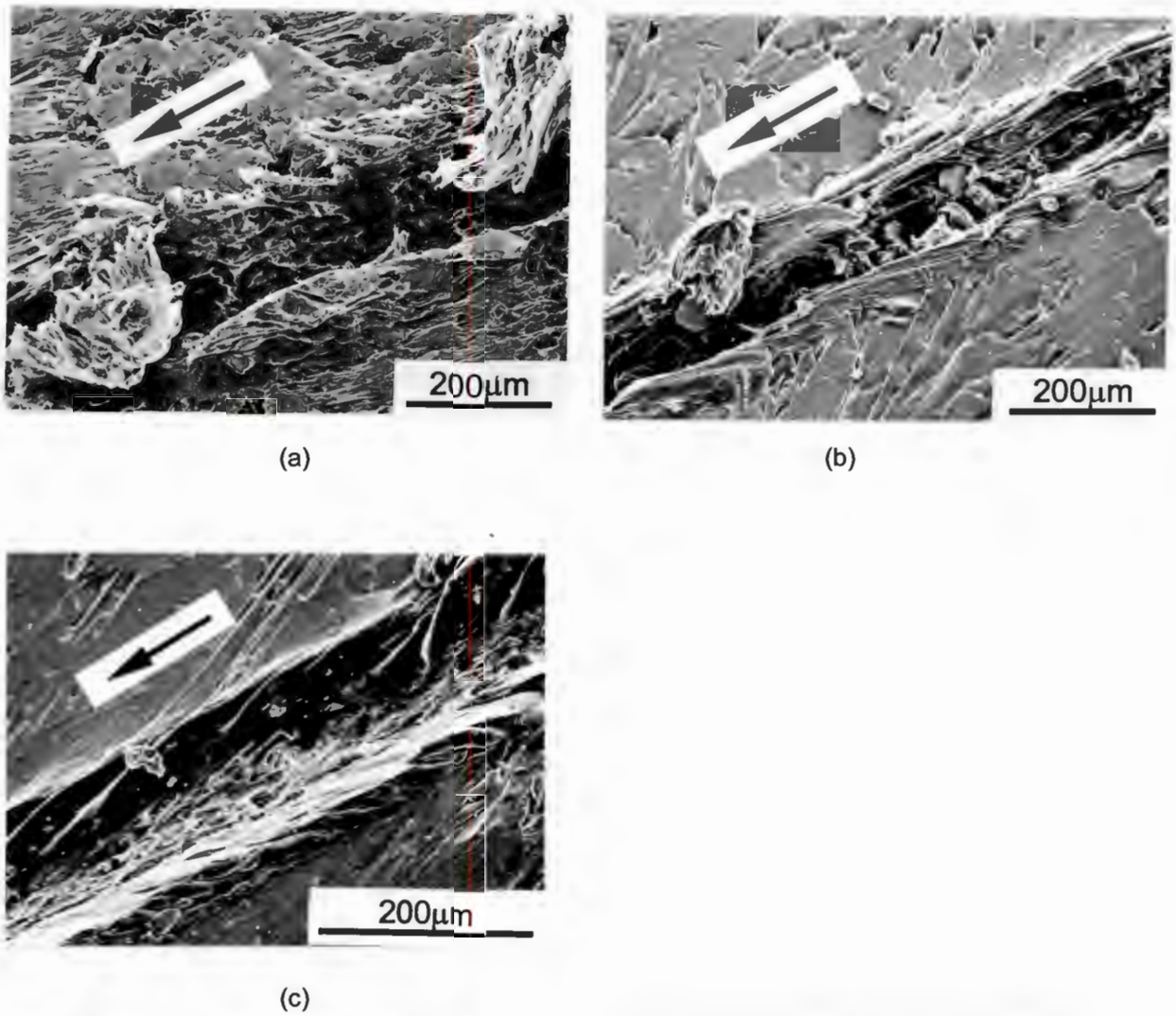

Figure 4.44: (a) Gross deformation of track ridge, stress whitening and formation of wear debris in a 60 wt% talc composite (15° indentor). Compare the deformation of the talc sample (a) with that of (b) a wollastonite composite under identical scratch conditions. (c) Ploughing scratch mode produced by a 45° indentor for a wollastonite composite.

4.3.3 Abrasive scrub tests

The abrasive scrub test is a unique testing method for determining a material's resistance to mild low stress cyclical abrasion. It is commonly used in the paint industry for testing the 'washability' and the loss of sheen/gloss of paints, but has also found use in the testing of the abrasion resistance of polymer coatings. In this study, the apparatus was used as a qualitative tool

to analyse and compare the various polymers and the filled composites with respect to their surface gloss and visual appearance. Four methods of wear assessment were used, *viz.*, material deformation, gloss measurement, surface roughness, and visual ranking.

The abrasive counterface used in the scrub tests is of paramount importance to the analysis of the results via light reflectance. Initial tests employed the use of the supplied nylon bristle brush (ASTM D2486), however due to the orientation of the bristles, a variation in the wear pattern on the sample surface was observed. Subsequent tests reported in this study were performed using a commercially available nylon scouring pad (No. 96 light duty scourer pad, supplied by 3M, South Africa) which produced a more consistent wear pattern.

Figure 4.45 shows the morphology of this abrasive pad as viewed in the scanning electron microscope. It consists of a network of nylon strands and bonded alumina particles.

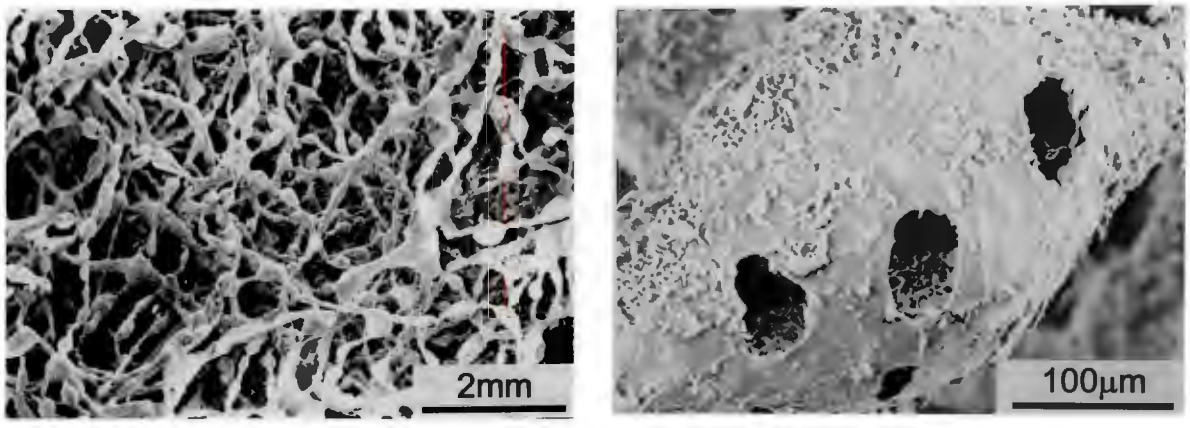

(a) (b)

Figure 4.45: Scanning electron micrographs of the network structure of the commercial nylon abrasive scourer pad used in the scrub tests. (a) Low magnification, (b) high magnification after testing showing the accumulation of polymer wear debris on the pad surface.

4.3.3.1 Result analysis by surface roughness

Surface roughness measurements of the worn surfaces of the samples were made after 10 000 abrasive cycles using a Taylor Hobson stylus profilometer. Ten measurements were taken for each sample and the average values are reported in Table 4.17 for the polypropylene and the comparative polymers.

Table 4.17: Surface roughness of the polypropylene and the comparative polymers after 10 000 cycles on the abrasive scrub tester.

Polymer	Surface roughness, R_a (μm)	Standard deviation
S1100L	1.5	0.18
S1147H	1.21	0.17
1040K	0.99	0.19
PMMA	3.54	0.56
PC	1.06	0.11
ABS	2.63	0.45

The brittle polymers, PMMA and ABS, show significantly higher R_a values, however PC has a surface roughness equivalent to that of the high crystalline polypropylene grades. An interesting point to note is the difference in R_a value between the S1100L PP and the two nucleated PP grades.

The surface roughness results of the filled composites, measured after 10000 abrasive cycles, are summarised in Table 4.18. No apparent trends were observed in the performance of the different individual fillers. Roughness values were in the range from 1.05 to 2.15 μm. Filler content of the composites appears to be the controlling factor with lower R_a values observed for the lower filler content composites. One anomaly is featured: the *Steaplast* talc showing R_a values of 1.7 μm and 1.05 μm at filler contents of 20 wt% and 40 wt%, respectively.

Table 4.18: Surface roughness values of the selected filled composites after 10 000 cycles on the abrasive scrub tester.

Polymer	Filler	Filler content (wt %)	Surface roughness, R_a (μm)	Standard deviation
S1100L			1.5	0.18
	talc	40	1.4	0.2
		60	2.0	0.2
S1147H			1.21	0.17
	Steaplast talc	20	1.7	0.3
		40	1.05	0.1
	wollastonite (15μm)	20	1.44	0.25
		40	1.4	0.12
	china clay	40	2.15	0.15

4.3.3.2 Result analysis by gloss measurement

The results of the gloss measurements during the scrub abrasive tests are summarised in Tables 4.19 and 4.20. Values recorded are the average of three readings for each sample. The tests were performed using a commercial nylon scourer pad under unlubricated conditions. The gloss readings are normalised according to the specular gloss of a black glass standard. It is important to analyse these results in conjunction with the other three methods of assessment as inconsistency can occur due to the nature of the gloss measurement. In particular, variation in the pigmentation of the polymer samples affects the gloss readings (see Appendix C).

Table 4.19: Normalised gloss readings for polypropylene and the comparative polymers at 60° and 85°.

		No. of cycles		
Polymer	**Angle (°)**	**0**	**1000**	**5000**
S1100L	60	0.48	0.17	0.24
	85	0.45	0.36	0.42
PMMA	60	0.94	0.19	0.21
	85	1.0	0.54	0.68
PC	60	1.41	0.44	0.36
	85	1.16	0.67	0.69
ABS	60	0.83	0.13	0.16
	85	1.03	0.39	0.47

A ranking order of the comparative polymers can be structured in the form: PC > PMMA > ABS > PP. Gloss measurements were taken at two angle geometry's, 60° and 85°, as the PMMA, PC, and ABS polymers can be classified as high-gloss materials. Table 4.19 shows the large fall-off in surface reflectance for these polymers when measured at 60°. At the 85° geometry this fall-off is not as significant as a transition to a predominantly matt surface occurs with the increasing number of abrasive scrub cycles.

Table 4.20: Abrasive scrub test results for the selected filled composites. (Normalised gloss readings at 85°.

			No. of cycles			
Polymer	**Filler**	**Filler content (wt%)**	**0**	**1000**	**5000**	**10 000**
S1100L			0.45	0.36	0.42	0.46
	talc	40	0.34	0.22	0.33	0.42
		60	0.25	0.17	0.30	0.38
S1147H			0.47	0.37	0.44	0.47
	Steaplast talc	20	0.37	0.31	0.37	0.41
		40	0.26	0.23	0.29	0.35
	wollastonite (15 μm)	20	0.34	0.26	0.35	0.40
		40	0.29	0.22	0.31	0.39
	china clay	40	0.17	0.13	0.24	0.33

Gloss measurement of the filled composites was performed at the 85° angle geometry as this is the preferred geometry for predominantly matt samples. As with the surface roughness measurements, there is little difference observed in the performance of the filled composites. Differences are noted with respect to the filler content with the lower wt% composites showing higher gloss readings. A slight difference is noted in the gloss readings of the S1100L and S1147H polypropylene samples. The high crystallinity sample (S1147H) exhibits nominally higher gloss readings at all recorded intervals during the abrasive scrub test.

A further feature of all the results is the observed pattern of measured gloss with increasing number of abrasive cycles. The lowest gloss readings were measured after 1000 abrasive cycles. Further abrasion up to 10 000 cycles showed a steady increase in the measured gloss, with readings on completion of the tests being, in some cases, higher than the initial values.

Figure 4.46 illustrates this pattern and also shows the influence of the mineral fillers and the filler content on the surface gloss readings.

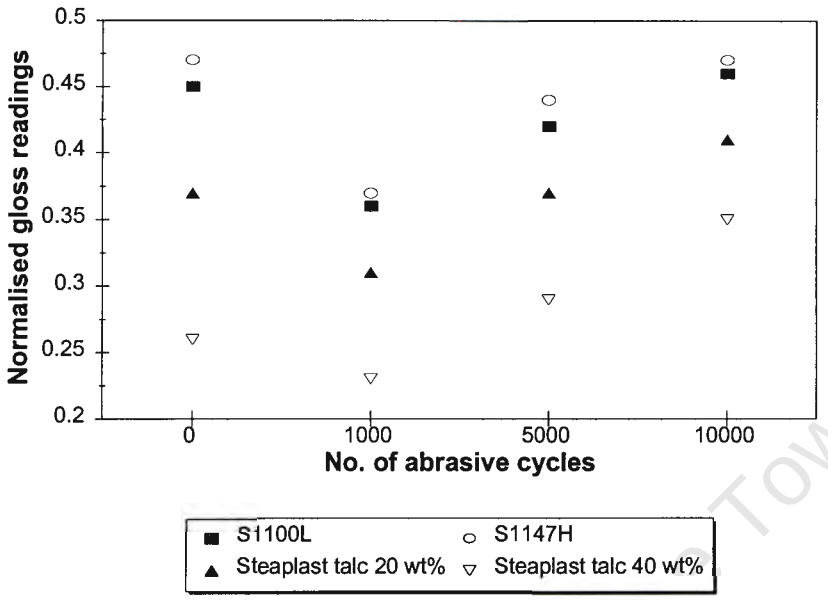

Figure 4.46: The general trend of gloss readings is illustrated. Surface gloss is at a minimum after 1000 abrasive cycles followed by a steady increase until test completion. The high-crystallinity S1147H polypropylene grade exhibits marginally improved surface gloss over the S1100L grade. The addition of filler particles reduces the surface gloss and this is further dependent on the filler content of the composite.

4.3.3.3 Result analysis by material deformation

Scanning electron micrographs of selected tested samples are shown in Figure 4.47. The worn surfaces of the PMMA and ABS are typically brittle, while the tougher PC and the polypropylene samples show more ductile wear behaviour. Observation of the worn surfaces of the filled composites showed breakdown of the included filler particles by the cyclical nature of the abrasive test and large-scale deformation on the sample surface. The *Steaplast* talc samples exhibited slightly less surface deformation, in line with the enhanced adhesion between the filler particles and the matrix polypropylene.

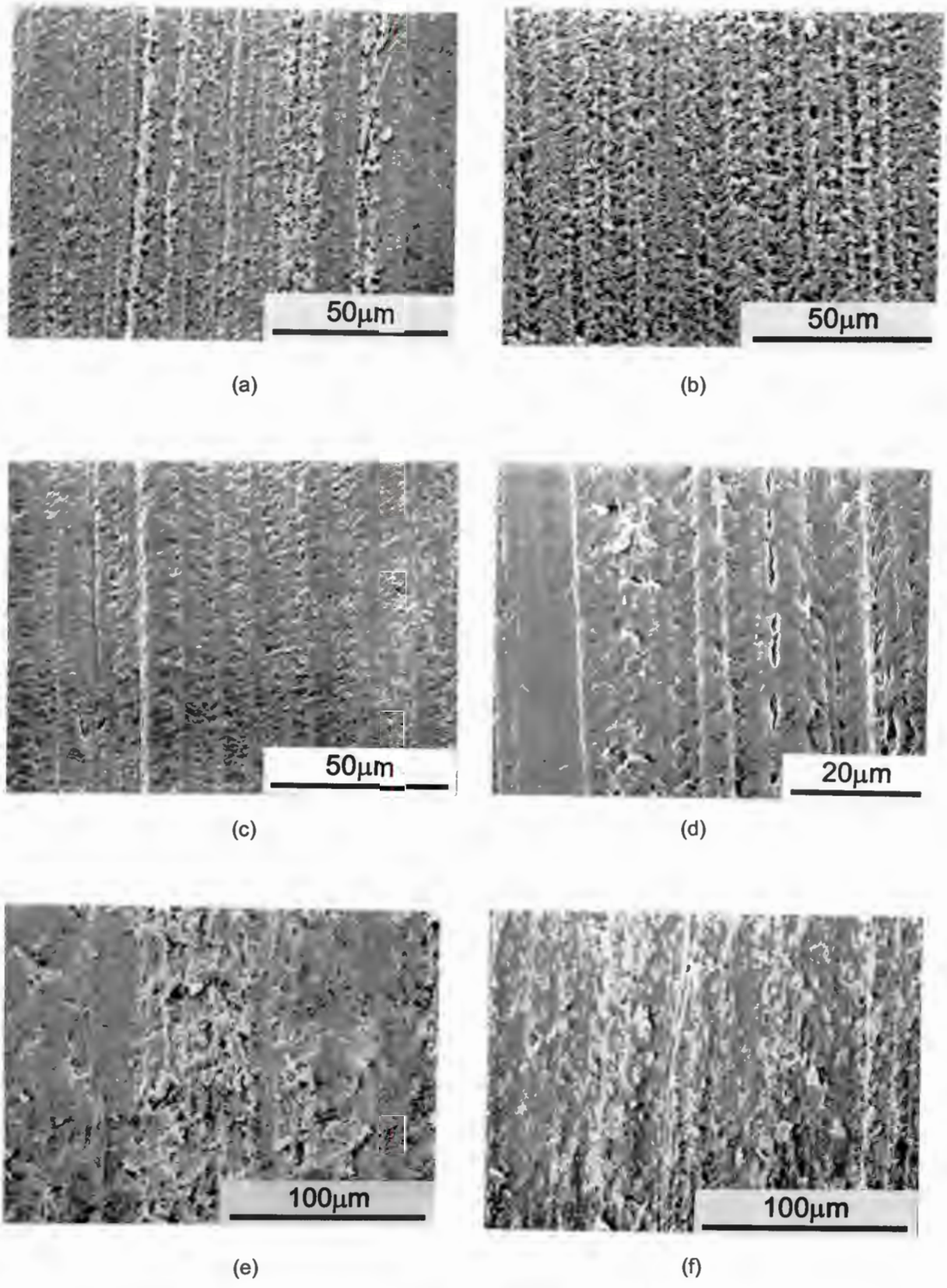

Figure 4.47: Scanning electron micrographs showing the abraded surfaces of the various polymers after 10 000 abrasive scrub cycles. (a) PMMA and (b) ABS both exhibit brittle wear characteristics; (c) PC and (d) PP show predominantly ductile wear surfaces; (e) 60 wt% talc exhibits filler breakdown due to the cyclical test system. (f) *Steaplast* talc showing less surface deformation as a result of the enhanced interfacial adhesion.

4.3.3.4 Result analysis by visual assessment / ranking

Although this method of assessment is highly subjective, it is widely used as a qualitative means of analysis specifically when materials are used in applications where visual effects and appearance are key requirements.

The abraded samples were assessed for scratch visibility under both direct outdoor light and illuminated indoor conditions.

A ranking order for the comparative polymers was established in the form: ABS > PMMA > PP > PC. Difficulties arose when assessing these polymers due to the distinct differences in the pigmentation of each sample. The PMMA and ABS samples are both white, while the PP and PC samples are transparent. Thus, although a ranking can be established between the ABS and PMMA samples, it is unwise to compare these polymers with the transparent samples.

For the filled composite materials, the variation in colouring due to the filler inclusions is an important parameter in the visual ranking system according to the visibility of surface scratching. Inclusion of filler particles to the polypropylene matrix introduces a natural pigmentation effect which ranges from dark grey (fly ash) to light brown (*Steaplast* talc). Furthermore, visual 'streaking' effects are often noted on injection moulded articles when a high filler content is incorporated or when the moulding conditions are not at optimum levels.

The ranking order of the selected filled composites is of the form:

Low scratch visibility:	talc 60 wt%
	Steaplast talc 40 wt%
	china clay 40 wt%
Medium scratch visibility:	wollastonite 40 wt%
	talc 40 wt%
High scratch visibility	*Steaplast* talc 20 wt%
	wollastonite 20 wt%
	(unfilled polypropylene)

The classification depicted above shows several trends. Firstly, the high filler content composites are rated above those of lesser filler content. Secondly, the variegated moulding effect present in several of the high wt% samples is able to 'hide' the appearance of the surface scratch marks. This effect, in conjunction with the variant pigmentation of the samples, is of prime importance for scratch visibility.

CHAPTER 5

DISCUSSION

5.1 INTRODUCTION

This thesis presents the results obtained when a series of composite materials are subjected to abrasive wear; the combination of a ductile thermoplastic polymer and harder, brittle mineral fillers is investigated. The addition of the fillers to the polypropylene matrix has been shown to have a deleterious effect on both the tensile properties and the abrasive wear performance of the composites. By characterising the mechanical properties of the materials, their response in tribological situations can be better interpreted and predicted. It should be realised that although analogies can be drawn between the mechanical deformation and the abrasive wear processes, in terms of the material deformation, the local stresses and strain rates present during abrasive wear tests are considerably higher than those encountered during tensile testing.

5.2 MECHANICAL PROPERTIES

5.2.1 Effect of the base polypropylene homopolymer

It is well known that the mechanical properties of a polymer can be influenced by a variety of factors. Tensile behaviour, for example, is highly sensitive to changes in strain rate and temperature which can cause ductile-brittle transitions to occur in the polymer. Under the controlled conditions of a uniaxial tensile test, the three unfilled PP grades show behaviour typical of a semi-crystalline polymer. Differences are noted for the parameters of E_{mod},

tensile yield stress, and elongation at break. These parameter variations can be analysed through microstructural aspects, in particular those of molecular weight and crystallinity.

The engineering stress-strain curves of the three PP homopolymers show similar characteristic behaviour, as illustrated in Figure 4.5. This behaviour is typified by the initial homogeneous deformation occurring with a steady increase in load with increasing strain. In the tensile tests, a drop in the engineering stress is observed and the yield point is defined as the point of maximum load. As the polymer yields, displacement of neighbouring chain segments occurs through a change of conformation. This is accompanied by the destruction of the original spherulitic microstructure, as spherulites become elongated in the direction of the principal tensile stress[127]. The yield point of the polymer indicates a point of plastic instability which manifests itself in the formation of a neck, and the development of a triaxial stress system. Microvoid formation, observed as stress whitening in the neck region, is a consequence of the constraint from the surrounding unyielded material. Further deformation of the polymer occurs as successive material yields and becomes drawn into the neck region. This large scale plastic deformation gives rise to shear, and the extensional deformation of the molecular chains resulting in chain alignment along the gauge length of the sample. The gauge length thus stabilises through strain hardening and propagates further until the axial stresses on the molecular chains reach a critical limit and fracture occurs. In the case of the S1100L grade, cold drawing of the entire gauge length occurs before final fracture in a fibrillar manner. The process of strain hardening of a polymer is more clearly seen when plotting a true stress-true strain curve which takes into account the change in cross-sectional area of the specimen. Figure 5.1 illustrates this phenomenon for the S1100L homopolymer. Although strain hardening occurs in the S1147H and 1040K polymer grades, fracture occurs at much lower elongation as noted in Figures 4.5b and c.

Close observation of all the PP samples prior to fracture indicated that the surface layer of material failed first with subsequent final fracture of the 'core' material. DSC scans of polymer material prepared from the skin (outer 20 μm layer) and core regions of a 1040K polypropylene tensile bar display significant variation in crystallinity. These sections were cut from an untested polymer sample and are compared to the results of material taken from the drawn neck region of a similar sample following tensile testing. The DSC results are shown in Table 5.1.

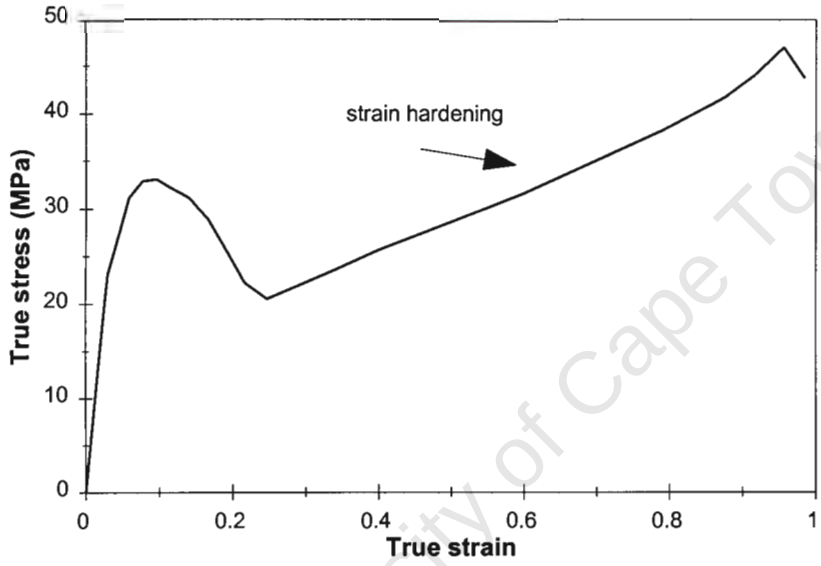

Figure 5.1: The true stress-true strain curve plotted for the homopolymer grade S1100L, illustrating the process of strain hardening occurring as the stable neck region cold draws during a uniaxial tensile test. Crosshead speed = 50 mm min^{-1}.

Table 5.1: Variation in crystallinity for the skin and core regions of a tensile bar due to differential thermal conditions during injection moulding. The crystallinity of the drawn material in the neck region is included for comparison.

Polymer material (1040K)	Crystallinity (%)
Outer skin layer (untested material)	41.6
Core region (untested material)	48.0
Material from drawn neck region (after testing)	48.7

The core region of the tensile bar exhibits higher crystallinity than the outer skin layer due to the thermal gradients present during the cooling cycle of the injection moulding process. The higher amorphous content of the outer layer arises through quench cooling, whereas the lower cooling rate experienced by the bulk material, due to the low thermal conductivity of the polymer, allows chain relaxation, crystallisation, and isotropic spherulite growth. Similar results have been noted by other authors[125,126]. In comparison, the crystallinity of the material from the drawn neck region is similar to that of the core material. The 1040K polypropylene grade exhibits low elongation to break and thus the cold drawn neck region is not as developed as for the S1100L grade (Figure 4.6). Under these conditions, where elongation of 200 to 300% is typical, crystallinity would be enhanced due to the improved orientation of the molecular chains in the direction of cold drawing during tensile testing[18].

Several microstructural factors are responsible for the variation in tensile and flexural behaviour of the three PP grades as noted in Table 4.3 and Figure 4.22. The nucleated grades S1147H and 1040K show improved strength and stiffness, but reduced elongation in comparison to the S1100L grade. A higher crystallinity, smaller average spherulite size, and a higher molecular weight influence these properties. The influence of molecular weight and crystallinity are the dominant features though they can produce contrasting effects. In particular, high molecular weight polymers have longer chains and thus more entanglements and tie molecules per chain leading to an expected increase in strength. The longer chains have, however, been associated with a reduction in crystallinity[27]. Properties of semi-crystalline polymers above their glass transition points that depend on short and rapid molecular displacements (such as melting points, stiffness, and tensile yield strength) reflect the greater controlling influence of crystallinity, while flow properties that involve larger molecular displacements (such as ultimate tensile strength) depend more strongly on molecular weight.

Spherulite boundaries are enriched with low molecular weight material, impurities, chain ends, and defects. Furthermore, during cooling and crystallisation, amorphous material is rejected from the forming crystal lamellae and accumulates at these boundaries. These boundaries are thus inherent points of weakness in the polymer microstructure. Yielding in polypropylene is associated with the deformation and reorientation of the spherulite structure. Tie molecules, which form interspherulitic links, provide the load-bearing strength of the polymer. Large spherulites, which have fewer tie molecules interlinking them, are thus more susceptible to crack propagation along the spherulite boundaries and are unable to sustain high applied stresses prior to yielding[127]. The addition of the nucleating agents to the S1147H and 1040K polypropylene grades enhances the crystallinity of the polymer and reduces the spherulite size, thus increasing the number of interlinking tie molecules. This results in higher yield stresses compared to the unnucleated PP grade, S1100L, as seen in Table 4.3.

The flexural modulus is not strongly affected by molecular weight and is predominantly a function of the degree of crystallinity as it involves short molecular displacements. The greater presence of interlinking tie molecules in the nucleated polypropylene grades (S1147H and 1040K) creates strong interspherulitic bonds and restricts the molecular deformation of the polymer. A consequence of the increase in stiffness of these nucleated polypropylene grades is an associated decrease in elongation in comparison to the S1100L PP grade. As the molecular deformation is restricted, it becomes easier to break primary valence bonds by chain scission than to overcome the chain entanglements and intermolecular forces[27]. This is further enhanced by the nucleated polypropylene grades having higher molecular weights, and hence longer chain lengths and a higher number of chain entanglements.

5.2.2 Effect of mineral fillers on the mechanical behaviour

The results of the uniaxial tensile tests have shown that the addition of the mineral fillers reduces the yield strength and ductility of the composites and that there is a variation in the behaviour of the individual fillers which can be related to their physical properties. Similarly, improvement in flexural stiffness is attained with the filler inclusions.

The improvement in flexural stiffness of the filled composites, as shown in Figure 4.23, is directly related to the mechanical restraint imposed on the ductile polypropylene matrix by the filler particles, leading to decreased mobility and deformation of the polymer molecules. This mechanical restraint is dependent both on the interparticulate spacing, and the properties of the filler particles and the polymer matrix[48].

Two primary factors are responsible for the deterioration in tensile properties. By introducing the mineral fillers into the polypropylene matrix the effective cross-sectional area of the specimen which is able to support an applied load is reduced. This is exacerbated by the lack of bonding between the two constituents. Secondly, because of the large disparities in the elastic and plastic properties of the fillers and the matrix, the fillers act as stress concentrators, providing nucleation sites for plastic deformation and crack initiation to occur. During tensile deformation in polymers, the basic micromechanical deformation mechanisms involve shear yielding and crazing. In particulate-filled composites yielding is accompanied by debonding at the particle-matrix interface if the interfacial adhesion is weak[128]. Interfacial debonding usually occurs first at the poles of the filler particles followed by propagation around the particle surface, as shown in Figure 5.2. This debonding causes microvoids to form which reflect light due to refractive index differences between the two phases and becomes visible as stress whitening. This stress whitening occurs almost immediately on elongation of composites containing large particle fillers or when the filler content is high.

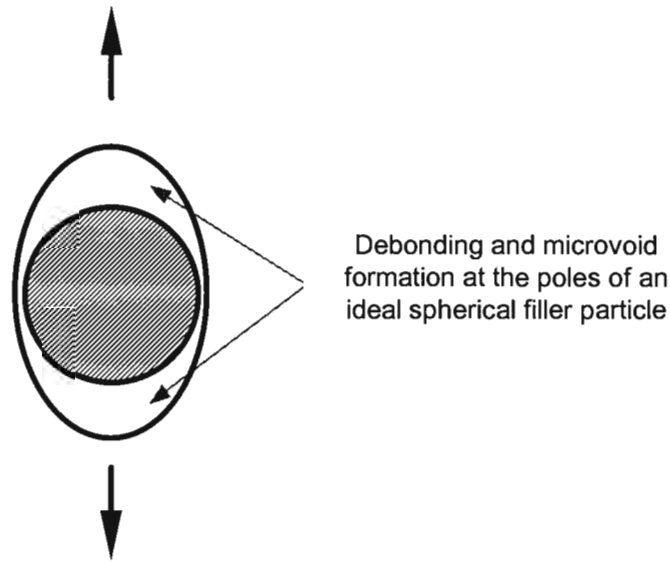

Figure 5.2: Schematic illustrating the process of interfacial debonding occurring predominantly at the poles of an ideal spherical filler particle during tensile deformation. The direction of the applied stress is shown by the arrows. [After Pukanszky *et al.*[128]].

The controlling influence of crystallinity on the tensile properties has already been discussed in the previous section. In general, although contrasting reports have been published[41], the addition of mineral fillers will inhibit the development and perfection of the crystalline structure of the matrix polymer and thus a decrease in tensile properties is expected unless compensated for by other means, for example, physical interaction between the matrix and the filler particles. The tensile behaviour will thus be analysed in terms of the physical properties of the included fillers as these parameters all contribute to the overall performance of the composite materials. Specifically, the effects of filler shape, size, weight fraction, and surface treatment will be discussed.

5.2.2.1 Effect of filler particle shape

The aspect ratio of the filler particles has a major influence on the tensile and flexural properties of the composites. Analysis of the tensile strength of the composites (Figure 4.9) shows the talc and china clay fillers, which have the highest aspect ratios, to have the highest tensile strengths. In the case of the talc-filled materials, an improvement over the unfilled polypropylene material

is observed at levels up to 40 wt%, while the china clay composites show no drop-off in yield strength over a similar filler content range. During the injection moulding process the talc platelets become aligned in the direction of the applied stress in the moulded tensile bar. Limited surface interaction can thus occur between the large surface areas of the aligned talc platelets resulting in the mechanical restraint of the ductile polymer matrix and limited ductility and high elastic stiffness. This effect of restricting the deformation of the polypropylene, as illustrated in Figures 4.7 and 4.13, is emphasised at high filler loading where the interparticulate spacing is small. An additional effect of this enhanced physical surface interaction is the improvement in stress transfer across the filler-matrix interface. The talc particles can thus support some of the applied load leading to the improvement in tensile strength over the other filled composites. The alignment of the talc particles further limits the extent of interfacial debonding due to stress concentration effects and thus the effective cross-sectional area of the sample is not lowered significantly. In addition, the mechanical restraint imposed on the polypropylene matrix by the aligned talc particles results in significantly lower strains to failure. At these low strains the mechanical restraint phenomenon dominates the fracture process and thus the stress concentration effects do not come into play prior to tensile failure.

For the other fillers with smaller aspect ratios, no particle alignment occurs during processing and thus less surface interaction and stress transfer can occur, resulting in a loss of load-bearing area, and hence a decrease in the yield strength of the composites. The tensile strength and modulus properties are thus dominated by the effects of stress concentration introduced by the presence of the filler particles. The wollastonite fibres show limited alignment as they do not readily orient side by side, resulting in an intermediate stress response as observed in Figure 4.9. The 'isotropic' fillers show greater elongation to failure due to the reduction of mechanical restraint of the ductile polypropylene matrix. The polypropylene is thus able to deform around the filler inclusions in a fibrillar manner as shown in Figure 5.3. Fracture is

dominated by the stress concentration effects of the included fillers, and the reduced polypropylene cross-sectional area, and occurs when the polymer fibrils can no longer support the applied load.

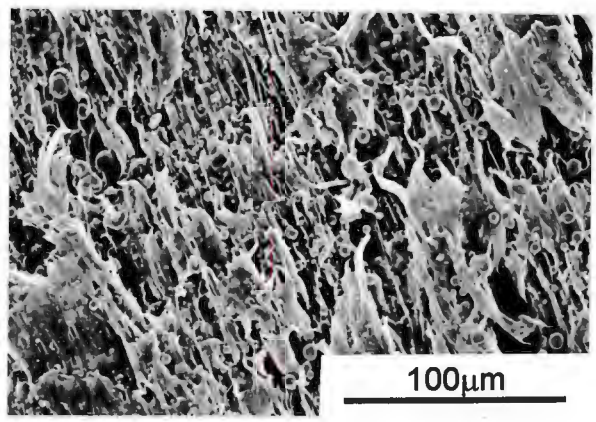

Figure 5.3: Side view of a fly ash composite tensile specimen illustrating the lack of mechanical restraint of the ductile polypropylene matrix by the filler particles and the formation of load-bearing fibrils.

5.2.2.2 Effect of filler particle size

Although the talc and china clay fillers show superior tensile properties due to their platelet shape, differences are noted with respect to their individual particle sizes. The larger talc grade particles have an average particle size of 10 μm in comparison to the 2 μm and 4 μm sized grades of *Steaplast* talc and china clay, respectively. Although the *Steaplast* talc filler has a higher surface area than the larger (10 μm) talc filler (see Appendix A), there is less filler particle alignment in the *Steaplast* composites, as compared in Figures 4.4d and 4.13. The larger talc-filled composites thus have a greater effective surface area available for filler-matrix interaction and stress transfer to occur, leading to higher tensile strength and elastic modulus values and the associated decreased ductility of the talc composites.

It has been shown by other authors that the tensile strength of a composite is inversely proportional to the diameter of the filler particles[36] when purely

spherical particles were considered and no other effects taken into account. The performance of the 'isotropic' $CaCO_3$ and fly ash-filled composites in this study affirm this theory with the large fly ash fillers showing the greatest decrease in tensile strength whereas the smaller (< 1 μm) $BaSO_4$ composites, although still displaying a fall-off in tensile strength with increasing filler content, perform significantly better than the respective $CaCO_3$- and fly ash-based materials (see Figure 4.9). As a consequence of the significantly higher density of the $BaSO_4$ in comparison to the other fillers, the volume fraction of filler particles in the $BaSO_4$-PP composites is greatly reduced, and hence the interparticulate spacing is increased. The small $BaSO_4$ particles at low filler concentration are free to move with the polypropylene matrix and hence the deformation of the ductile matrix is not inhibited. This viscous drag of the small filler particles can contribute to the apparent strength increase, as seen in Figure 4.9[31]. Furthermore, the effects of microvoid formation and the associated decrease in cross-sectional load-bearing area are not as significant for the $BaSO_4$-PP composites. With an increase in the filler particle size, the size of the voids initiated by debonding at the filler-matrix interface increase, lowering the load-bearing cross-sectional area of the composite, and hence the tensile yield strength. Figure 5.4 illustrates a schematic representation of the debonding behaviour with respect to the different filler particle shapes and sizes[129].

Evidence of interfacial debonding during tensile testing is shown in Figure 5.5a and b. Two test specimens, one an unfilled polypropylene and one a 20 wt% fly ash-filled composite were allowed to yield but not fracture during a tensile test before the applied load was removed. These test pieces were then cross-sectioned through the neck region and the surfaces examined in the scanning electron microscope. The unfilled sample showed no large-scale material deformation in this region whereas the fly ash composite is characterised by debonding at the filler-matrix interface and the growth of microvoids from these sites.

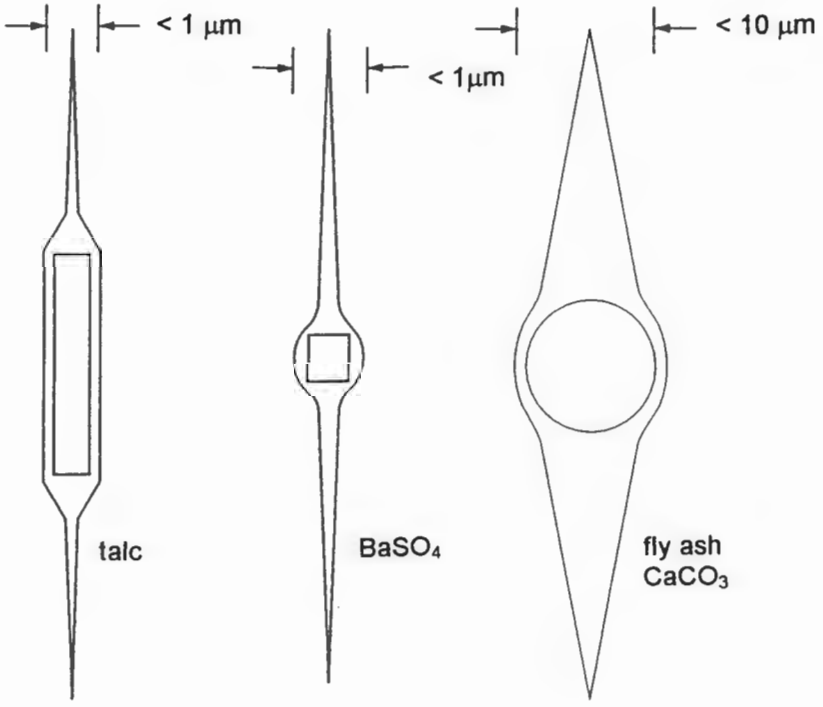

Figure 5.4: Schematic representation of the formation and growth of microvoids in a bulk polymer showing the influence of filler particle shape and size. [After Sole and Ball[129]].

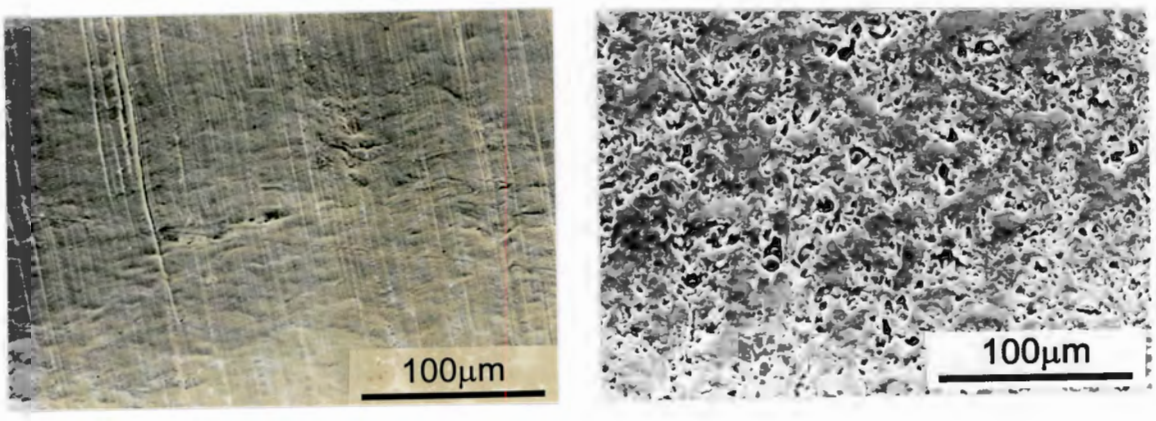

(a) (b)

Figure 5.5: Scanning electron micrographs of the cross-sections of 'necking' regions of (a) an unfilled polypropylene specimen, and (b) 20 wt% fly ash composite tensile test specimen. The samples are sectioned transverse to the tensile axis after loading to 20% elongation. The addition of the filler particles to the ductile matrix results in the initiation of microvoids during tensile testing leading to a decrease in tensile strength.

5.2.2.3 Effect of filler content

The decrease in tensile strength and elongation to failure with increasing filler content is directly related to the higher number of sites available for microvoid initiation to occur, and the decrease in effective load-bearing area of the polypropylene matrix. Furthermore, the increased filler content of the composites reduces the effective crystallinity of the polypropylene matrix. Similarly, a higher filler content results in enhanced mechanical restraint of the ductile matrix leading to the improved stiffness of the composites.

5.2.2.4 Effect of filler surface treatments

The *Steaplast* talc and the china clay fillers are both surface modified to improve the interfacial adhesion during polymer compounding. This improved adhesion was most evident for the *Steaplast* talc filler as seen in Figure 4.4d. Opposing reports by other authors on the benefits of surface treatments are well documented. In general, the surface treatments improve the dispersion of the filler particles within the polymer matrix, with subsequent improvements in tensile strength and elongation [41,48,49]. Chacko *et al.*[39], however, observed that the improved filler dispersion led to a greater degree of interfacial debonding and a higher reduction in yield stress compared to non-surface treated particle agglomerates.

Improved tensile strength and negligible fall-off in tensile properties over the filler content range 0 to 40 wt% is evident for the china clay and *Steaplast* talc composites in Figures 4.9 and 4.11, respectively. These results, when compared to those of the larger non-surface treated talc filler, confirm the effectiveness of surface treatments in counteracting the physical surface interaction effects inherent for a larger surface area.

5.2.2.5 Overview

The wide range of fillers used in this study with varying particle shape, size, and density illustrate and confirm the major influence of these parameters on the tensile and flexural properties of ductile thermoplastic polymers, and in particular, polypropylene. Although each of these individual physical parameters is significant, it is important that their specific contributions to the mechanical performance of a polymer composite should be analysed as a whole.

5.3 ABRASIVE WEAR PROPERTIES

5.3.1 Influence of abrasive grit size on the wear rates

The interaction between the abrasive medium and the polymer surface results in the generation of stresses at the contact points, *i.e.* the asperities of the alumina particles. The extent of the material deformation and wear is primarily dependent on the magnitude of these stresses, although particle hardness, geometry, and cutting angle can be influential. These factors are not considered in this discussion as the alumina abrasive belts were all obtained from the same supplier and thus the particles can be considered to be uniform in these respects.

The coarse abrasive belts have a low distribution density of particles thus apply a high contact stress per particle. A greater depth of penetration into the softer polymeric material results together with severe plastic deformation, groove formation, and high wear rates. Abrasion against the finer abrasive belts is associated with a higher distribution density of alumina particles and thus a lower applied contact stress per particle. The depth of penetration into the polymer surface is reduced, and a higher proportion of recoverable

elastic, rather than plastic, deformation prevails; hence lower wear rates are experienced.

As shown in Figure 4.37, there is a significant levelling off of the wear rate with increasing alumina particle size for the unfilled polypropylene samples. A critical particle diameter of about 70 μm is observed, above which the wear rate becomes insensitive to the abrasive particle size. In the abrasive particle size range 0 to 70 μm, the average applied load acting on each alumina particle is steadily increased. Consequently, the average depth of penetration of these particles into the polymer surface increases, with associated greater mass loss during abrasion. Above the critical particle diameter of 70 μm, the depth of penetration of the alumina particles into the polymer surface is restricted by the plastic constraint of the bulk polypropylene. This constraint becomes the dominant parameter for further deformation to occur. A further increase in the abrasive particle size, and hence an increase in the load per abrasive particle, does not result in a further significant increase in the penetration depth of these abrasive particles into the polymer surface. The wear rate thus reaches a uniform level.

With the addition of the mineral fillers to the ductile polymer matrix the critical abrasive particle size becomes less well defined with increasing filler content. For the 60 wt% filled composites, the greatest increase in wear rate is seen over the abrasive particle range of 0 to 40μm. Above this point, there is some decrease in wear rate with increasing abrasive particle size, however a uniform steady-state level is not attained. With the addition of the mineral fillers to the polypropylene matrix the bulk hardness of the composites is increased. The effective load per abrasive particle required to reach the 'saturation' depth of penetration into the composite surface is thus much greater than for the unfilled polymer, hence the increasing wear rates. Furthermore, with increasing filler content, there is a change in the dominant wear mechanism of the composite as the filler inclusions reduce the ability of the polymer matrix to absorb plastic strain energy. As the polymer surface

abrades against the alumina belt, a higher proportion of deformed material reaches its plastic limit and is removed as wear debris. In the case of the high filler content composites, much of the measured mass loss can be attributed to the removal of the filler particles from the polymer. This is exacerbated by the lack of adhesion between the two phases.

5.3.2 Effect of the base polypropylene homopolymer

The abrasive wear resistance of the three unfilled polypropylene grades decreases in the order 1040K > S1147H > S1100L, however this difference in behaviour is more apparent for wear results against the coarse grit Al_2O_3 belt. In Figure 5.6 the wear rates against the 80 grade belt for the three PP grades are plotted against calculated values according to the Ratner-Lancaster and Briscoe correlation's[73,74]. In these two models polymer wear rates are shown to decrease with an increasing strain to failure. However the three similar PP polymers exhibit an opposite trend with the less ductile 1040K grade showing the lowest wear rate. The influence of yield strength and elongation to failure of the three polypropylene grades, on the abrasive wear rates can be understood in terms of the abrading counterface. During abrasion against both fine and coarse abrasive belts, plastic deformation dominates the wear process for the polypropylene samples, as seen in the scanning electron micrographs of Figure 4.29. This indicates that the yield strength of the polymers has been exceeded.

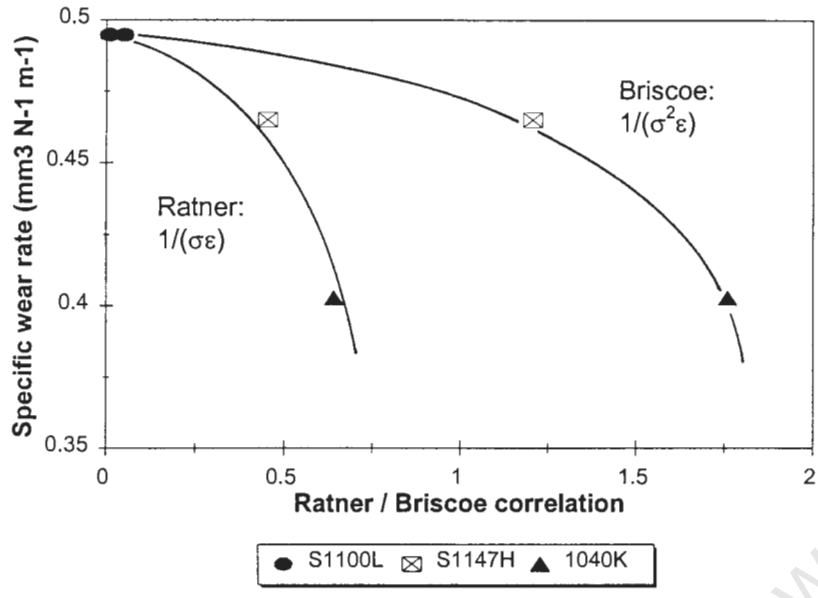

Figure 5.6: The specific wear rates against the 80 grit Al_2O_3 belt for the PP grades 1040K, S1147H and S1100L plotted against the Ratner-Lancaster and Briscoe correlation's.

5.3.2.1 Abrasion against the coarse abrasive belts

The difference in abrasive wear rates against the coarse abrasive belts of the three unfilled PP grades can be understood by using a model of a single alumina particle penetrating the polymer surface, shown schematically in Figure 5.7.

The distribution density of alumina particles on the coarse 80 grade abrasive belts is low and thus the effective applied load per abrasive particle is high. The depth of penetration of the abrasive particles into the polymer surface is dependent on the hardness, and thus the yield strength of the polymer. The 1040K PP grade has a higher yield strength associated with a higher crystallinity, smaller spherulite size, and a greater number of interconnecting tie molecules. This PP grade is thus more resistant to surface penetration by the alumina particles than the softer S1100L polypropylene grade, as illustrated in Figure 5.7. As the abrasive particle moves across the polymer surface it will plough a groove in the softer material; the depth of the groove is

related to the initial depth of penetration. As the effective load on the abrasive particle is high, the polymer material in this groove yields under plastic deformation conditions. Although not all of the deformed material is removed from the surface, the volume of the groove can be correlated to the measured wear rates. Thus, although the S1100L PP grade has a superior elongation to failure than the nucleated 1040K grade, and can thus accommodate a higher plastic strain during abrasion, the high applied stress per abrasive particle ensures that the plastic limit of both materials is exceeded. The higher yield strength and hence the smaller groove volume of material of the 1040K polypropylene thus dominates the wear process under coarse abrasive conditions.

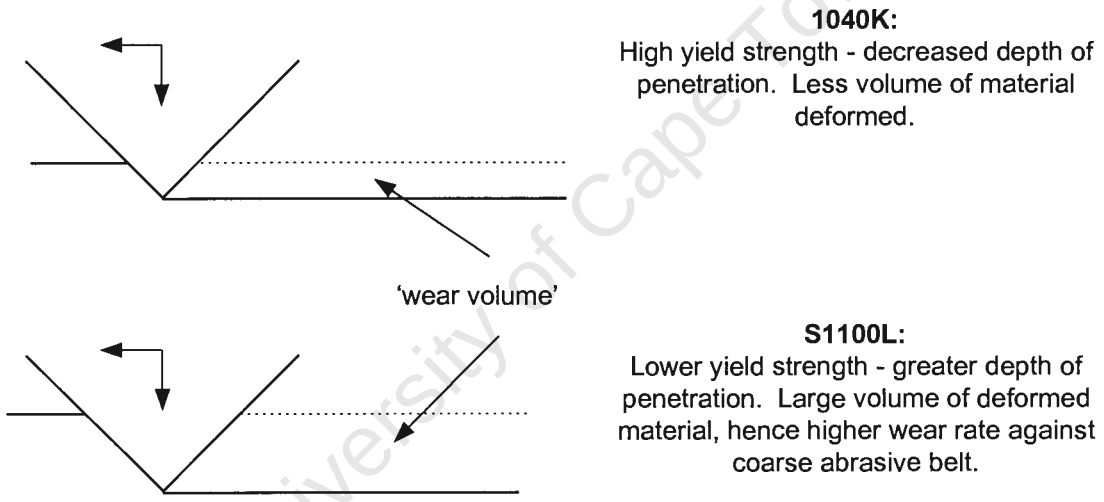

Figure 5.7: Schematic illustrating the influence of yield strength on the wear rates of the polypropylene grades 1040K and S1100L under coarse abrasive conditions.

5.3.2.2 Abrasion against the fine abrasive belts

The high abrasive particle distribution density of the fine abrasive belts gives rise to a low applied stress per particle. Consequently, the influence of the variation in polymer yield strength is not as marked since the penetration depth of the abrasive particles is significantly reduced. Furthermore, due to the reduced load per abrasive particle, much of the abrasive energy per single particle traverse, is dissipated in the microploughing deformation of the polymer

and only a small part is consumed by microcutting and material removal mechanisms. The low strain to failure of the nucleated PP grades is negated by this effect. The 'wear volume' of plastically deformed material produced during the microploughing process is thus equivalent for the three polypropylene grades and similar wear rates are exhibited under these mild abrasive conditions.

5.3.3 Abrasive wear behaviour of the comparative polymers

The wear performance of the selected polymers show general agreement with Ratner's correlation for the factor $(\sigma\varepsilon)^{-1}$ as shown in Figure 5.8. The values for PMMA, and the two nucleated polypropylene grades, S1147H and 1040K are lower than the relationship suggests. In the case of the PMMA, this could be attributed to the high hardness and yield strength of the polymer which resists penetration of the abrasive particles, whereas the lower elongation to failure of the nucleated PP grades contributes to the deviation from the Ratner model.

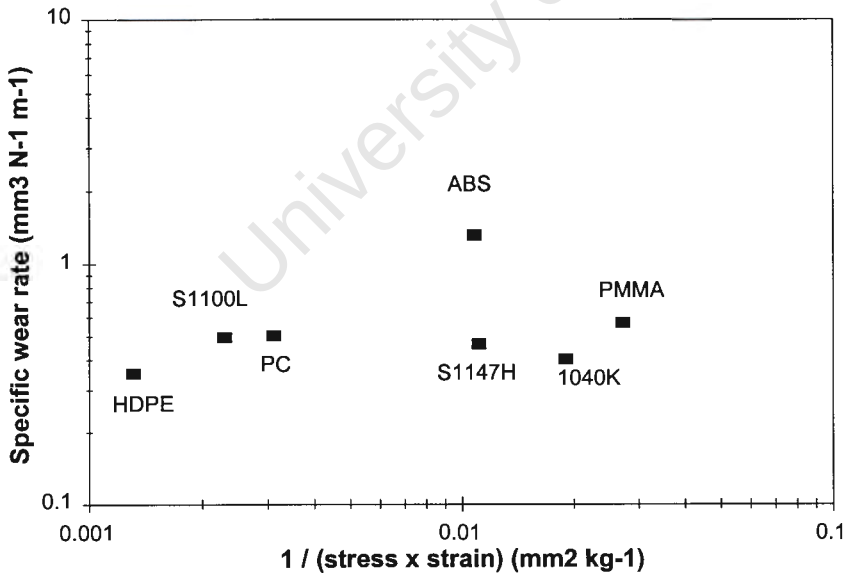

Figure 5.8: The relationship between the specific wear rate measured for abrasion against the coarse 80 Al_2O_3 belt and the Ratner factor $(\sigma_f\varepsilon_f)^{-1}$.

The HDPE polymer shows the lowest wear rate and a ductile deformation mechanism associated with a large strain to failure. The PC, ABS, and

PMMA samples have reduced elongation and all exhibit brittle wear mechanisms as observed in Figure 4.30. This deformation mode is dominated by a microcracking mechanism as the strain to microfracture of these polymers is low. Surface cracks produced by the contact stresses propagate until wear particles break from the surface without notable plastic deformation.

5.3.4 Effect of mineral fillers on the abrasive wear rate

The abrasive wear modes of the filled polypropylenes are typical of ductile polymers, exhibiting extensive plastic deformation as the dominant feature. The addition of the mineral fillers to the polymer matrix has a detrimental effect on the wear resistance at both high- and low-contact stress abrading conditions, *i.e.* against coarse and fine abrasive papers. Although this increase in wear rate occurs within one order of magnitude the effect is significant. The wear behaviour of the filled composites will be discussed in terms of the abrading alumina particles, the physical properties of the fillers, and the mechanical properties of the composites. Furthermore, the following discussion draws analogies between the tensile stress/strain behaviour, and the wear performance of the respective filled and unfilled polypropylenes. This analogy is illustrated in the schematic of Figure 5.9.

During the steady-state situation for repeated abrasion, the amount of material undergoing deformation and removal from the surface is dependent firstly on the ability of the filled composite to resist penetration by the alumina particles, and secondly, to accommodate plastic strain generated by the high contact stress conditions prevalent during the abrasive process. The resistance to penetration is largely dependent on the yield stress of the composite, while the accommodation of plastic strain is related to the material's microtoughness or energy to fracture which can be calculated from the area under the stress-strain curve.

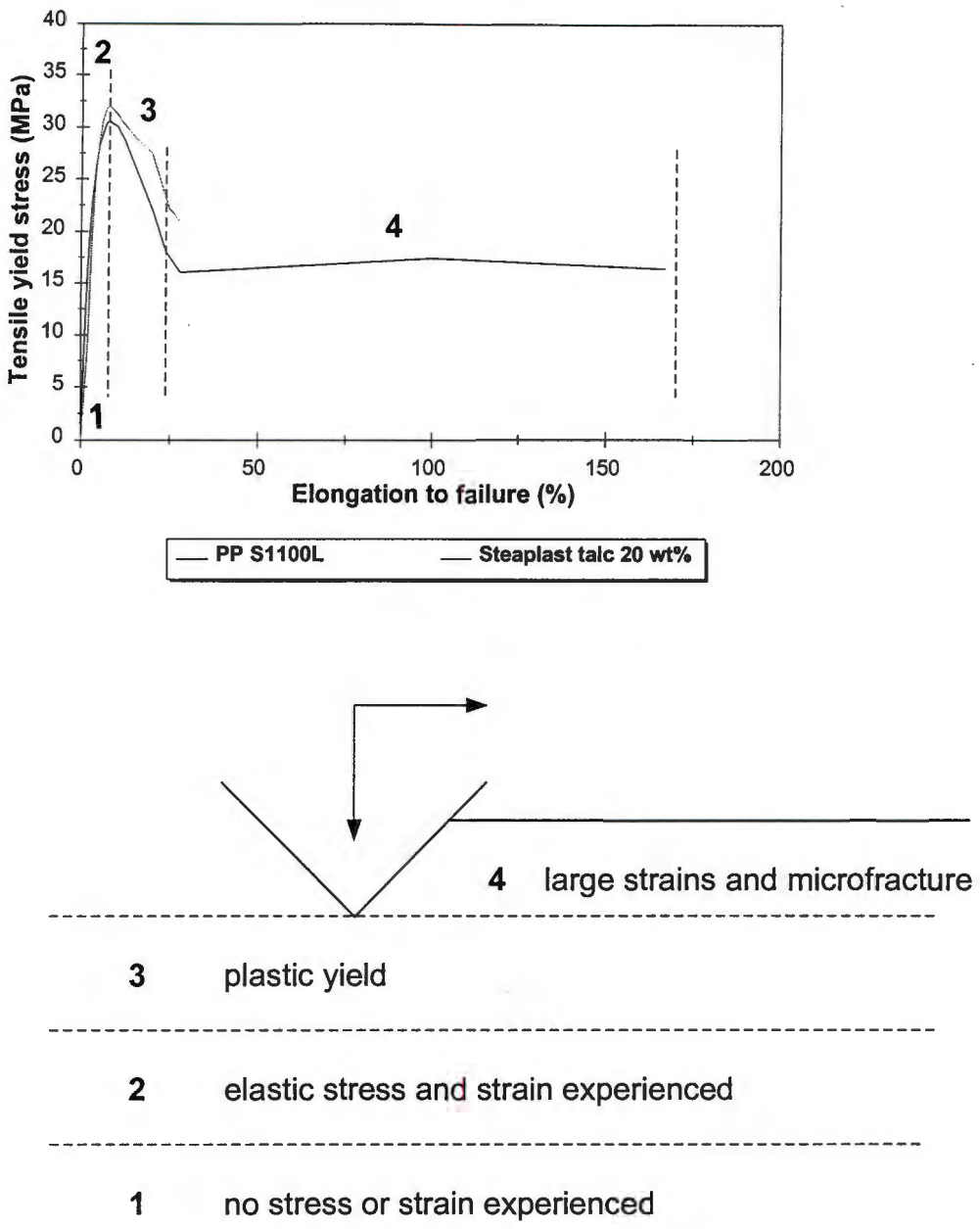

Figure 5.9: Schematic illustrating the analogy between the tensile stress/strain behaviour and the steady-state abrasive wear performance of an unfilled polypropylene (S1100L), and a filled composite (Steaplast talc).

The addition of the fillers marginally improves the surface hardness of the polypropylene, however, with the exception of the platelet fillers, a decrease in tensile yield stress is noted. The accommodation of plastic strain is thus the dominant factor affecting the wear resistance of the filled composites.

Comparing the tensile curves of the selected unfilled polypropylene, S1100L, and the filled composite, 20 wt% Steaplast talc, in Figure 5.9, it is observed that the matrix polymer exhibits a far greater energy to fracture and can thus accommodate plastic strain generated under the abrasive conditions to a greater extent. The strain to failure of the filled composites is limited by the initiation of microfractures at the filler-matrix interface arising from the discontinuities in the elastic and plastic properties of the two phases, and the absence of any significant interfacial bonding. Plastic strain energy absorbed by the polymer material during abrasion is not able to be effectively transferred across the phase interface and is liberated through the formation of microfractures and debris particles. Thus under steady-state repeated abrasion, the filled composites exhibit much higher wear rates than their respective unfilled base polymer. Table 5.2 details the disparities in elastic properties for the polypropylenes and the various mineral fillers. Furthermore, the increasing filler content of the composites favours a ductile to brittle transition in the wear mode. In addition to the ductile microploughing mechanism, a microcracking mechanism associated with brittle material deformation exists, leading to a higher volumetric loss of material from the surface.

Table 5.2: Summary of the Young's Moduli for the polymers and fillers used in this study. [Values for the fillers are from Katz and Milewski[31]].

Material	Young's Modulus (GPa)
PP S1100L	1.4
PP S1147H	1.5
PP 1040K	1.9
talc	196
fly ash	590
$CaCO_3$	255
$BaSO_4$	294
china clay	196
wollastonite	294

5.3.4.1 Abrasion under high applied contact stresses

The worn surfaces of each composite are covered with wide abrasive wear tracks whose width generally exceeds that of the constituent filler particles in the material. Typical groove widths measured from the scanning electron micrographs are of the order of 70 to 100 μm. Thus the alumina abrasive particles 'see' the bulk composition of the sample during abrasion. With large alumina abrasive particles (260 μm) the material displaced from the surface during plastic deformation incorporates both the soft ductile polymeric matrix and the harder filler particles which are removed either as a whole or fractured by the high contact stresses applied by the large alumina particles. The weak adhesion at the filler-matrix interface contributes to the initiation of microfracture in these areas and the removal of filler particles from the bulk composite.

5.3.4.2 Abrasion under low applied contact stresses

The worn surfaces of the samples abraded against the finer grit sizes show similar wear tracks to those produced by the coarse alumina particles. The typical widths of these tracks for the 600 grade abraded samples are in the range 7 to 10 μm. The influence of the included filler particles is much greater under these abrasive conditions as the filler size and the wear groove widths are of similar magnitude. The harder filler particles can withstand the contact stresses from the alumina abrasive particles and restrict the deformation and removal of the surrounding ductile polymer, thus contributing to the decreased wear rates observed. In particular, the large wollastonite filler particles show improved wear rates over the unfilled materials. Figure 5.10 shows the wear surface of a coarse grade wollastonite-filled sample. The scar produced by the alumina particle is indicated by the arrow. Due to the reduced applied load acting at this point, the wollastonite fibre is able to withstand the stress and thus no breakdown of the fibre is seen.

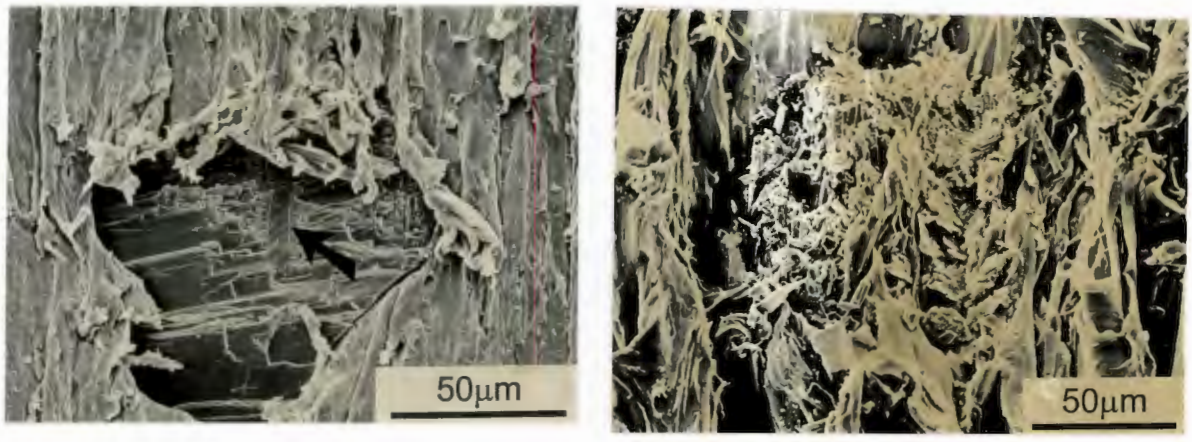

(a) (b)

Figure 5.10: Wear surface of a coarse wollastonite filled composite after abrasion by (a) the fine 600 grade Al_2O_3 belt and (b) the coarse 80 grade Al_2O_3 belt, illustrating the influence of the relative size difference between the abrasive particles and the filler constituent. Against the fine abrasive the decreased contact stress per abrasive particle is insufficient to cause breakage of the wollastonite fibre. The wear scar produced by the alumina on the particle fibre is indicated by the arrow. At higher contact stress conditions filler breakage occurs as the filler particles shatter on contact with the highly loaded alumina particles. These filler particle fragments are easily removed and contribute to the higher wear rates.

5.3.4.3 Influence of mechanical properties on the wear rates of the filled composites

From earlier discussion it is noted that the limited capacity of the filled composites to absorb plastic strain during abrasion is related to their deteriorating wear resistance when compared to the unfilled polypropylenes. In Figure 5.11 the specific wear rates of the range of filled composite materials against the 80 and 600 grade alumina belts are plotted as a function of the Ratner correlation (the reciprocal of $\sigma_f\varepsilon_f$). Although a general trend identifying higher wear rates with reduced stress and strain at fracture is seen, the dependence is not strong.

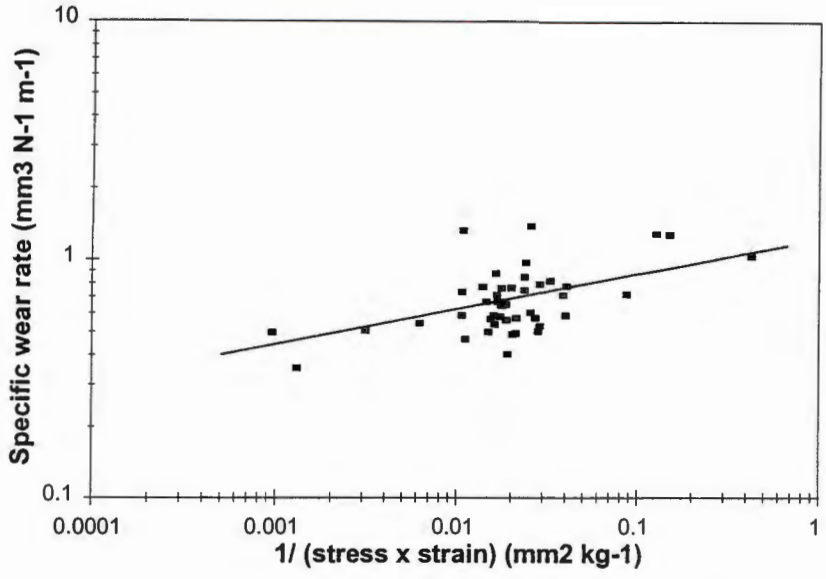

Figure 5.11a: Correlation between the reciprocal of the stress and strain at fracture $(\sigma_f \varepsilon_f)^{-1}$ and the specific wear rate for the filled composites abraded against the coarse 80 Al_2O_3 belt.

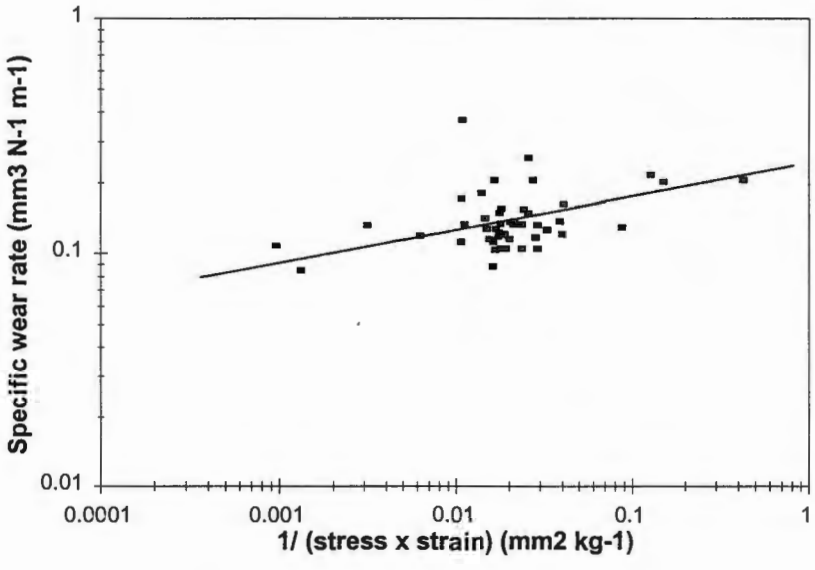

Figure 5.11b: Correlation between the reciprocal of the stress and strain at fracture $(\sigma_f \varepsilon_f)^{-1}$ and the specific wear rate for the filled composites abraded against the fine 600 Al_2O_3 belt.

By isolating the individual filler types a clearer trend can be distinguished. Figures 5.12a and b reflect the respective trends for the talc- and fly ash-filled composites. These two fillers correlate well with the Ratner model at all levels of abrasion, however, as noted from the logarithmic scale of the graphs,

relative differences exist in the abrasion modes of the respective filled composites. These can be related to the variations in the physical properties of the two fillers. This is better illustrated in Figure 5.13 which plots the wear rates (600 grit Al_2O_3 belt) of the two filled composites as a function of both elongation to failure and filler content.

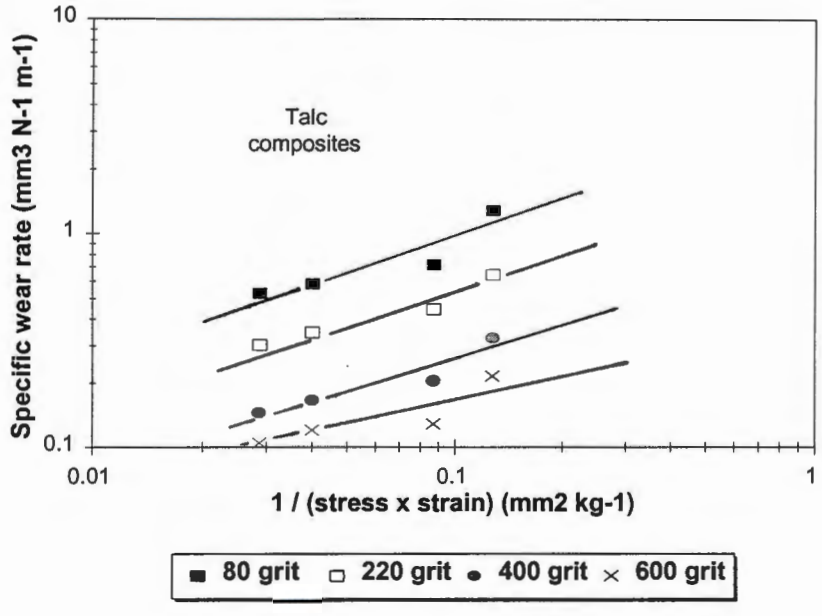

Figure 5.12a: The specific wear rates of the talc-filled composites at all levels of abrasive wear illustrating close correlation with the Ratner model.

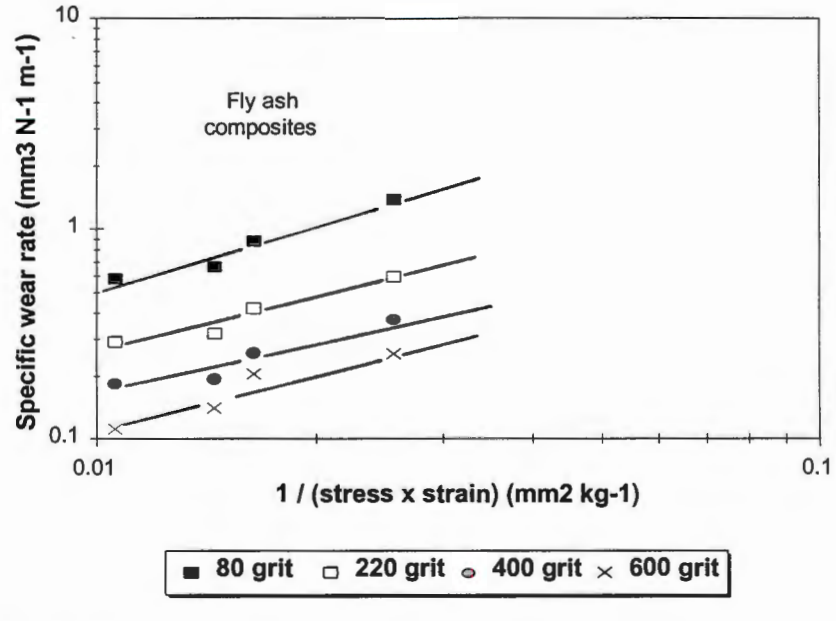

Figure 5.12b: Specific wear rates of the fly ash-filled composites at all levels of abrasive wear showing close correlation with Ratner's model.

In Figure 5.13 both the talc and fly ash composites display a negative correlation between the specific wear rate and the elongation to tensile failure. Furthermore, it is interesting to note that although the 60 wt% fly ash composite has a greater ductility than a 10 wt% talc-filled material, the talc blend shows a wear rate of less than half that of the fly ash sample.

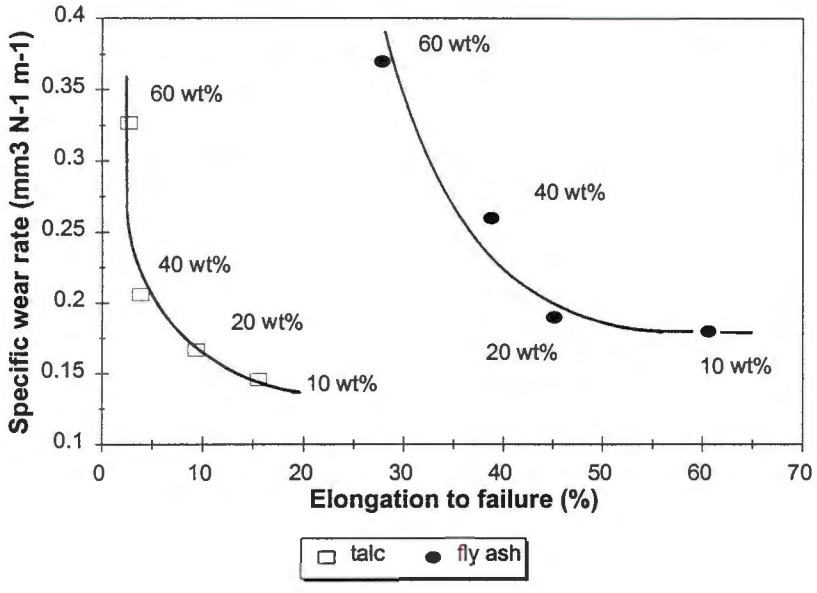

Figure 5.13: Variation in specific wear rate, measured against the 600 grade alumina abrasive belt, with elongation to failure for composites containing fly ash and talc fillers. The low strain to failure of the talc based composites is evident.

The wear behaviour of the talc composites is strongly governed by the shape of the filler particles. The anisotropy of the talc platelets promotes mechanical restraint of the polymer matrix and hence a higher yield strength and associated increased resistance to penetration and plastic deformation. The talc composites can thus better withstand penetration by the small alumina particles and less wear debris is generated. Consequently, against the finer grit abrasive belts, the talc-filled composites show improved wear resistance at low filler content over both the unfilled polypropylene and the other filled composites. At higher levels of filler content, the limited strain to failure of the composite begins to dominate and the wear rate increases.

In contrast, the large isotropic fly ash particles do not have the same interfacial properties and the polymer matrix is not constrained from plastic deformation, even at high filler contents, leading to higher strain to failure than the talc composites. During abrasion the high filler content and large particle size provides extensive sites for microvoid initiation and coalescence to occur, leading to a high volume loss of material, both of the polypropylene matrix and the debonded fly ash particles. The differences in wear deformation of the talc and fly ash composites are observed in the high magnification electron micrographs in Figure 4.36.

Although the Ratner correlation holds true for the specific fillers investigated in this study, it is of limited value when comparing fillers of different physical properties.

5.4 SINGLE-POINT SCRATCH TESTS

In this section an attempt is made to correlate the wear rates and material deformation mechanisms prevalent during bulk abrasive wear with the deformation produced by a single-track scratch test. Moreover, the single-point test procedure is used as a qualitative method for ranking the materials in terms of their scratch resistance.

5.4.1 Polypropylene and the comparative polymers

The calculated scratch hardness values according to eqn. 2.19, *viz.* $H_s = x\, 4W / \pi d_s^2$, for the PP and comparative polymers, are shown in Figures 5.14 and 5.15 as functions of the applied load on a Rockwell C diamond indentor and the included half-angle (α), of the stainless-steel indentors, respectively.

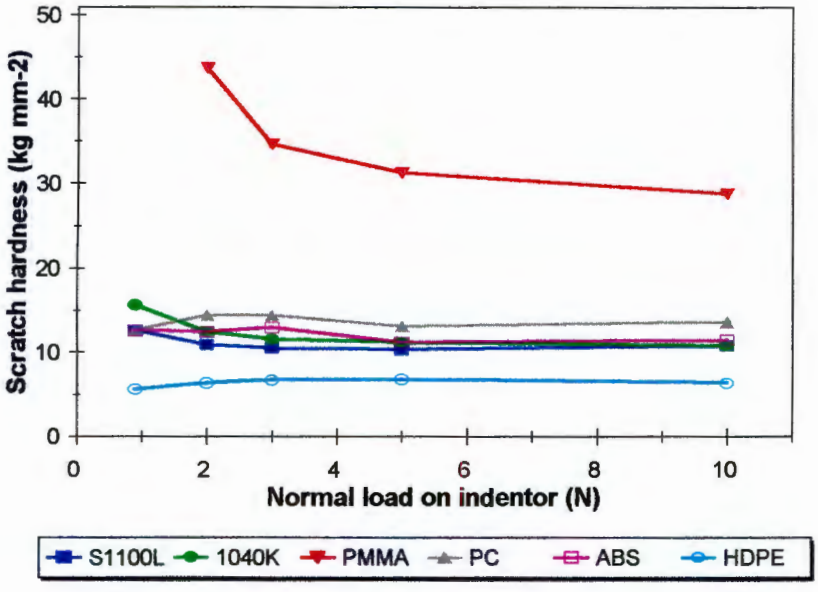

Figure 5.14: The calculated scratch hardness values for polypropylene and the comparative polymers as a function of the applied load on a Rockwell C diamond indentor.

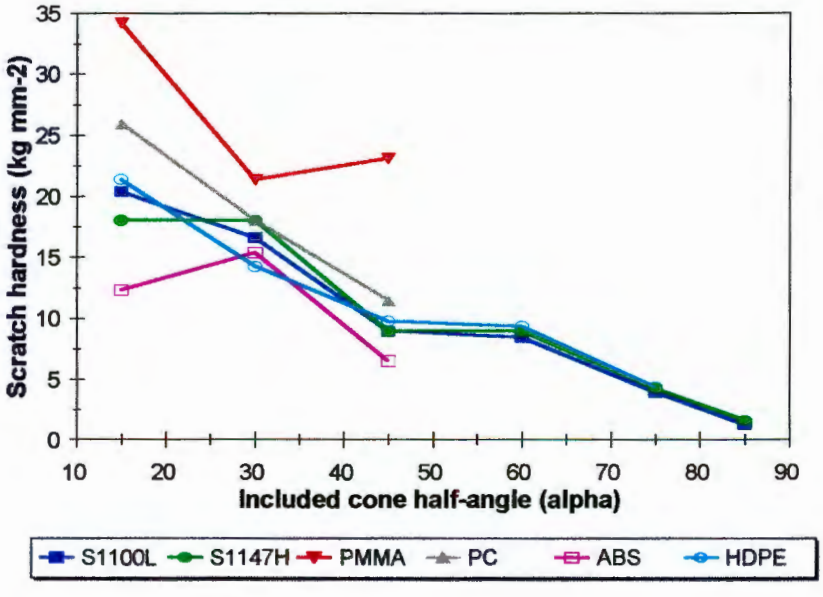

Figure 5.15: Calculated scratch hardness values for polypropylene and the comparative polymers as a function of the included half-angle, (α), of the steel scratch indentor. Applied load = 2 N.

For the unfilled polypropylenes and the comparative polymers the scratch hardness is generally independent of the applied load on the indentor above a critical load of 5 N. Below this load the hardness is dependent on the relative elastic and plastic contributions to the material's response to

indentation. The PMMA sample illustrates this in Figure 5.14; at low applied loads an elastic response is dominant, resulting in reduced scratch track widths and an increased scratch hardness; as the applied load increases there is a transition to a more dominant plastic response to indentation and hence lower scratch hardness values. A direct correlation between the measured normal hardness and the calculated scratch hardness is difficult due to the differences in indentor geometry and the applied load used for the respective tests. However, as Figure 5.16 shows, a relationship does exist between the two measured hardness values for the comparative polymers. This suggests that surface hardness is an important parameter for improved scratch resistance of a polymer.

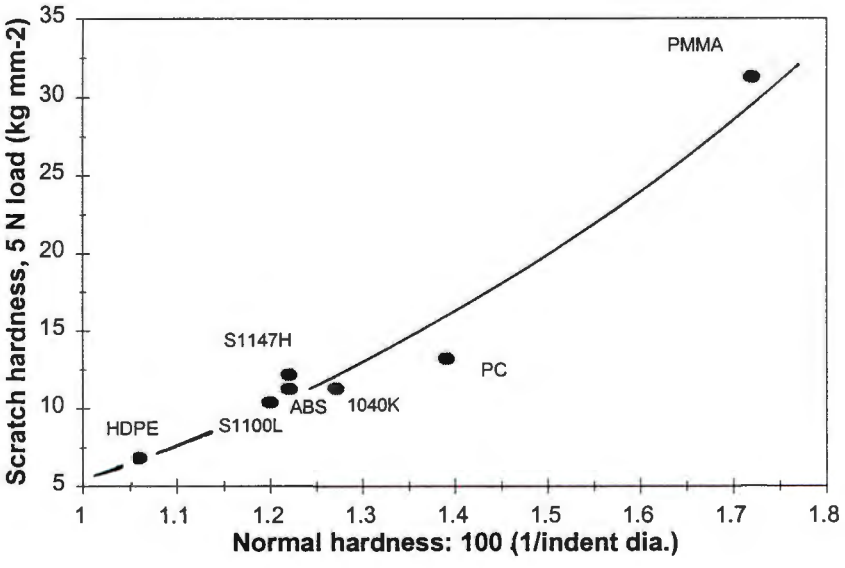

Figure 5.16: Plot illustrating the relationship for the comparative polymers between the measured scratch hardness (Rockwell C indentor at 5 N load), and the normal bulk hardness measured by the steel ball indentation method.

The transition in material deformation mechanisms with the variation in indentor angle, indicated in Table 4.16, can be analysed in terms of the stress system at the contact points.

At large included angles the contact stress is low with corresponding low tangential forces. The characteristic clear track morphologies (Figure 4.43d) with negligible deformation are indicative of the influence of yield strength and hardness in controlling the scratch indentation. The presence of the friction force during the scratching process causes the polymer to yield at a lower point than during normal hardness testing. In the case of PMMA and PC, the high yield stress of these two polymers ensures that deformation under conditions of large included indentor angle is entirely elastic in nature and, following recovery, the scratch tracks are indistinguishable.

As the included indentor angle is reduced, both the strain and the contact tensile stress in the polymer increases. The distinctive convex deformation banding visible in the type A scratches is related to the compressive tangential forces prevalent during scratching. As the scratch indentor moves across the polymer surface, the material in front of the indentor is pushed forward by compressive shear stresses acting in this zone. Ni and Le Faou[122] suggest that the convex nature of the bands corresponds to the surface Von Mises shear stress in the material and that this shear yield stress is the controlling parameter for the initiation of this scratch morphology. Deformation arises when the applied shear yield stress exceeds that of the polymer, however the spacing of the deformation bands can also be related to the adhesion/friction between the contact points, leading to a 'stick-slip' situation. 'Stick-slip' action will occur if the frictional force at the contact points is high, as is evident in the scratch tracks of several of the filled composites in Figure 4.40. If, however, the shear yield stress of the polymer is lower than the interfacial frictional force at the contact asperities, wear of the polymer by roll formation can occur as shown in Figure 4.39b. Aharoni[130] suggested that wear by roll formation can occur if the polymer in

the sliding couple is an elastic or ductile material with the ability to undergo bulk deformation under the applied normal pressure. Furthermore, he suggests that the magnitude of the contact pressure is critical in that with too low a pressure, ploughing wear would dominate, with material removal in the form of chips or slivers; under too high a contact pressure, surface shear yielding effects would dominate with the formation of the convex deformation bands (as seen for polypropylene). Thus in these scratch tests for the ductile polypropylene polymers, a mixed mode of deformation occurs, with both roll formation and shear yielding present. A schematic representation of the mechanism of roll formation is illustrated in Figure 5.17.

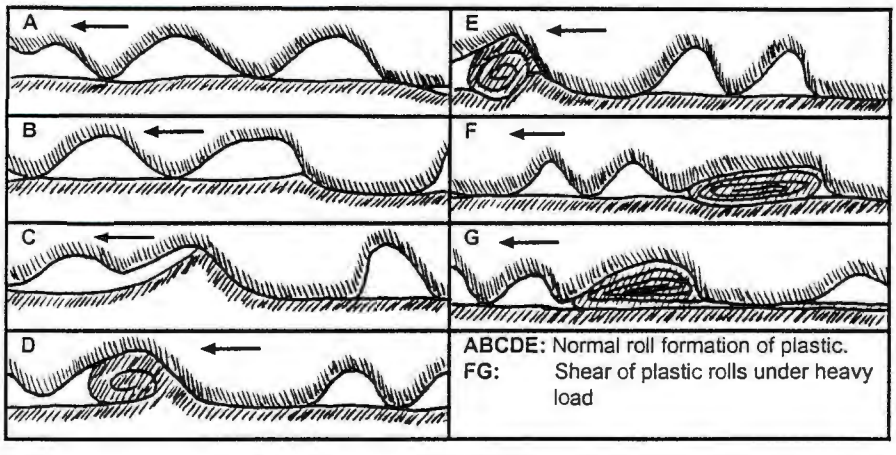

Figure 5.17: Schematic representation of the mechanism of wear by roll formation in elastic or ductile polymers. [After Aharoni[130]].

To confirm the shear yield stress theory, polypropylene samples were heat treated in an air furnace for three hours at varying temperatures and scratch tested under similar conditions. The annealed samples exhibited higher crystallinities and associated improved yield strengths over the control sample. Furthermore, decreased scratch widths were measured and the inter-shear ridge spacing of the typical type A scratches was found to be significantly reduced, as shown in Figure 5.18. Table D.3, Appendix D details

the results of the heat treatment, crystallinity determination, and the mechanical testing.

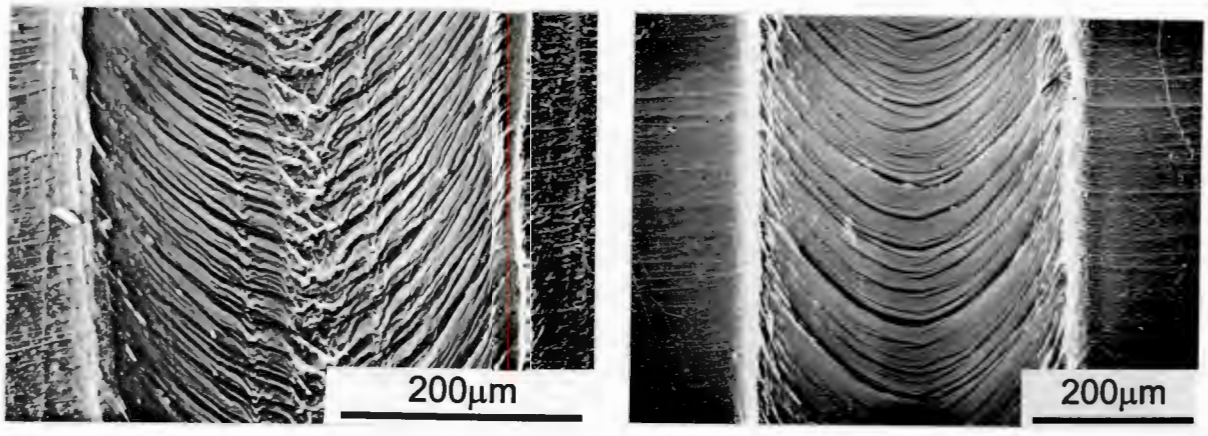

(a) (b)

Figure 5.18: (a) Type A scratch morphology of a polypropylene sample heat treated at 140°C for 3 h. The scratch track width and the spacing of the characteristic deformation shear ridges is decreased in comparison to the (b) unannealed polymer.

The type B scratch morphologies are typical of those produced on relatively brittle materials. Under high applied loads or sharp indentor conditions, the contact stress and the tangential forces at the interface zone are increased, decreasing the critical normal load for fracture to occur. As the indentor moves forward the adhesion/friction forces between the surfaces are sufficient to generate tensile stresses in the scratch track zone behind the indentor. The reduced strain to failure of the PMMA, PC, and ABS leads to tensile failure and the formation of half-moon cracks in the track as shown in Figure 5.19 and the scanning electron micrographs in Figures 4.43e and 4.43f. These results are in agreement with those of other authors[105,121].

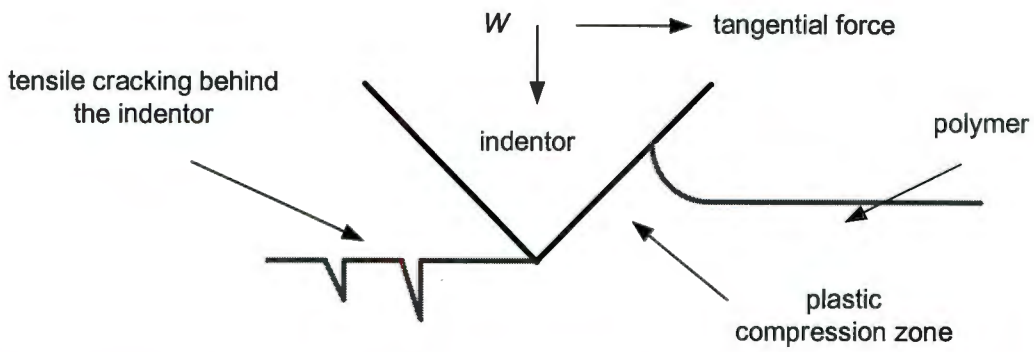

Figure 5.19: Schematic representation of a Type B scratch morphology typical of the brittle polymers PMMA, PC, and ABS, illustrating the tensile cracking occurring in the wake of the indentor. [Adapted from Williams[105]].

Scratch testing at indentor half-angles (α) of 15° and 30° produces severe cutting deformation. However, this deformation mode is dependent on the specific polymer. In the case of the PMMA, PC, and ABS polymers, the mode is brittle in nature with tensile cracking originating from the scratch track edges (Figure 4.43b). It is noted that the transition from this cutting mechanism to the onset of Type B scratch morphologies is related to the relative ductility of the three polymers.

The PP and HDPE samples display ductile cutting modes as seen in Figures 4.43a and 4.43g. During scratching of the polypropylene, the flow stress of the polymer is exceeded resulting in material removal from the scratch track. In contrast, the scratch track of the ductile HDPE shows deep grooving of the polymer, but no material removal is evident. This is indicative of the high strain to failure of the HDPE.

5.4.2 Polypropylene and the filled composites

The calculated scratch hardness values (eqn. 2.19) for the unfilled PP S1100L and the selected filled composites are shown as a function of the applied load in Figure 5.20.

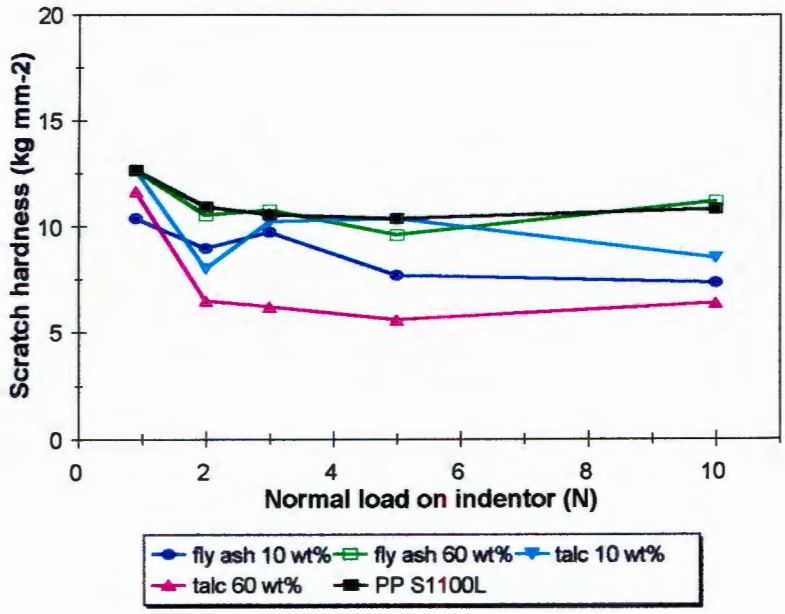

Figure 5.20: The calculated scratch hardness values for the selected filled PP composites as a function of the applied load. The scratch hardness is noted to be influenced by both the filler type and content.

Whereas the surface hardness is influential in improving the scratch resistance of the unfilled polymers, the addition of the filler particles introduces a further parameter into the scratch deformation mechanisms of the composites. Consequently, although a similar relationship is observed when plotting the measured scratch hardness against the bulk indentation hardness for selected filled polypropylene composites, there is more scatter to the results, as shown in Figure 5.21.

As seen in Figures 5.20 and 5.21, the softer unfilled polypropylene exhibits an equivalent scratch hardness to the harder filled composites. Under normal static loading conditions, the addition of the hard filler particles to the soft polymer matrix improves the bulk hardness of the composite. This is most

evident for the 60 wt% fly ash composite; the fly ash particles having a Mohs hardness of 5, the highest of the filler materials. Under dynamic scratch conditions, two opposing deformation mechanisms are present. Although the lower yield stress of the filled composites should result in greater penetration of the conical indentor into the polymer surface resulting in wider scratch tracks, the improvement in bulk hardness through the inclusion of the hard filler particles counteracts this effect. Thus the unfilled polypropylene grades show equivalent scratch hardness values to these filled composites.

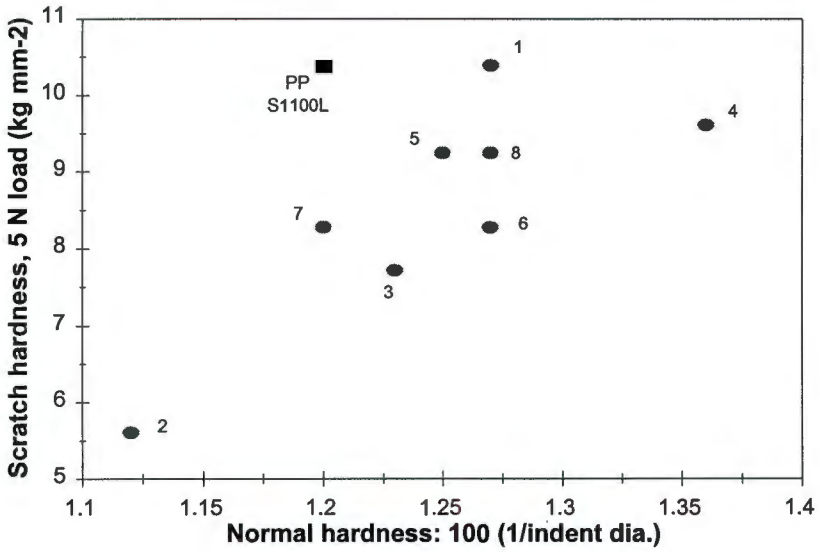

Figure 5.21: Graph illustrating the relationship between the measured scratch hardness (Rockwell C indentor at 5 N load), and the bulk indentation hardness for selected filled polypropylene composites. [1: talc 10 wt%, 2: talc 60 wt%, 3: fly ash 10 wt%, 4: fly ash 60 wt%, 5: wollastonite 10 wt%, 6: wollastonite 40 wt%, 7: *Steaplast* talc 10 wt%, 8: *Steaplast* talc 40 wt%].

The large talc-filled composites however, display divergent behaviour from that expected. The scratch behaviour of the talc-filled composites, which showed higher yield strengths than the unfilled polypropylenes, is dominated by severe material deformation and stress whitening, with the talc platelets being removed in 'leaves' from the scratch track as a result of the high strains generated behind the indentor (Figure 4.41c). The measured scratch track widths are hence greater due to the enhanced extent of lateral deformation. This deformation mechanism is emphasised at high filler contents where the

energy to fracture of these composites is greatly reduced. The low static bulk hardness values of the high filler content talc composites is attributed to enhanced deformation and slip occurring between the aligned filler platelets in the polymer matrix.

At higher applied loads (10 N), the filled composites show increasing scratch track widths to those measured for the unfilled polypropylene grades (Table 4.15). This is indicative of the decreased yield strength of the composites allowing greater indentor penetration under high load, and the prevalence of a 'stick-slip' deformation mechanism as seen for the wollastonite and *Steaplast* talc composites in Figure 4.40. This phenomenon points to enhanced interfacial friction at the contact surface resulting in an increase in the lateral extent of material deformation and hence a decrease in the scratch hardness. It is interesting to note that in the scratch tests performed using a 10 N applied load, the unfilled polypropylene and the 60 wt% fly ash composites showed equivalent scratch hardness values, illustrating the effect of the inclusion of high hardness fillers.

5.5 ABRASIVE SCRUB TESTS

The common perception of a material's scratch resistance is based on the appearance of a surface whitening, *i.e.* visible surface damage occurring usually under low applied stress conditions. This stress whitening is considered to be due to microvoid formation in the bulk polymer during scratch deformation. This leads to a difference in the refractive index between the polymeric material and the voids, and hence the whitening effect. It is particularly prevalent in the single-point scratch tests where high localised contact stresses are created. The addition of the mineral filler particles assist in the microvoid formation due to the lack of interfacial adhesion. Also, the darker pigmentation of the composites, induced by the filler addition, leads to a more visible and undesirable whitening effect.

The low stress conditions and the nature of the abrasive counterface used in the abrasive scrub tests do not result in the same level of surface whitening as attained during single-point scratch tests. The visual assessment and ranking of the materials is based on the overall appearance of the worn surface.

5.5.1 Polypropylene and the comparative polymers

The wear deformation of the PMMA and the ABS polymers is characteristically brittle with polymer debris broken off the surface in chips during the abrasive cycles (Figure 4.47a and b). This surface damage correlates with the high surface roughness values measured for the two polymers after testing, and is summarised in Table 4.17. In contrast, the PC, although it is inherently brittle, has higher toughness and is able to withstand the cyclical fatigue-like nature of the abrasive scrub pattern more readily. Thus the wear surface shows reduced damage in comparison to the PMMA and ABS. The wear surfaces of the PP grades, shown in Figure 4.47d, exhibit predominantly ductile features associated with their higher elongation to fracture. Grooving of the surface is observed but extensive surface damage is limited. This is reflected in the lower surface roughness values measured for both PC and PP. It is also apparent that the enhanced crystallinity of the S1147H and 1040K PP grades enables them to resist indentation and surface damage by the abrasive pad.

The gloss measurements of the polymers, summarised in Table 4.19, are similar and describe a progressive transition from a high gloss surface to a matt finish. It is noticeable that gloss measurement with the 60° geometry (glossy surfaces) shows the PC sample to be superior to both ABS and PMMA, which correlates to the reduced surface damage seen in the electron micrographs in Figure 4.47. Crystallinity has some effect on the gloss measurements, with the S1147H sample showing consistently, if not

significantly higher, gloss readings than the S1100L grade. This effect of crystallinity has been observed by other authors[131].

5.5.2 Polypropylene and the filled composites

The surface damage of the filled composites features large scale deformation and fatigue cracking and the breakdown of the filler particles; this latter effect is influenced by the filler size. The coarse wollastonite fibres do not readily break down under the small local contact stresses present during testing. This surface damage is reflected in the high surface roughness, R_a, values measured for each sample after test completion. The extent of damage, as given by the R_a value, is directly related to the filler content. At high filler loading a larger proportion of filler is exposed at the sample surface and hence subjected to the abrasive process. The surface-treated *Steaplast* talc composites do not follow this trend as the enhanced interfacial adhesion leads to a reduced probability of filler damage and removal; hence the lower measured R_a values as shown in Table 4.18.

The patterns associated with the reduction in surface gloss as a function of the number of abrasive cycles for the filled composites reflect the influence of both bulk crystallinity and the filler content. It is known that the inclusion of mineral fillers reduces the bulk crystallinity of a polymer. This in turn leads to a reduction in surface gloss which is allied to the increased number of filler particles exposed at the sample surface at high filler loading. In addition, SEM observation of the unworn composite surfaces shows that at high filler content the surface is highly 'textured' and voids and discontinuities exist due to the exposure of the filler particles and the lack of adhesion to the polypropylene matrix. Since the gloss reading is based on a reflectance principle, a 'textured' surface will produce more light scattering and hence lower recorded gloss values.

The decrease in gloss reading after the initial 1000 abrasive cycles, as illustrated in Figure 4.46, is associated with the maximum degree of light scattering from the surface, *i.e.,* at this point the entire sample surface has not been fully abraded due to the nature of the abrasive counterface, and there is thus a significant contrast between the initial scratch tracks produced and the unworn surface. After further abrasion, a consistent wear pattern is obtained and is associated with a transition to a characteristic matt finish. This is emphasised in the higher gloss readings obtained after both 5000 and 10 000 abrasive cycles when using the 85° gloss geometry for matt surfaces.

The transition from 'glossy' to 'matt' correlates well with the ranking order proposed through visual assessment of the samples. The high filler content composites, which are inherently less glossy than the unfilled polypropylene and low wt% grades, are able to 'hide' the matt scratching effect to a better extent. This is further enhanced by the variegated colouring of some of the samples due to moulding inconsistencies; the limited stress whitening effect can be camouflaged by the mottled appearance of the sample.

The factor of pigmentation is a further influential parameter in the scratch resistance. Whereas the dark grey fly ash samples were ranked poorly in terms of visual scratch resistance, the lighter colours of the *Steaplast* talc and wollastonite composites were noticeably better able to reduce the scratch visibility to the naked eye.

CHAPTER 6

CONCLUSIONS

The tensile strength of the unfilled polypropylene grades is dependent on the crystallinity and tie molecule density of the polymer. Crystalline enhancement with the aid of nucleating agents increases the stress required to initiate yielding. However, the higher crystallinity and tie molecule density increase the polymer chain interactions and lead to a reduction in the strain to failure.

The addition of mineral fillers to the ductile polypropylene matrix decreases the crystallinity of the composite and leads to a deterioration in tensile properties. This is exacerbated by the lack of interfacial adhesion and the large elastic and plastic mismatch between the two phases which promotes shear yielding and debonding at the polymer-filler interface. Stress transfer across this interface is limited thus contributing to a lower effective cross-sectional area for load bearing. The tensile properties are sensitive to the variation in the shape and size of the filler particles. Large platelet talc composites show improved tensile strength over the other materials due to improved interfacial stress transfer associated with the filler anisotropy and alignment.

The abrasive wear behaviours of the three unfilled polypropylene grades differ under conditions of high and low applied contact stress. Under high applied stress conditions, the polymers do not follow the accepted Ratner-Lancaster inverse correlation with increasing work to fracture, but are dependent primarily on the difference in tensile yield strength and hence the resistance to penetration of the abrasive particles. Under low stress conditions, where the abrasive particle distribution density is high, equivalent wear rates are observed for the three unfilled polypropylene grades. This is attributed to a greater abrasive energy dissipated through the increased

number of penetration and ploughing events, than for cutting and material removal.

Under conditions of severe abrasive wear corresponding to a high applied stress, the mineral fillers increase the abrasive wear rate of polypropylene. This behaviour is related to the composites' reduced ability to accommodate plastic strain generated during abrasion. Wear rates for the filled composites correlate reasonably well with the established Ratner-Lancaster theory but this model is limited in application when comparing fillers of different physical properties. The addition of mineral fillers to the polymer matrix favours a transition from a ductile to brittle wear mode with increasing filler content. An additional wear process of microcracking, contributing to brittle wear debris formation and the increased wear rates is observed. Under mild abrasive wear conditions the applied contact load per abrasive particle is reduced. The wear rates under these conditions show some dependence on the shape and relative size of the filler particles and can lead to improved wear performance, in the case of the wollastonite- and talc-filled composites.

The damage modes of the unfilled polypropylene grades, the filled composites, and the comparative polymers worn under single-point scratch conditions correlate with, and model those deformation modes produced under abrasion conditions. The surface hardness of the unfilled polymers is a controlling parameter in the scratch resistance behaviour which is in contrast to the theories of bulk abrasive wear. In the case of the filled composites, the scratch resistance is influenced predominantly by the specific physical properties of the filler materials.

Five different scratch track morphologies have been identified and related to the transitions in wear mode with changing abrasive counterface geometry. These transitions are observed as a result of the relative contributions of viscoelastic-plastic deformation and recovery, brittle fracture and microcracking, and shear yielding and ploughing to the scratch wear process.

The single-point scratch tests highlight the effect of visible stress whitening and surface damage of the polymers under scratch testing. This effect is more prevalent in the filled composites due to the presence of the filler particles acting as stress concentrators in the ductile polypropylene matrix. In applications where the visual appearance and scratch resistance of the polymer is of prime importance, colouration and surface texture are observed to be an effective means of scratch 'hiding'.

This investigation has demonstrated the role played by mineral fillers in the tensile and abrasive wear behaviour of polypropylene and compared the performance of filled polypropylenes to that of several other polymers with potential use in projected application areas. Whereas, a high tensile yield strength coupled with a high energy to fracture are beneficial to bulk abrasive wear conditions, surface hardness and effective and variegated colouration play important roles in the scratch resistance of the polymers. In particular, the surface hardness of polypropylene is limited by molecular constraints, thus scratch 'hiding' through colouration and texture will be important if polypropylene-based polymers are to be successfully used in a wide range of domestic and consumer articles.

REFERENCES

1.) Vogtländer P., "*Customer focus, creativity and change: The way ahead for polymers*", **Proc. IOM Int. Polypropylene Conf.,** London, 24-25 Oct., 1994.

2.) "Polifin: Aperitif for Stock Exchange", Corporate Special report, **Financial Mail**, October 11, 1996, p68-84.

3.) **Kirk-Othmer Encyclopedia of Chemical Technology,** 3rd Edn., Vol 16, John Wiley and Sons, Inc., 1981, p453-467.

4.) Graff G., "*Advanced formulations expand PP properties*", **Modern Plastics International,** October 1995, p63.

5.) **Modern Plastics International,** January 1996, p46-47.

6.) Genin R. and Seiler E., "*Substitution, the motor for growth*", **Proc. IOM Int. Polypropylene Conf.,** London, 24-25 Oct., 1994, p3-15.

7.) Hay J. N., "*Recent developments in polymer materials*", **Engineering Plastics**, **Metals and Materials**, May 1989, p275-279.

8.) Marcus K., Polifin PP Division, unpublished data.

9.) Mills N. J., **Plastics: Microstructure, Properties and Applications**, Edward Arnold Publ., London, 1986, p47-49.

10.) Cowie J. M. G., **Polymers: Chemistry and Physics of Modern Materials,** 2nd Edn., Blackie and Son Ltd., London, 1991, p8, 129, 140.

11.) Spaleck W., Bachmann B., and Winter A., *"New isotactic polypropylenes via metallocene catalysts",* **Proc. IOM Int. Polypropylene Conf.,** London, 24-25 Oct., 1994.

12.) Varga J., *"Review: Supermolecular structure of isotactic polypropylene"*, **J. Mater. Sci.,** Vol 27, 1992, p2557-2579.

13.) Padden F. J. and Keith H. D., *"Spherulitic crystallization in polypropylene",* **J. Appl. Physics,** Vol 30 (10), 1959, p1479-1484.

14.) Tjong S. C., Shen J. S., and Li R. K. Y., "*Mechanical behaviour of injection moulded β-crystalline phase polypropylene",* **Polym. Eng. Sci.,** Vol 36 (1), 1996, p100-105.

15.) Bassett D. C., **Principles of Polymer Morphology**, Cambridge University Press, Cambridge, 1981, p7-11.

16.) Meares P., **Polymers: Structure and Bulk Properties**, D. Van Nostrand Company Ltd., London, 1965.

17.) Williams D. J., **Polymer Science and Engineering,** Prentice-Hall Inc., London, 1971, p174-176.

18.) McCrum N. G., Buckley C. P., and Bucknall C. B., **Principles of Polymer Engineering**, Oxford University Press, Oxford, 1988, p42-45.

19.) Billmeyer F. W.(Jr.), **Textbook of Polymer Science,** 3rd Edn., John Wiley and Sons, Inc., 1984, p16-18.

20.) Phillips R., Herbert G., News J., and Wolkowicz M., "*High modulus polypropylene: Effect of polymer processing variables on morphology and properties*", **Polym. Eng. Sci.,** Vol 34 (23), 1994, p1731-1743.

21.) **Plastics Technology,** January 1996, p38-41.

22.) Marcus K., Steinhobel C., Domingo M. and Marshall N., "*The physical, mechanical and rheological properties of polypropylene: The influence of molecular weight averages and molecular weight distribution*", **Proc. Int. GPC Symposium '96**, Sept. 8-11, 1996, San Diego, California, (in press).

23.) Tzoganakis C., Vlachopoulos J., Hamielec A. E., and Shinozaki D. M., "*Effect of molecular weight distribution on the rheological and mechanical properties of polypropylene*", **Polym. Eng. Sci.,** Vol 29 (6), 1989, p390-396.

24.) Martin J. R., Johnson J. F., and Cooper A. R., "*Mechanical properties of polymers: The influence of molecular weight and molecular weight distribution*", **J. Macromol. Sci. Revs., Macromol. Chem.,** C8 (1) 1972, p57-199.

25.) Frontini P. M. and Fave A., "*The effect of annealing temperature on the fracture performance of isotactic polypropylene*", **J. Mater. Sci.,** Vol 30, 1995, p2446-2454.

26.) Balta Calleja F. J., Martinez Salazar J., and Asano T., "*Phase changes in isotactic polypropylene measured by microhardness*", **J. Mater. Sci. Lett.,** Vol 7, 1988, p165-166.

27.) Nunes R. W., Martin J. R., and Johnson J. F., "*Influence of molecular weight and molecular weight distribution on mechanical properties of polymers*", **Polym. Eng. Sci.,** Vol 22 (4), 1982, p205-228.

28.) Greco R. and Ragosta G., "*Isotactic polypropylenes of different molecular characteristics: Influence of crystallization conditions and annealing on the fracture behaviour*", **J. Mater. Sci.,** Vol 23, 1988, p4171-4180.

29.) Wu W. and Black W. B., "High-strength polyethylene", **Polym. Eng. Sci.,** Vol 19 (16), 1979, p1163-1169.

30.) Hartmann B., Lee G. F., and Wong W., "*Tensile yield in polypropylene*", **Polym. Eng. Sci.,** Vol 27 (11), 1987, p823-828.

31.) Katz H. S and Milewski J. V., **Handbook of Fillers for Plastics,** Van Nostrand Reinhold, New York, 1987, p3-7.

32.) Brydson J. A., **Plastics Materials,** 4th Edn., Butterworth Scientific, London, 1982, p116-118.

33.) Kerner E. H., "*The elastic and thermo-elastic properties of composite media*", **Proc. Phys. Soc. London,** Vol 69 (B), 1959, p808-813.

34.) Lewis T. B. and Nielsen L. E., "*Dynamic mechanical properties of particulate-filled composites",* **J. Appl. Polym. Sci.,** Vol 14, 1970, p1449-1471.

35.) Halpin J. C. and Kardos J. L., "*The Halpin-Tsai equations: A review*", **Polym. Eng. Sci.,** Vol 16 (5), 1976, p344-352.

36.) Leidner J. and Woodhams R. T., "*The strength of polymeric composites containing spherical fillers*", **J. Appl. Polym. Sci.,** Vol 18, 1974, p1639-1654.

37.) Ramsteiner F. and Theysohn R., *"On the tensile behaviour of filled composites*", **Composites,** Vol 15 (2), 1984, p121-128.

38.) Turcsanyi B., Pukanszky B., and Tudos F., "*Composition dependence of tensile yield stress in filled polymers*", **J. Mater. Sci. Lett.,** Vol 7, 1988, p160-162.

39.) Chacko V. P., Farris R. J., and Karasz F. E., "*Tensile properties of $CaCO_3$-filled polyethylenes*", **J. Appl. Polym. Sci.,** Vol 28, 1983, p2701-2713.

40.) Chacko V. P., Karasz F. E., Farris R. J., and Thomas E. L., "*Morphology of $CaCO_3$-filled polyethylenes*", **J. Appl. Polym. Sci.,** Vol 20, 1982, p2177-2195.

41.) Liu Z. and Gilbert M., "*Structure and properties of talc-filled polypropylene: Effect of phosphate coating*", **J. Appl. Polym. Sci.,** Vol 59, 1996, p1087-1098.

42.) Jancar J., "*Influence of filler particle shape on elastic moduli of PP/$CaCO_3$ and PP/$Mg(OH)_2$ composites*", **J. Mater. Sci.,** Vol 24, 1989, p3947-3955.

43.) Jancar J. and Kucera J., "*Yield behaviour of polypropylene filled with $CaCO_3$ and $Mg(OH)_2$: 'Zero' interfacial adhesion*", **Polym. Eng. Sci.,** Vol 30 (12), 1990, p707-713.

44.) Jancar J. and Kucera J., "*Yield behaviour of PP/$CaCO_3$ and PP/$Mg(OH)_2$ composites: 'Enhanced' interfacial adhesion*", **Polym. Eng. Sci.,** Vol 30 (12), 1990, p714-720.

45.) Jancar J. and Dibenedetto A. T., "*The mechanical properties of ternary composites of polypropylene with inorganic fillers and elastomer inclusions*", **J. Mater. Sci.,** Vol 29, 1994, p4651-4658.

46.) Pukanszky B., Tudos F., Jancar J., and Kolarik J., "*The possible mechanisms of polymer-filler interaction in polypropylene-$CaCO_3$ composites*", **J. Mater. Sci. Lett.,** Vol 8, 1989, p1040-1042.

47.) Harper J. F., Birchenough C., and Haworth B., "*The influence of filler coatings on the mechanical properties of filled polyethylene*", **Proc. MOFFIS-93 Int. Symp.,** Namur, Belgium, April 13-16, 1993, p67-70.

48.) Maiti S. N. and Sharma K. K., *"Studies on polypropylene composites filled with talc particles",* **J. Mater. Sci.,** Vol 27, 1992, p4605-4613.

49.) Maiti S. N. and Mahapatro P. K., "*Mechanical properties of i-PP / $CaCO_3$ composites*", **J. Appl. Polym. Sci.,** Vol 42, 1991, p3101-3110.

50.) Dongming L., Wenge Z., and Zongneng Q., "*The J-integral toughness of PP/$CaCO_3$ composites*", **J. Mater. Sci,** Vol 29, 1994, p3754-3758.

51.) Jancar J., Dibenedetto A. T., and Dianselmo A., "*Effect of adhesion on the fracture toughness of calcium carbonate-filled polypropylene*", **Polym. Eng. Sci.,** Vol 33 (9), 1993, p559-563.

52.) Hornsby P. R. and Watson C. L., *"Interfacial modification of polypropylene composites filled with magnesium hydroxide*", **J. Mater. Sci.,** Vol 30, 1995, p5347-5355.

53.) Miyata S., Imahashi T., and Anabuki H., "*Fire-retarding polypropylene with magnesium hydroxide*", **J. Appl. Polym. Sci.,** Vol 25, 1980, p415-425.

54.) Harper J. F. and Cook M., "*Filler morphology and surface treatment effects in fire retardant polypropylene copolymers*", **Proc. 5th SPSJ Int. Polymer Conf.,** Osaka, Japan, 1994, p82.

55.) Busigin C., Lahtinen R., Martinez G. M., Thomas G., and Woodhams R. T., "*The properties of mica-filled polypropylenes*", **Polym. Eng. Sci.,** Vol 24 (3), 1984, p169-174.

56.) Jarvela P. A. and Jarvela P. K., "*Multicomponent compounding of polypropylene*", **J. Mater. Sci.,** Vol 31, 1996, p3853-3860.

57.) Halling J., **Introduction to Tribology,** Wykeham Publications Ltd., London, 1976, p1.

58.) Friedrich K., "*Wear of reinforced polymers by different abrasive counterparts*", in **Friction and Wear of Polymer Composites,** K. Friedrich (ed.), Vol 1, Composite Materials Series, Elsevier Science Publ., Amsterdam, 1986, p233-287.

59.) Bahadur S., "*Wear research and development*", **J. Lub. Tech.,** ASME Trans., Vol 100, 1978, p449-454.

60.) Czichos H., "*Introduction to friction and wear*", in **Friction and Wear of Polymer Composites,** K. Friedrich (ed.), Vol 1, Composite Materials Series, Elsevier Science Publ., Amsterdam, 1986, p1-23.

61.) Evans D. C. and Lancaster J. K., "*The wear of polymers*", **Wear, Treatise on Materials Science and Technology,** Vol 13, D. Scott (ed.), Academic Press Inc., 1979, p85-140.

62.) Briscoe B. J., "*Wear of polymers: an essay on fundamental aspects*", **Trib. Int.,** Vol 14, 1981, p231-243.

63.) Marcus K., **Micromechanisms of polymer sliding wear,** Ph.D Thesis, Univ. of Cape Town, 1992.

64.) Lancaster J. K., "*Material-specific wear mechanisms: relevance to wear modelling*", **Wear,** Vol 141, 1990, p159-183.

65.) Steijn R. P., "*Characteristics of polymer wear*", in **Wear Tests for Plastics: Selection and Use,** ASTM STP 701, R.G. Bayer (ed.), ASTM, 1979, p3-17.

66.) Hutchings I. M., **Tribology: Friction and Wear of Engineering Materials,** Edward Arnold, London, 1992, p122-127, 133-150.

67.) Khruschov M. M., "*Principles of abrasive wear*", **Wear,** Vol 28, 1974, p69-88.

68.) Organization for Economic Co-operation and Development (O.E.C.D.), "*Friction, Lubrication, Wear terms and definitions*", **Research Group on the Wear of Engineering Materials,** Paris, 1968.

69.) Lancaster J. K., "*Abrasive Wear*", in **Tribology in Particulate Technology,** B. J. Briscoe and M. J. Adams (eds.), IOP Publishing Ltd., 1987, p321-334.

70.) Lancaster J. K., "*Abrasive wear of polymers*", **Wear,** Vol 14, 1969, p223-239.

71.) Greenwood J. A. and Williamson J. B. P., "*Contact of nominally flat surfaces*", **Proc. R. Soc. London,** Vol A 295, 1966, p300-319.

72.) Ratner S. B., Farberova I. I., Radyukevich O. V., and Lure E. G., "*Connection between wear resistance of plastics and other mechanical properties*", **Sov. Plastics,** Vol 12 (7), 1964, p37. [cited in ref. 70].

73.) Lancaster J. K. "*Relationships between the wear of polymers and their mechanical properties*", **Tribology Convention,** Proc. IMechE, Paper 12, Vol 183, Part 3P, 1968-1969, London, p98-106.

74.) Briscoe B. J. and Ni Z., "*The friction and wear of γ-irradiated polytetrafluoroethylene*", **Wear,** Vol 100, 1984, p221-242.

75.) Giltrow J. P., "*A relationship between abrasive wear and the cohesive energy of materials*", **Wear,** Vol 15, 1970, p71-78.

76.) Vaziri M., Spurr R. T., and Stott F. H., "*An investigation of the wear of polymeric materials*", **Wear,** Vol 122, 1988, p329-342.

77.) Czichos H., "*Influence of adhesive and abrasive mechanisms on the tribological behaviour of thermoplastic polymers*", **Wear,** Vol 88, 1983, p27-43.

78.) Santner E. and Czichos H., "*Tribology of polymers*", **Trib. Int.,** Vol 22 (2), 1989, p103-109.

79.) Bohm H., Betz S., and Ball A., "*The wear resistance of polymers*", **Trib. Int.,** Vol 23 (6), 1990, p399-406.

80.) Thorp J. M., "*Abrasive wear of some commercial polymers*", **Trib. Int.,** Vol 15 (2), 1982, p59-68.

81.) Archard J. F., "*Contact and rubbing of flat surfaces*", **J. Appl. Phys.,** Vol 24 (8), 1953, p981-988.

82.) Nathan G. K. and Jones W. J. D., "*The empirical relationship between abrasive wear and the applied conditions*", **Wear,** Vol 9, 1966, p300-309.

83.) Misra A. and Finnie I., "*On the size effect in abrasive and erosive wear*", **Wear,** Vol 65, 1981, p359-373.

84.) Cortellucci R., Heim C. J., Koshy T. D., and Phillips P. J., "*Abrasion of plastics*", **Wear,** Vol 47, 1978, p397-405.

85.) Hollander A. E. and Lancaster J. K., "*An application of topographical analysis to the wear of polymers*", **Wear,** Vol 25, 1973, p155-170.

86.) Tabor D., "*A simplified account of surface topography and the contact between solids*", **Wear,** Vol 32, 1975, p269-271.

87.) Larsen-Badse J., "*Influence of grit size on the groove formation during sliding abrasion*", **Wear,** Vol 11, 1968, p213-222.

88.) Larsen-Badse J., "*Influence of grit diameter and specimen size on wear during sliding abrasion*", **Wear,** Vol 12, 1968, p35-53.

89.) Date S. W. and Malkin S., "*Effects of grit size on abrasion with coated abrasives*", **Wear,** Vol 40, 1976, p223-235.

90.) Friedrich K. and Cyffka M., "*On the wear of reinforced thermoplastics by different abrasive papers*", **Wear,** Vol 103, 1985, p333-344.

91.) Roberts J. C. and Chang H., "*Two-body abrasion of some polymers against 6-50μm SiC abrasives*", **Wear,** Vol 79, 1982, p363-374.

92.) Sin H., Saka N., and Suh N. P., "*Abrasive wear mechanisms and the grit size effect*", **Wear,** Vol 55, 1979, p163-190.

93.) Bahadur S. and Gong D., "*The action of fillers in the modification of the tribological behaviour of polymers*", **Wear,** Vol 158, 1992, p41-59.

94.) Briscoe B. J. and Tweedale P. J., "*A view of polymer composite tribology*", **Tribology of Composite Materials,** ASM Int. Conf. Proc., P. K. Rohatgi, P. J. Blau, and C. S. Yust (eds.), 1990, p15-23.

95.) Tanaka K. and Kawakami S., "*Effect of various fillers on the friction and wear of polytetrafluoroethylene-based composites*", **Wear,** Vol 79, 1982, p221-234.

96.) Anderson J. C., "*High density and ultra-high molecular weight polyethylenes: their wear properties and bearing applications*", **Trib. Int.,** Vol 15 (1), 1982, p43-47.

97.) Cirino M., Friedrich K., and Pipes R. B., "*The effect of fibre orientation on the abrasive wear behaviour of polymer composite materials*", **Wear,** Vol 121, 1988, p127-141.

98.) Cirino M., Pipes R. B., and Friedrich K., "*The abrasive wear behaviour of continuous fibre polymer composites*", **J. Mater. Sci.,** Vol 22, 1987, p2481-2492.

99.) McGee A. C., Dharan C. K. H., and Finnie I., "*Abrasive wear of graphite fibre-reinforced polymer composite materials*", **Wear,** Vol 114, 1987, p97-107.

100.) Bijwe J., Logani C. M., and Tewari U. S., "*Influence of fillers and fibre reinforcement on abrasive wear resistance of some polymeric composites*", **Wear,** Vol 138, 1990, p77-92.

101.) Rutherford K. L. and Hutchings I. M., "*A micro-abrasive test, with particular application to coated systems*", **Surf. Coat. Tech.,** Vol 79, 1996, p231-239.

102.) Briscoe B. J., Evans P. D., and Lancaster J. K., "*Single point deformation and abrasion of γ-irradiated polytetrafluoroethylene*", **J. Phys. D: Appl. Phys.,** Vol 20, 1987, p346-353.

103.) Denape J., Etienne P., Paris J.-Y., Phalippou J., and Sempere R., "*Tribological analysis of friction damage on coated plastics through the third body concept*", **Proc. 22nd Leeds-Lyon Symp. on Tribology,** Lyon, France, 5-8 September, 1995, in Tribology Series , Vol 31, D. Dowson *et al.* (eds.), p479-488.

104.) Hurlbut C. S., **Dana's Manual of Mineralogy**, 18th Edn., John Wiley and Sons, Inc., New York, 1971, p128-130.

105.) Williams J. A., "*Analytical models of scratch hardness*", **Trib. Int.,** Vol 29 (8), 1996, p675-694.

106.) Hutchings I. M., "*Ductile-brittle transitions and wear maps for the erosion and abrasion of brittle materials*", **J. Phys. D: Appl. Phys.,** Vol 25, 1992, pA212-A221.

107.) Briscoe B. J., Evans P. D., Biswas S. K., and Sinha S. K., "*The hardnesses of polymethylmethacrylate*", **Trib. Int.,** Vol 29 (2), 1996, p93-104.

108.) Grasmeder J. R., "*Scratch resistant polypropylene compounds*", **Proc. IOM Int. Polypropylene Conf.**, London, 24-25 Oct., 1994, p98-108.

109.) Erichsen Testing Equipment Data Sheet: Gr.14-413/E, VI/93.

110.) Ford Laboratory Test Method BN 108-13.

111.) Jeffs D. G., "*Polymer treated minerals as fillers in scratch resistant PP mouldings*", **Proc. Polypropylene '94: Applications, Markets and Business Development,** Session III, Speaker 2-1, Zurich, October 4-5, 1994, p1-13.

112.) ASTM Standard D4213-92.

113.) ASTM Standard D1044-85.

114.) ASTM Standard D523-85.

115.) British Standard BS 2782, Part 3: Method 370, 1990.

116.) Lawn B. and Wilshaw R., "*Review: Indentation fracture: principles and applications*", **J. Mater. Sci.,** Vol 10, 1975, p1049-1081.

117.) Conway J. C. and Kirchner H. P., "*The mechanics of crack initiation and propagation beneath a moving sharp indentor*", **J. Mater. Sci.,** Vol 15, 1980, p2879-2883.

118.) Bull S. J. and Page T. F., "*High-dose ion implantation of ceramics: benefits and limitations for tribology*", **J. Mater. Sci.,** Vol 23, 1988, p4217-4230.

119.) Briscoe B. J., Biswas S. K., Sinha S. K., and Panesar S. S., "*The scratch hardness and friction of a soft rigid-plastic solid*", **Trib. Int.,** Vol 26 (3), 1993, p183-193.

120.) Briscoe B. J., Sebastian K. S. and Adams M. J., "*The effect of indentor geometry on the elastic response to indentation*", **J. Phys. D: Appl. Phys.,** Vol 27, 1994, p1156-1162.

121.) Bethune B., "*The surface cracking of glassy polymers under a sliding spherical indentor*", **J. Mater. Sci.,** Vol 11, 1976, p199-205.

122.) Ni B. Y. and Le Faou A., "*Scratching behaviour of polymer films using blunt spherical styli*", **J. Mater. Sci.,** Vol 31, 1996, p3955-3963.

123.) Campbell D. and White J. R., **Polymer Characterisation: Physical Techniques,** Chapman and Hall, London, 1989, p302-313.

124.) Greco R., Martuscelli E., Ragosta G., and Jinghua Y., "*Polyolefin blends: Morphology, thermal behaviour and mechanical properties of PP-EPR alloys crystallised at low undercoolings*", **J. Mater. Sci.,** Vol 23, 1988, p4307-4314.

125.) Trotignon J.-P. and Verdu J., "*Skin-core structure - Fatigue behaviour relationships for injection moulded parts of polypropylene*", **J. Appl. Polym. Sci.,** Vol 34, 1987, p1-18.

126.) Fujiyama M. and Azuma K., "*Skin/core morphology and tensile impact strength of injection moulded polypropylene*", **J. Appl. Polym. Sci.,** Vol 23, 1979, p2807-2811.

127.) Way J. L. and Atkinson J. R., "*Some studies of deformation processes in fully-spherulitic polypropylene*", **J. Mater. Sci.,** Vol 6, 1971, p102-109.

128.) Pukanszky B., van Es M., Maurer H. J., and Vörös G., "*Micromechanical deformations in particulate filled thermoplastics: volume strain measurements*", **J. Mater. Sci.,** Vol 29, 1994, p2350-2358.

129.) Sole B. M. and Ball A., "*On the abrasive wear behaviour of mineral filled polypropylene*", **Trib. Int.,** Vol 29 (6), 1996, p457-465.

130.) Aharoni S. M., "*Wear of polymers by roll formation*", **Wear,** Vol 25, 1973, p309-327.

131.) Grasmeder J. R., Private communication.